ISSN 2221-6413 (Print), ISSN 2223-2559 (Online)
Coden: PJSIB5 58(2) 59-116 (2015)

Pakistan Journal of Scientific and Industrial Research

Series A: Physical Sciences

Vol. 58, No.2, May-June, 2015

(for on-line access please visit web-site http://www.pjsir.org)

Published by
Scientific Information Centre
Pakistan Council of Scientific and Industrial Research
Karachi, Pakistan

Pakistan Journal of Scientific and Industrial Research
Series A: Physical Sciences

Pakistan Journal of Scientific and Industrial Research started in 1958, has been bifurcated in 2011 into:

Series A: Physical Sciences [**ISSN 2221-6413 (Print); ISSN 2223-2559 (online)]** (appearing as issues of January-February, May-June and September-October) and
Series B: Biological Sciences [**ISSN 2221-6421 (Print); ISSN 2223-2567 (online)]** (appearing as issues of March-April, July-August and November-December).
Each Series will appear three times in a year.

This Journal is indexed/abstracted in Biological Abstracts and Biological Abstracts Reports, Chemical Abstracts, Geo Abstracts, CAB International, BioSciences Information Service, Zoological Record, BIOSIS, NISC, NSDP, Current Contents, CCAB, Rapra Polymer Database, Reviews and Meetings and their CD-ROM counterparts etc.

Subscription rates (including handling and Air Mail postage): ***Local:*** Rs. 2500 per volume, single issue Rs. 425; ***Foreign:*** US$ 450 per volume, single issue US$ 75.

Electronic format of this journal is available with: Bell & Howell Information and Learning, 300, North Zeeb Road, P.O. 1346, Ann Arbor, Michigan 48106, U.S.A; Fax.No.313-677-0108; http://www.proquest.com

Photocopies of back issues can be obtained through submission of complete reference to the Executive Editor against the payment of Rs. 25 per page per copy (by Registered Mail) and Rs. 115 per copy (by Courier Service), within Pakistan; US$ 10 per page per copy (by Registered Mail) and US$25 per page per copy (by Courier Service), for all other countries.

Printed and Published by: PCSIR Scientific Information Centre, PCSIR Laboratories Campus, Shahrah-e-Dr. Salimuzzaman Siddiqui, Karachi-75280, Pakistan.

Editorial Address

Executive Editor
Pakistan Journal of Scientific and Industrial Research, PCSIR Scientific Information Centre
PCSIR Laboratories Campus, Shahrah-e-Dr. Salimuzzaman Siddiqui, Karachi-75280, Pakistan
Tel: 92-21-34651739-40, 34651741-43; Fax: 92-21-34651738; Web: http://www.pjsir.org, E-mail: info@pjsir.org

AIMS & SCOPE

Pakistan Journal of Scientific and Industrial Research (PJSIR) was started in 1958 to disseminate research results based on utilization of locally available raw materials leading to production of goods to cater to the national requirements and to promote S&T in the country. Over the past 55 years, the journal conveys high quality original research results in both basic and applied research in Pakistan. A great number of major achievements in Pakistan were first disseminated to the outside world through PJSIR.

It is a peer reviewed journal and published in both print and electronic form. Original research articles, review articles and short communications from varied key scientific disciplines are accepted however, papers of Pure Mathematics, Computer Sciences and Medical Sciences are not entertained.

From 54th Volume in 2011, it has been bifurcated into Series A: Physical Sciences & Series B: Biological Sciences. Each series appears three times in a year as follows:

Physical Sciences in January-February, May-June and September-October issues. It includes research related to Natural Sciences, Organic Chemistry, Inorganic Chemistry, Industrial Chemistry, Physical Chemistry, Environmental Sciences, Geology, Physics, Polymer Sciences and Technology.

Biological Sciences in March-April, July-August and November-December issues. Papers included in this series are from Agriculture, Agronomy, Botany, Biochemistry, Biotechnology, Food Sciences, Genetic Engineering, Pharmaceutical Sciences, Microbiology, Marine Sciences, Soil Sciences, Tissue Culture, Zoology and Technology.

Due to many global issues, we are encouraging contributions from scientists and researchers from all across the globe with the sole purpose of serving scientific community worldwide on the whole and particularly for our region and third world countries.

Pakistan Journal of Scientific and Industrial Research
Series A: Physical Sciences
Vol. 58, No. 2, May-June, 2015

Contents

Preparation and Characterisation of Some Transition Metal Complexes of Niacinamide (Vitamin B_3)
Md. Mahmudul Hasan, Md. Elius Hossain, M. Ershad Halim and Md. Qamrul Ehsan **59**

Electroless and Electrodeposition of Silver from a Choline Chloride-Based Ionic Liquid
Muhammad Rostom Ali, Muhammad Ziaur Rahman and Siddhartha Sankar Saha **66**

An Assessment of Cleaning Amenability of Salt Range Coal Through Physical Cleaning Methods
Muhammad Shahzad, Syed Muhammad Tariq, Mansoor Iqbal, Syed Mahmood Arshad and Shahab Saqib **74**

Variability in Foliar Phenolic Composition of Several *Quercus* Species in Northern Mexico
Jorge Armando Arámbula-Salazar, Norma Almaraz-Abarca, José Javier Corral-Rivas, Eli Amanda Delgado-Alvarado, Raúl Díaz-Moreno and Eusebio Montiel-Antuna **79**

Automated Method for Delineating Watershed, Drainage Pattern and Calculation of Flow Accumulation in Punjab Province using Digital Elevation Model
Umair bin Zamir and Jamil Hassan Kazmi **90**

DSC Cure Kinetics of an Unsaturated Polyester Resin Using Empirical Kinetic Model
Iram Abdullah **99**

Amenability of Carboxylic Acids Adsorption on Surface of Activated Carbon
Tayyba Aftab, Naeem Abbas, Muhammad Irfan, Farah Deeba, Naz Imtiaz and Rauf Ahmad Khan **106**

Evaluation of Pesticide Residues in Drinking Water in Different Areas of Khyber Pakhtunkhwa, Pakistan
Muhammad Nasimullah Qureshi and Inayat Ur Rahman **111**

Pak. j. sci. ind. res. Ser. A: phys. sci. 2015 **58** (2) 59-65

Preparation and Characterisation of Some Transition Metal Complexes of Niacinamide (Vitamin B_3)

Md. Mahmudul Hasan, Md. Elius Hossain, M. Ershad Halim and Md. Qamrul Ehsan*
Department of Chemistry, University of Dhaka, Dhaka-1000, Bangladesh

(received September 18, 2013; revised June 27, 2014; accepted July 9, 2014)

Abstract. Niacinamide forms metal complexes of general formula $[M(C_6H_6N_2O)_2]Cl_2$; where M = Mn(II), Co(II), Ni(II), Cu(II) and Zn(II) in the aqueous medium. The complexes were formulated by comparing the experimental and calculated data for C, H, N and metal. The prepared complexes were characterised by different physicochemical methods. The UV-vis, FTIR spectral analysis and thermo gravimetric analysis (TGA). TGA of these complexes have been discussed. Magnetic susceptibility values indicate that all complexes except Zn complex are paramagnetic in nature. The redox properties of the metal ions in the Mn, Cu and Zn complexes have been discussed from the cyclic voltammetric studies. In all cases the systems are quasi reversible.

Keywords: niacinamide, magnetic susceptibility, metal complexes, thermo gravimetric analysis

Introduction

The vitamins are a disparate group of compounds. They have little in common either chemically or in their metabolic functions. Nutritionally, they form a cohesive group of organic compounds that are required in the diet in small amounts (micrograms or milligrams per day) for the maintenance of normal health and metabolic integrity (Bender, 2003). Considering the significant role of metal ions in vast number of widely different biological processes many scientists are working in the field of interaction of metals with different vitamins. A great deal of work has been done in the field of preparation and characterisation of metal-vitamin compounds (Mamun *et al*., 2011; Rahman *et al*., 2011; Ehsan *et al*., 2004; 2001; Haider *et al*., 1988; 1987).

Niacinamide named as vitamin B_3 is one of the most important member of water-soluble vitamins (B-vitamins). Vitamin B_3 functions as coenzyme in oxidation and reduction reactions, functional part of NAD and NADP, role in intracellular calcium regulation and cell signaling. Vitamin B_3 deficiency causes pellagra, characterised by a photosensitive dermatitis, like severe sunburn, typically with a butterfly-like pattern of distribution over the face, affecting all parts of the skin that are exposed to sunlight. Similar skin lesions may also occur in areas not exposed to sunlight, but subject to pressure, such as the knees, elbows, wrists, and ankles. Advanced pellagra is also accompanied by a dementia or depressive psychosis, and there may be diarrhoea (Bender, 2003). Studies of metal-niacinamide complexes are therefore, very important from the physiological activity point in the living system.

The niacinamide is a 3-substituted derivative of pyridine. It has three donor atoms (2N and 1O). The coordination chemistry of niacinamide is important since there are possibilities to form variety of complexes with d-block metal ions. In this communication preparation and characterisation of niacinamide complexes of first row transition metals namely; Mn, Co, Ni, Cu and Zn have been reported, all in the + 2 oxidation state.

Materials and Methods

Analytical grade reagents (BDH and Aldrich) were used in all preparative and analytical works. Micro-analysis for C, H and N were performed on an automatic micro-analyser in the Laboratory of Organic Structural Chemistry (Prof. Shinmyozu Lab.), Department of Molecular Chemistry, Graduate School of Sciences & IMCE, Kyushu University, Japan. Metal content of the complexes were quantitatively determined by complexometric method. Chloride content of all the complexes were qualitatively tested by $AgNO_3$ solution. The melting point of all the complexes were measured in a heating device with a thermometer, MEL-TEMP II Laboratory Devices made in USA. Infrared spectra of the complexes were recorded on a calibrated Fourier Transformation Infrared Spectrophotometer (Shimadzu FTIR IR prestige-21 S/N) in the range of 500-4500 cm^{-1} as KBr pellets at QC Department of Beximco

*Author for correspondence; E-mail: mqehsan@yahoo.com

Pharmaceuticals, Bangladesh. The electronic spectra of niacinamide and its complexes were recorded on a Shimadzu UV-visible recording spectrophotometer (UV-160A) in the wavelength range 200-1100 nm using nujol mull technique. The thermo gravimetric analysis of the complexes was carried out with a computer controlled TA-60WS thermo gravimetric analyser and TGA-50H detector made in Japan at Centre of Excellence, Dhaka University. The magnetic properties of the complexes were studied at ambient temperature on a magnetic susceptibility balance (Magway MSB Mk1 Sherwood Scientific Ltd., Cambridge, England). The cyclic voltammogram of the complexes were studied with Epsilon, a PC controlled potentiostat; developed by Bioanalytical Systems, Inc. USA.

Preparation and formulation. All the complexes were prepared by following a general procedure. In all cases 20 mmol niacinamide and 20 mmol metal salt were dissolved separately in deionised water. These two solutions were filtered separately and mixed together. The resultant mixture was concentrated by heating carefully with moderately low flame in a Bunsen burner. Then the concentrated solution was allowed to cool at room temperature. The precipitate obtained was filtered, washed with water and dried over silica gel in a desiccator. All the complexes were stable in light and air. Preparation of the complexes are shown in scheme 1.

The formulation of the complexes was done by comparing the experimental and calculated data for elemental analysis. The micro analytical data of C, H, N and M content in the prepared complexes are given below:

A $[Mn(C_6H_6N_2O)_2]Cl_2$**:** calcd, (%): C, 38.91; H, 3.27; N, 15.13; Mn, 14.85.
anal Found, (%): C, 38.22; H, 3.23; N, 14.86; Mn, 12.60.
B $[Co(C_6H_6N_2O)_2]Cl_2$**:** calcd, (%): C, 38.50; H, 3.23; N, 14.97; Co, 15.76.
anal Found, (%): C, 38.42; H, 3.24; N, 14.99; Co, 13.75.
C $[Ni(C_6H_6N_2O)_2]Cl_2$**:** calcd, (%): C, 38.52; H, 3.24; N, 14.98; Ni, 15.70.
anal Found, (%): C, 37.62; H, 3.19; N, 14.69; Ni, 13.60.
D $[Cu(C_6H_6N_2O)_2]Cl_2$**:** calcd, (%): C, 38.03; H, 3.20; N, 14.80; Cu, 16.77.
anal Found, (%): C, 37.95; H, 3.13; N, 14.78; Cu, 14.48.
E $[Zn(C_6H_6N_2O)_2]Cl_2$**:** calcd, (%): C, 37.85; H, 3.18; N, 14.72; Zn, 17.18.
anal Found, (%): C, 37.66; H, 3.27; N, 14.65; Zn, 14.96.

Results and Discussion

Metal complexes of niacinamide have been synthesised in the aqueous medium following a general procedure. The complexes have the general formula:

$[M(C_6H_6N_2O)_2]\ Cl_2$; M = Mn(II), Co(II), Ni(II), Cu(II) and Zn(II)

The complexes are soluble in water but insoluble in most of the common organic solvents. The physical appearance of the complexes are $[Mn(C_6H_6N_2O)_2]Cl_2$ (light pink), $[Co\ (C_6H_6N_2O)_2]\ Cl_2$ (orange), $[Ni\ (C_6H_6N_2O)_2]Cl_2$ (yellowish green), $[Cu(C_6H_6N_2O)_2]Cl_2$ (light green), $[Zn(C_6H_6N_2O)_2]Cl_2$ (colourless). Melting point of the complexes are more than 200 °C. The high melting point and the solubility nature of the complexes indicate that they are ionic in nature to some extent.

IR Spectral analysis. The IR spectral analysis confirm the formation as well as similar bonding nature of all the complexes. The IR absorption spectra of niacinamide and Cu-niacinamide complex are compared in Fig. 1. The tentative assignments have been done on the basis of standard references (Silverstein *et al*., 2005, Banwell *et al*., 2003, Pavia *et al*., 2001) and presented in Table 1.

In all the complexes a strong peak at ~3157 to 3203 cm^{-1} appears due to symmetric N-H stretching vibration. Asymmetric N-H stretching vibration appears at ~ 3319 to 3402 cm^{-1}. Whereas, for the ligand a strong broad peak at 3165 cm^{-1} and 3365 cm^{-1} was due to symmetric and asymmetric N-H stretching vibration of $–NH_2$ group, respectively. The change in sharpness and position of the peaks in the complexes with respect to that of ligand is due to the fact that the nitrogen participate in the coordination.

All the complexes absorb strongly at ~1664 to 1708 cm^{-1} due to C=O stretching vibration. Strong sharp band appear at ~1602 to 1624 cm^{-1} due to aromatic C=C stretching vibration. For ligand a strong peak at 1678 cm^{-1} and 1618 cm^{-1} are due to C=O and aromatic C=C stretching vibrations. At ~1375 to 1398 cm^{-1} all the complexes absorb

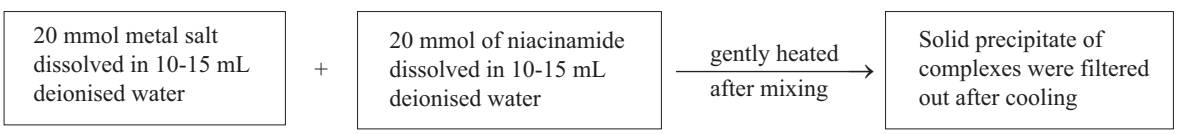

Scheme 1. Preparation of complexes.

Table 1. Comparison of IR bands of niacinamide and its complexes

Compound	υ (NH) str. (sym) cm^{-1}	υ (NH) str. (asym) cm^{-1}	υ (CH) str. aromatic cm^{-1}	υ (C=O) str. cm^{-1}	υ (C=C) str. aromatic cm^{-1}	υ (NH) bending cm^{-1}	υ (CN) str. cm^{-1}
Niacinamide	3165	3365	2783	1678	1618	1576	1394
$[Mn(C_6H_6N_2O)_2]Cl_2$	3203	3342	2365	1670	1622	1601	1375
$[Co(C_6H_6N_2O)_2]Cl_2$	3196	3319	2754	1666	1602	1568	1396
$[Ni(C_6H_6N_2O)_2]Cl_2$	3196	3367	2752	1664	1624	1605	1398
$[Cu(C_6H_6N_2O)_2]Cl_2$	3157	3402	2360	1708	1605	-	1379
$[Zn(C_6H_6N_2O)_2]Cl_2$	3184	3344	2762	1674	1603	1568	1375

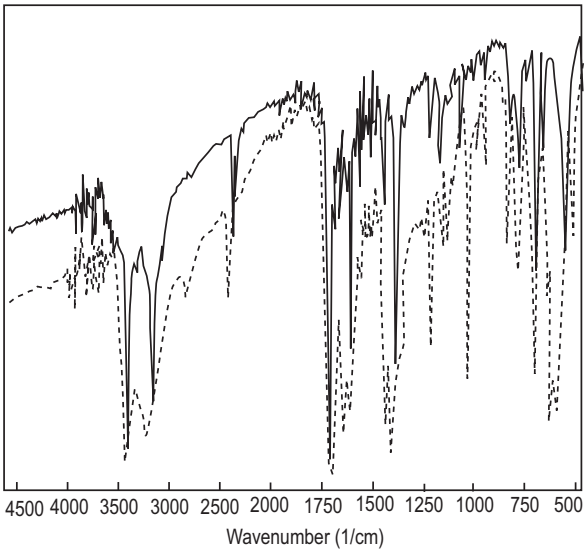

Fig. 1. Comparison of the FTIR spectra of (a) $[Cu(C_6H_6N_2O)_2]Cl_2$ and (1) Niacinamide ($C_6H_6N_2O$) in the region 500 to 4500 cm^{-1}.

due to C-N stretching vibration. A strong sharp peak at 1394 cm^{-1} appeared due to C-N stretching vibration for ligand. A sharp peak for aromatic =C-H stretching vibration appears at 2360 to 2762 cm^{-1} in the complexes. The sharpness of the peaks due to C=O, C=C and CN bands and their displacement with respect to that of ligand confirmed the formation of the complexes.

UV-vis spectral analysis. The electronic absorption spectra of the niacinamide complexes and their characteristic absorption bands with tentative assignments are presented in Fig 2 and Table 2, respectively. The assignments have been done on the basis of some standard references (Banwell *et al*., 2003; Pavia *et al*., 2001).

The $n \rightarrow \sigma^*$ absorption bands due to the transition of nitrogen lone pair to the anti bonding orbital of C-N bond

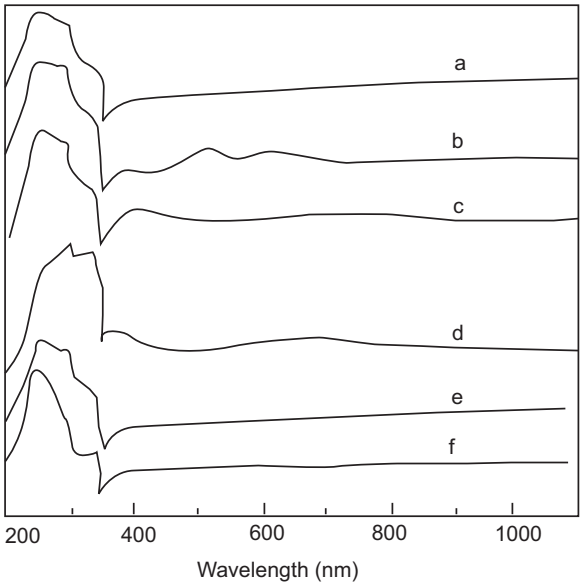

Fig. 2. The UV absorption spectrum in the region 200 to 1100 nm of (a) $[Mn(C_6H_6N_2O)_2]Cl_2$ (b) $[Co(C_6H_6N_2O)_2]Cl_2$ (c) $[Ni(C_6H_6N_2O)_2]Cl_2$ (d) $[Cu(C_6H_6N_2O)_2]Cl_2$ (e) $[Zn(C_6H_6N_2O)_2]Cl_2$ and (1) niacinamide ($C_6H_6N_2O$).

Table 2. Absorption bands of niacinamide and its complexes

Compound	Absorption bands λ_{max} (nm)			
	d→d*	n→π*	n→σ*	π→π*
Niacinamide ($C_6H_6N_2O$)	-	343	300	250
$[Mn(C_6H_6N_2O)_2]Cl_2$	-	340	298	263
$[Co(C_6H_6N_2O)_2]Cl_2$	520, 620	342	299	263
$[Ni(C_6H_6N_2O)_2]Cl_2$	700	340	299	265
$[Cu(C_6H_6N_2O)_2]Cl_2$	650	341	299	262
$[Zn(C_6H_6N_2O)_2]Cl_2$	-	338	299	255

Table 3. Weight loss at different stages of TG analysis of niacinamide and metal-niacinamide complexes

Compound	Sample weight (mg)	TG analysis Transition temp. (°C)	% Wt. loss		Comments
$[Cu(C_6H_6N_2O)_2]Cl_2$	10.373	32-60	6		The weight loss may be due to loss of adhere water
		60-250	No loss		No chemically bound water
		250-350	57		The weight loss may be due to loss of CO_2, HCl, NH_3, H_2
		350-580	5		It may be due to loss of CH_4
		580-580 (10 min.) Residue = 26%	6		The rest of the organic part may be lost

Table 4. Magnetic properties of the complexes of niacinamide

Compound	χ_A (cgs) x 10^{-3}	μ_{eff} BM (at 300K) Found	Theo.	No. of unpaired electron	Config. g.	Inference
$[Mn(C_6H_6N_2O)_2]Cl_2$	10.63	5.50	5.7-6.0	5	d^5	Paramagnetic
$[Co(C_6H_6N_2O)_2]Cl_2$	11.47	5.20	4.3-5.2	3	d^7	Paramagnetic
$[Ni(C_6H_6N_2O)_2]Cl_2$	3.598	2.94	3.0-3.3	2	d^8	Paramagnetic
$[Cu(C_6H_6N_2O)_2]Cl_2$	1.09	1.62	1.7-2.2	1	d^9	Paramagnetic
$[Zn(C_6H_6N_2O)_2]Cl_2$	-ve	0*	-	0	d^{10}	Diamagnetic

* = The negative value of χ_A indicates that the tube and sample have a net diamagnetism. In that case μ_{eff} can be considered as zero.

appeared at 299 nm instead of 300 nm in niacinamide. The bands due to $\pi \rightarrow \pi^*$ transition in the metal complexes at ~ 255-263 nm are somewhat broad and seem to be overlapped with the $n \rightarrow \sigma^*$ bands. The $n \rightarrow \pi^*$ transition bands in the complexes are observed in the region 338-340 nm whereas the ligand absorb at 343 nm. The broad bands for the coloured complexes in the range of 520-700 nm were clearly due to the d-d transitions which is absent for the complex with d^{10} system.

The presence of $\pi \rightarrow \pi^*$, $n \rightarrow \pi^*$ and $n \rightarrow \sigma^*$ bands in all the complexes indicate the presence of the functional groups of the parent ligand (e.g. -C=O, $-NH_2$). Shifting of the absorption bands in the complexes and appearing of a new band for d-d transitions also indicate the probability of forming M←L coordination bonds in the complexes. Again the positions of the absorption bands also indicate the similar bonding pattern of the complexes.

Thermo gravimetric analysis. Thermo gravimetric TG curves of the complexes and the ligand are compared in Fig. 3 and the characteristic features of decomposition of $[Cu(C_6H_6N_2O)_2]Cl_2$ are tabulated in Table 3.

Thermo gravimetric analysis (TGA) reveals that niacinamide and its complexes are not accompanied by any chemically bonded water or water of crystallization. The pattern of the thermo grams also confirm the complexation between metal and niacinamide.

Magnetic properties. Magnetic moments of all the complexes were measured using a manual magnetic susceptibility balance. The measured values agree with the divalent oxidation state of the metals (Table 4).

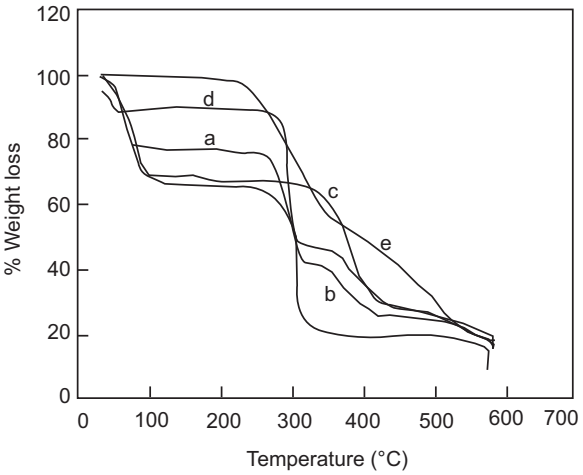

Fig. 3. TG curves of (a) $[Mn(C_6H_6N_2O)_2]Cl_2$ (b) $[Co(C_6H_6N_2O)_2]Cl_2$ (c) $[Ni(C_6H_6N_2O)_2]Cl_2$ (d) $[Cu(C_6H_6N_2O)_2]Cl_2$ (e) $[Zn(C_6H_6N_2O)_2]Cl_2$ (1) Niacinamide ($C_6H_6N_2O$).

The μ_{eff} values of the complexes demonstrate that all the complexes are sufficiently pure. The complexes of Mn(II), Co(II), Ni(II) and Cu(II) are high spin paramagnetic as suggested by their measured and standard magnetic moment values (Mamun *et al*., 2011, Rahman *et al* 2011). The $[Zn(C_6H_6N_2O)_2]Cl_2$ complex is diamagnetic as the complex is d^{10} system. The deviation of magnetic moment value of copper ion may be due to some experimental errors.

Cyclic voltammetric studies. The redox behaviour of Mn(II), Cu(II) and Zn(II) in the coordinated and uncoordinated states were examined using cyclic voltammetric technique. All the solutions in the present study were prepared in freshly prepared KCl solution. The surface of the working electrode was polished with powdered alumina and rinsed thoroughly with deionised water before doing the experiments. The solution system was deoxygenated by purging with N_2 gas and was homogenised by stirring with a magnetic stirrer. The cyclic voltammograms of the solution were recorded with respect to saturated Ag/AgCl reference electrode.

CV studies of redox behaviour of Cu(II) in $CuCl_2$ and $[Cu(C_6H_6N_2O)_2]C_2$. The redox behaviour of Cu(II) in $CuCl_2$ and $[Cu(C_6H_6N_2O)_2]Cl_2$ were observed in 0.1M KCl using cyclic voltammetric technique on glassy carbon electrode within the potential window 1200-1300 mV at room temperature. The voltammogram of the complex is compared with that of the free metal and niacinamide in Fig. 4.

The CV of Cu(II) in $CuCl_2$ shows two cathodic peaks at potential 45.4 mV and -212.2 mV, and two anodic peaks at potential 241.0 mV and 88.4 mV, respectively. In the metal complex, there were two cathodic peaks at potential 121.8 mV, and -188.4 mV, and two anodic peaks at potentials 174.2 mV, and 55.0 mV, respectively. The voltammograms indicate that there were two one-electron transfer processes i.e.,

The peak positions deviated noticeably in the complex system compared to that of free metal. However, the peak currents for both the anodic and cathodic peaks in the voltammogram of the complex are remarkably lower than that of metal salt.

$$\text{Cathodic: Cu(II)} \xrightarrow{+\,e^-} \text{Cu(I)} \xrightarrow{+\,e^-} \text{Cu(0)}$$

$$\text{Anodic: Cu(0)} \xrightarrow{-\,e^-} \text{Cu(I)} \xrightarrow{-\,e^-} \text{Cu(II)}$$

Scan rate variation. The cyclic voltammograms of 1 mM $[Cu(C_6H_6N_2O)_2]Cl_2$ at different scan rates are shown in Fig. 5. The current potential data, peak potential separation and peak current ratio of the voltammograms are recorded in Table 5.

The voltammograms of the metal complex at different scan rates expressed that with the increase of scan rate the peak currents for both cathodic and anodic peaks increases. Both the cathodic peaks shifted towards negative while the anodic peaks shifted towards positive direction with the increase of scan rate. The peak separation for the first pair of cathodic and anodic peaks increases with the increase of scan rate.

Randless-sevcick plot. A plot of peak current (first pair of peak) vs SQRT of scan rate (Fig. 6) for the metal complex showed that with the increase of scan rate peak, current for both cathodic and anodic peaks increases.

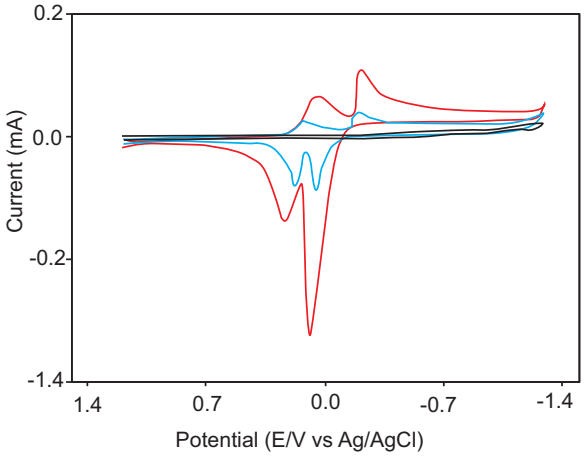

Fig. 4. CVs 1mM $CuCl_2$, 1mM $[Cu(C_6H_6N_2O)_2]Cl_2$ and 1mM niacinamide in 0.1M KCl at 100 mV/s.

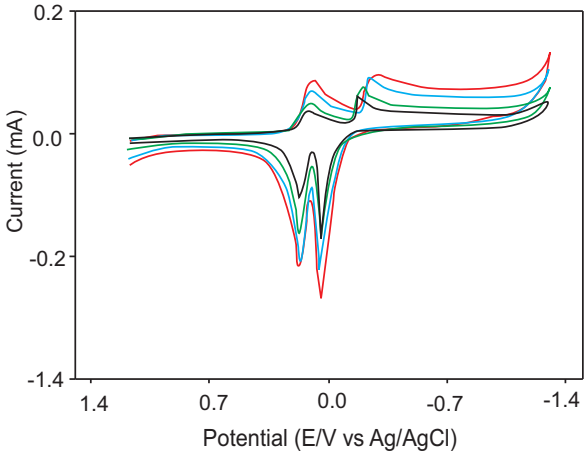

Fig. 5. CVs of 1mM $[Cu(C_6H_6N_2O)_2]Cl_2$ in 0.1M KCl at 300, 200, 100 and 50 mV/s.

Table 5. Current- Potential data, peak potential separation, peak current ratio of the voltammogram of 1 mM $[Cu(C_6H_6N_2O)_2]Cl_2$ in 0.1 M KCl at different scan rates

v Vs^{-1}	$v^{1/2}$ Vs^{-1}	E_{pc1} Volt (+)	E_{pc2} Volt (-)	E_{pa1} Volt (+)	E_{pa2} Volt (+)	i_{pc1} mA (+)	i_{pc2} mA (+)	i_{pa1} mA (-)	i_{pa2} mA (-)	ΔE_p Volt	i_{pa1}/i_{pc1}
0.05	0.2236	0.1218	0.1693	0.1742	0.0502	0.0187	0.0341	0.054	0.075	0.0475	2.8877
0.10	0.3162	0.1218	0.1884	0.1742	0.0550	0.0251	0.0393	0.081	0.089	0.0666	3.2271
0.20	0.4472	0.1074	0.2361	0.1742	0.0597	0.0363	0.0457	0.105	0.113	0.1287	2.8926
0.30	0.5477	0.0979	0.2838	0.1742	0.0597	0.0441	0.0504	0.109	0.133	0.1859	2.4716

v = scan rate; $v^{1/2}$ = SQRT of scan rate; E_{pc1} = cathodic peak potential for 1st peak; E_{pc2} = cathodic peak potential for 2nd peak, E_{pa1} = anodic peak potential for 1st peak; E_{pa2} = anodic peak potential for 2nd peak; i_{pc1} = cathodic peak current for 1st peak, i_{pc2} = cathodic peak current for 2nd peak; i_{pa1} = anodic peak current for 1st peak; i_{pa2} = anodic peak current for 2nd peak, ΔE_{p1} = peak potential separation for 1st pair of peak; i_{pa1}/i_{pc1} = peak current ratio for 1st pair of peak

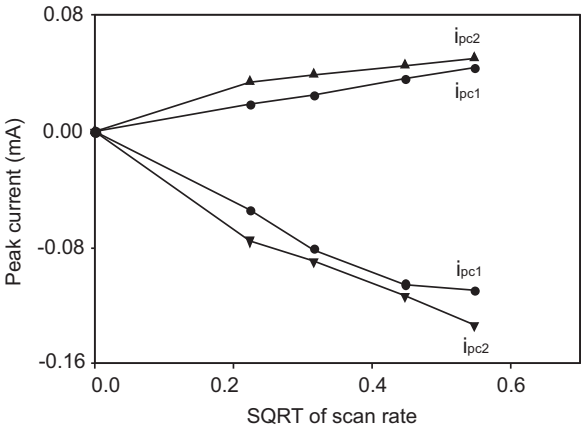

Fig. 6. Variation of peak current with SQRT of scan rate.

The shifting of the peaks in the complex compared to that of free metal confirmed the complexation of Cu(II) with niacinamide. The peak potential separation increases with scan rate due to slow electron transfer kinetics or ohmic potential (iR) drop. The linear increase of peak current with SQRT of scan rate revealed that the electrode process is diffusion controlled. The values of peak current ratio indicate that the process is quasi reversible (Akhtar *et al.,* 2008; Shaikh *et al.*, 2006; Wang 2006; Bard and Faulkner 2001; Brett and Brett, 1993).

Redox behaviour of the complexes $[Mn(C_6H_6N_2O)_2]Cl_2$and $[Zn(C_6H_6N_2O)_2]Cl_2$ were also studied. The Mn-complex showed two pair of redox signals. The probable electron transfer processes are:

$$\text{Cathodic: } Mn(IV) \xrightarrow{+e^-} Mn(III) \xrightarrow{+e^-} Mn(II)$$
$$\text{Anodic: } Mn(II) \xrightarrow{-e^-} Mn(III) \xrightarrow{-e^-} Mn(IV)$$

The CV of $[Zn(C_6H_6N_2O)_2]Cl_2$ showed one pair of redox signals. The probable electron transfer processes are:

$$\text{Cathodic: } Zn(II) \xrightarrow{+2e^-} Zn(0)$$
$$\text{Anodic: } Zn(0) \xrightarrow{-2e^-} Zn(II)$$

The Mn and Zn complexes behaved almost similarly to that of the Cu-complex. In both the cases the electron transfer processes were diffusion controlled and quasi reversible.

Conclusion

(i) Niacinamide forms coordination complexes with Mn(II), Co(II), Ni(II), Cu(II) and Zn(II) in 2:1 ratio.
(ii) Weight losing pattern of all the complexes are similar indicating similar structure of the complexes.
(iii) All except Zn(II) produces paramagnetic complexes with the ligand.
(iv) The redox properties of the metal ions changes appreciably on complexation with niacinamide

Acknowledgement

The authors would like to acknowledge the support from Prof. Shinmyozu of the Laboratory of Organic Structural Chemistry, Department of Molecular Chemistry, Graduate School of Sciences & IMCE, Kyushu University, Japan, for supplying the elemental analysis data of the samples.

References

Akhtar, H.M.N., Shaikh, A.A., Ehsan, M.Q. 2008. Cyclic voltammetric study of the redox behavior of Fe(II)/Fe(III) systems forming during the oxidation of Fe(II) complexes with saccharin and 1,10- phenanthroline. *Russian Journal of Electrochemistry,* **44:** 1403-1408.

Banwell, C.N., McCash, E.M. 1995. *Fundamentals of Molecular Spectroscopy*, pp. 84-88, 189-192, 4th edition, McGraw-Hill International Limited, UK.

Bard, A.J., Faulkner, L.R. 2001. *Electrochemical Methods Fundamentals and Applications,* pp. 228-255, 2nd edition, John Wiley & sons, Inc., New York, USA.

Bender, D.A. 2003. *Nutritional Biochemistry of the Vitamins*, 512 pp., 2nd edition, Cambridge University Press, UK.

Brett, C.M.A., Brett, A.M.O. 1993. *Electrochemistry Principles, Methods and Applications,* pp. 174-191, Oxford University Press, New York, USA.

Ehsan, M.Q., Begum, S.M., Islam, S.M.S. 2004. Preparation and characterization of pyridoxine complexes of Fe(III), Mo(VI), Cd(II), Hg(II) and U(VI). *Journal Saudi Chemical Society,* **8:** 251-256.

Ehsan, M.Q., Khatun, S., Quyser, M.A. 2001. Preparation and characterisation of pyridoxine complexes of Mn(II), Co(II), Ni(II), Cu(II) and Zn(II). *Journal Saudi Chemical Society,* **5:** 59-65.

Haider, S.Z., Malik, K.M.A., Khan, M.S., Bakshi, P.K., Bhuiyan, A.A., Hursthouse, M.B. 1988. Preparation, characterization and properties of some metal-thiamine compounds of general formula ($C1_2H_{17}N_4OS)MCl_3$. 0.5 H_2O [M = Co(II), Zn(II) and Cd(II). *Journal of Bangladesh Academy of Sciences,* **12:** 197-206.

Haider, S.Z., Malik, K.M.A., Bakshi, P.K., Bhuiyan, A.A., Khan, M.S., Hursthouse, M.B. 1987. Preparation, characterization and properties of the metal-thiamine compounds $(C_{12}H_{18}N_4OS)CuCl_4$ and $(C_{12}H_{18}N_4OS)MCl_4$. H_2O [M = Co(II), Zn(II), Cd(II) and Hg(II)]. *Journal of Bangladesh Academy of Sciences,* **11:** 117-127.

Mamun, M.A., Ahmed, O., Bakshi, P.K., Yamauchi, S., Ehsan, M.Q. 2011. Synthesis and characterization of some metal complexes of cystine: $[Mn(C_6H_{10}N_2O_4S_2)]$; where M = Mn(II), Co(II), Ni(II), Cu(II), Zn(II), Cd(II), Hg(II) and Pb(II). *Russian Journal of Inorganic Chemistry,* **56:** 1972-1980.

Pavia, D.L., Lampman, G.M., Kriz, G.S. 2001. *Introduction to Spectroscopy,* pp. 26, 28, 357-386, 3rd edition, Harcourt College Publisher, Fort Worth, New York, USA.

Rahman, K.L., Mamun, M.A., Ehsan, M.Q. 2011. Preparation of metal Niacin complexes and characterization using spectroscopic and electrochemical techniques. *Russian Journal of Inorganic Chemistry,* **56:** 1436-1442.

Shaikh, A., Begum, M., Khan, A.H., Ehsan, M.Q. 2006. Cyclic voltammetric studies of the redox behavior of iron(III)-vitamin B6 complex at carbon paste electrode. *Russian Journal of Electrochemistry*, **42:** 620-625.

Silverstein, R.M., Webster, F.X., Kiemle, D.J. 2005. *Spectrometric Identification of Organic Compounds,* pp. 75-108, 7th edition, John Wiley & Sons, Inc., New York, USA.

Wang, J. 2006. *Analytical Electrochemistry,* pp. 29-40, 3rd edition, John Wiley & Sons, Inc., New York, USA.

Pak. j. sci. ind. res. Ser. A: phys. sci. 2015 **58** (2) 66-73

Electroless and Electrodeposition of Silver from a Choline Chloride-Based Ionic Liquid

Muhammad Rostom Ali[a]*, Muhammad Ziaur Rahman[a] and Siddhartha Sankar Saha[b]

[a]Department of Applied Chemistry and Chemical Engineering, University of Rajshahi, Rajshahi-6205, Bangladesh

[b]Department of Chemistry, Rajshahi University of Engineering and Technology, Rajshahi-6204, Bangladesh

(received June 26, 2013; revised March 24, 2013; accepted May 20, 2014)

Abstract. The electroless and electrolytic deposition of silver from a solution containing silver nitrate in either an ethylene glycol (EG)-choline chloride based or a urea-choline chloride based ionic liquids has been carried out onto steel and copper cathodes by simple immersion, constant current and constant potential methods at room temperature. It has been found that electroless silver deposits of up to several microns have been obtained by dip coating from both urea and EG based ionic liquids without the use of catalysts. The influences of various experimental conditions on electrodeposition and morphology of the deposited layers have been investigated by scanning electron microscopy (SEM) and X-ray diffraction (XRD). It has been observed that crack free bright metallic coloured silver coatings can be obtained from both EG and urea based ionic liquids at the applied deposition potentials up to -0.40 V and applied deposition current densities up to -5.0 A m^{-2} at room temperature. The cathodic current efficiency for the deposition of Ag is about 99%.

Keywords: cyclic voltammetry, electrodeposition, electroless deposition, ethaline, reline, silver

Introduction

The electroless and electrodeposition of silver metal onto copper substrate is an important industrial process that is used primarily by the manufactures of printed circuit boards to prevent degradation of exposed copper surfaces (conduction tracks) during the time that elapses between the manufacture of the circuit board and the assembly procedure incorporating the board or component into a finished device. Typically this can be up to several months. This method of protection for copper surfaces is very effective despite the fact that silver is thermodynamically much more susceptible to aerobic oxidation. This is because silver oxide and sulphide (formed as tarnish on silver surfaces), as well as the underlying silver metal, are very soluble in the tin- and tin/lead-based molten solder that are used to bond the circuit components to the copper tracks of the circuit board.

On the contrary, copper oxides are poorly soluble in the molten solder such that, aerobic oxidation of the copper surface prior to soldering inhibits interfacial wetting at the copper/solder interface and prevents bonding of the component. In a practical device, this results in failure of the joint either through poor conductivity or because of low mechanical stress tolerance. Solder fluxes are often used to mitigate this problem by preventing aerobic oxidation of copper surfaces, but this approach is not always successful or practical. Commercial electroless silver processes typically use an aqueous $AgNO_3$ solution in the presence of HNO_3. In addition to the social and environmental concerns that surround the use of strong inorganic acids, here the use of HNO_3, whilst necessary to the process, has an additional detrimental effect because there is competitive etching of the copper tracks during silver plating. This can be a serious problem for the electronics industry, particularly as integration densities continue to increase and consequently feature sizes become smaller. Many component failures arise because of copper etching (by the HNO_3) before the surfaces are silver plated. In addition, the aqueous process requires the use of colloidal catalyst (usually palladium metal) to sustain silver plating from beyond a few nanometers up to 1-5 μm in thickness (Djokic *et al*., 2002; Shipley, 1961).

Sun *et al*. (2003) and Endres (2002) reported that, recently ionic liquids have received a great deal of attention in the literature as alternative solvents and electrolytes for a number of electrochemical processes. These processes range in scope from fundamental academic investigations, for example, into the structure of the solid/liquid interfaces (Ohno, 2005), or into the mechanisms of ion diffusion, to industrial processes where, the ionic liquid has the potential to replace conventional noxious aqueous media (Abbott

*Author for correspondence; E-mail: dmrali@yahoo.com

et al., 2004a). A relatively new class of ionic liquid based on eutectic mixtures of choline chloride with a hydrogen bond donor species has been reported by Abbott and Mckenzie (2006) and Abbott *et al.* (2004b; 2003). Abbott *et al*. (2006a; 2006b) also reported that, these liquids can be used for deposition of a range of metal coatings including Zn, Cr, Sn, Cu, and Ag at high current efficiency and also for metal dissolution processes such as electropolishing. In many cases, the use of ionic liquids as solvents overcomes the need for strong inorganic acids (e.g., chromic acid, HF, H_3PO_4, H_2SO_4) and highly toxic salts (e.g., cyanide). The aim of the present work is to develop a coating of silver on copper substrate by electroless and electrolytic deposition methods from ionic liquids based on choline chloride and hydrogen bond donors such as ethylene glycol (EG) or urea.

Materials and Methods

Chemicals. Choline chloride [$HOC_2H_4N(CH_3)_3Cl$] (ChCl) (Aldrich 99%) which was recrystallised from absolute ethanol, filtered and dried under vacuum. Urea (Aldrich >99%) was dried under vacuum prior to use. Ethylene glycol (EG) (Aldrich >99%), silver nitrate ($AgNO_3$) (Merck 99.8%), and all other chemicals were used as received.

Preparation of ionic liquid. The eutectic mixtures were formed by stirring the two components together, in the stated proportions, at 75 °C until a homogeneous, colourless liquid formed. The molar ratio for the eutectic compositions was found to be 1:2 for choline chloride (ChCl) with ethylene glycol (EG) or urea. The ionic liquids, once formulated, were kept in a thermostatic oven at 30 °C prior to use.

Electrochemical and analytical study. Electrochemical investigations including potential step chronoamperometry, chronopotentiometry and cyclic voltammetry were carried out using a Hokudo Denko HAB151 Potentiostat/Galvanostat, Tokyo, Japan, equipped with a potential sweeper. Data were recorded in a computer through data acquisition system (USA) using WinDaq software. A three-electrode system consisting of a platinum ($50\times5\times0.1$ mm^3) working electrode, a silver ($50\times10\times0.2$ mm^3) counter electrode and a silver wire quasi-reference electrode were used in all electro-chemical studies. The working electrode was cleaned electrochemically in 1.5 mol/dm^3 H_2SO_4 1.0 mol/dm^3 H_3PO_4 mixtures then rinsed with deionised water, and finally dried with acetone prior to use in all measurements. All voltammograms were obtained at 30 °C with various scan rates ranging from 5 to 100 mV/s. A silver wire (immersed in ethaline/reline) quasi-reference electrode was used in all electrochemical experiments which have been shown to have stable reference potential in chloride based eutectics. All potentials in this work are quoted with respect to Ag/1:2 ChCl-EG/urea reference electrode (which will be written as Ag/Ag(I) (note that the reference potential will be changed slightly with melts of different compositions).

Deposition of silver. The electroless plating of silver were carried out in a glass beaker containing 15 cm^3 ionic liquids at room temperature (typically 25~30 °C) onto copper ($50 \times 10 \times 0.2$ mm^3) or mild steel ($50 \times 10 \times 0.2$ mm^3) substrates. Prior to deposition experiments, copper and steel substrates were mechanically polished to mirror finish by 600, 1000 and 2000 grit sandpaper. After polishing, the specimens were ultrasonically cleaned in deionised water, and finally dried with acetone. The substrates were then immediately immersed in ChCl:2EG (ethaline) and ChCl:2Urea (reline) ionic liquids containing $AgNO_3$ (0.01~0.10 mol/dm^3) at different time periods (1~5 min). The electrolytic deposition of silver were carried out onto copper and steel cathodes under constant current and constant potential methods from ionic liquids (ethaline/reline) containing $AgNO_3$ at room temperature. Following each deposition, the resulting deposit was soaked firstly in ethanol, then in deionised water, and finally washed with acetone to remove the residual ionic liquids. The deposit was then dried with cold air.

Deposit characterisation. The surface morphologies of the samples were then examined with scanning electron microscope (XL 30 SEM, PHILIPS) and its auxiliary X-ray energy dispersive spectroscope (EDX). X-ray diffraction analysis was also performed with a Philips PW 1716 diffractometer using CuK_α radiation (40 kV, 25 mA) to explore the crystal structure of the deposits.

Results and Discussion

Cyclic voltammetry of Ag(I) in ChCl:2EG (ethaline) and ChCl:2urea (reline) ionic liquids. The cyclic voltammograms recorded on a platinum electrode in 1:2:0.05 (mole ratio) ChCl:EG:$AgNO_3$ (a) and Ch Cl: urea:$AgNO_3$ (b) ionic liquids at 30 °C with a scan rate of 10 mV/s are shown in Fig. 1. The rest potentials are + 0.44 V in ethaline and +0.22 V in reline. The scan towards negative direction consists of first reduction waves C_1 in Fig. 1a and C'_1 in Fig.1 b with the currents starting to increase at -0.03 V (C_1) and + 0.013 V (C'_1). Additional reduction waves C_2 in Fig. 1a and C'_3 in Fig. 1b are observed with the currents increase starting

again at -1.10 V and -1.00 V, respectively. The reverse scan consists of first oxidation peaks P_{a1} in Fig. 1a (+ 0.11 V) and p'_{a1} in Fig. 1b (+ 0.146 V). Additional oxidation waves are also observed with the currents starting to increase at +1.02 V for ethaline and + 0.90 V for reline. From XRD and EDX analyses, pure silver has been detected in the deposit obtained at a deposition potential of -0.12 V (from the first reduction waves C_1 and C'_1) by constant potential method. Therefore, the increases of the negative currents in the first reduction waves C_1 and C'_1 are obviously associated with the reductions of silver ions to metallic state according to the following reaction.

$$Ag^{+}_{(ad)} + e^{-} \rightarrow Ag \qquad (1)$$

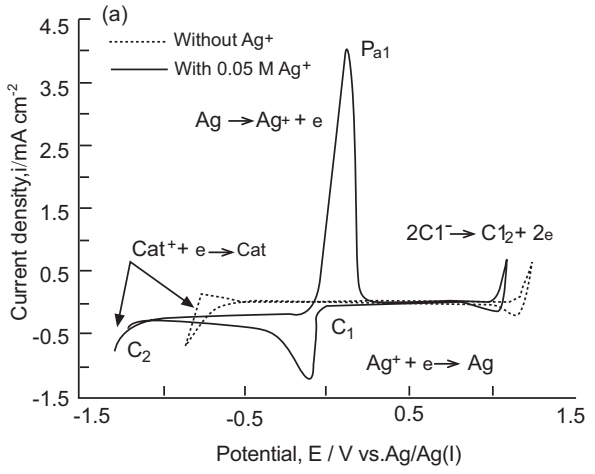

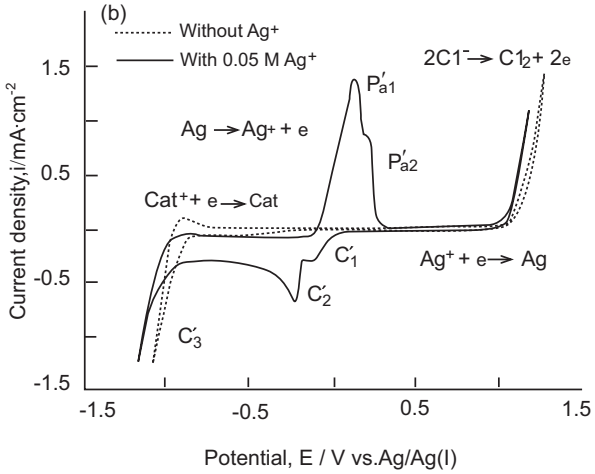

Fig. 1. Cyclic voltammograms recorded on a platinum electrode in ChCl:2EG (a) and ChCl:2urea (b) ionic liquids containing 0.05 M $AgNO_3$ at 30 °C with a scan rate of 10 mV/s.

Compared with the voltammograms obtained in the absence of $AgNO_3$, dotted curves in Fig.1a and Fig.1b, the reduction waves appeared at -0.72 V in ethaline and -0.90 V in reline correspond to the reduction of cationic species (Cat^+) into these ionic liquids, while the oxidation waves appeared at +1.2 V in ethaline and +1.0 V in reline correspond to the oxidation of chloride ions (anions) to molecular/gaseous chlorine according to following reaction.

$$2Cl^{-}_{(ad)} \rightarrow Cl_2 \uparrow + 2e^{-} \qquad (2)$$

Figure 2 shows the effect of sweeping potentials on the cyclic voltammograms recorded on a platinum electrode in 1:2:0.05 (mole ratio) ChCl:urea:$AgNO_3$ ionic liquids at 30 °C with a scan rate of 10 mV/s. It is readily seen from the voltammograms that the first reduction wave C'_1 corresponds to the second oxidation peak P'_{a2} and the second reduction wave C'_2 corresponds to the first oxidation peak P'_{a1}. Pure silver has also been detected in the deposit obtained at a deposition potential of -0.12 V and -0.22 V (from the first C'_1 and second reduction waves C'_2) by constant potential method. Therefore, the increases of the negative currents in the first and second reduction waves (C'_1 and C'_2) are also associated with the reductions of silver ions to metallic state.

It can be seen from the voltammograms that more cathodic limits lead to increasing charge for more anodic dissolution process. The two reduction waves and two oxidation peaks could be due to the deposition of silver with different

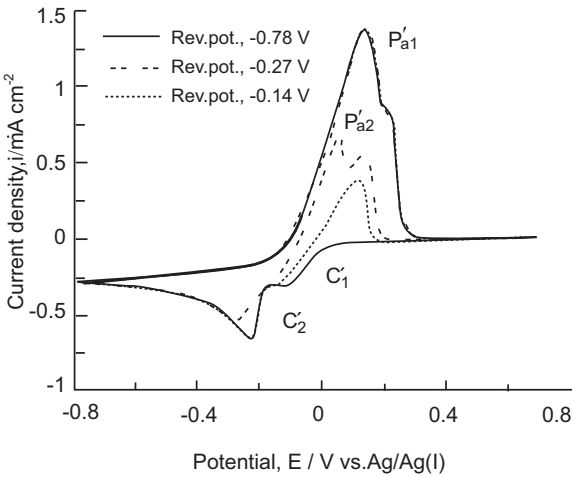

Fig. 2. Effect of sweeping potentials on the cyclic voltammograms recorded on a platinum electrode in ChCl:2urea ionic liquids containing 0.05 M $AgNO_3$ at 30 °C with a scan rate of 10 mV/s.

morphologies (Fig. 2). The two different morphologies must result from different growth mechanisms. One possibility could be the initial growth of a large number of nuclei on the surface where some of which stop growing giving a material with a different morphology. Alternatively, some aspect of the interfacial layer structure could neutralise the surface energy of the growing particle. Similar morphology had been reported by Abbott *et al*. (2010) for the deposition of aluminium from chloroaluminate based ionic liquids.

Figure 3 shows the effect of $AgNO_3$ concentrations on the cyclic voltammograms recorded on a platinum electrode in ChCl:2EG (a) and ChCl:2urea (b) ionic liquids at 30 °C with a scan rate of 10 mV/s. It is readily seen from the voltammograms that, the magnitudes of the current densities of first reduction waves C_1 and C'_1, which are attributed to the reductions of silver ions to metallic silver, increase with the increase of the $AgNO_3$ concentration added into the ionic liquids. The same phenomena are observed with the first oxidation peaks P'_{a1} (Fig. 3a) and P'_{a1} (Fig. 3b), which also shows the increase in current densities with the increase of $AgNO_3$ concentrations. As the magnitudes of the reduction current densities of silver (C_1 and C'_1) increase; the magnitudes of the oxidation peak current densities (P_{a1} and P'_{a1}) also increase, therefore, it is concluded that the first oxidation peaks P_{a1} and P'_{a1} are attributed to the dissolution of the deposited silver into this ionic liquid.

The effect of scan rates on the cyclic voltammograms recorded on a platinum electrode in ChCl: 2EG: 0.05 $AgNO_3$ (a) and ChCl:2urea:0.05$AgNO_3$ (b) ionic liquids at 30 °C are presented in Fig. 4. For a reversible system, peak potential

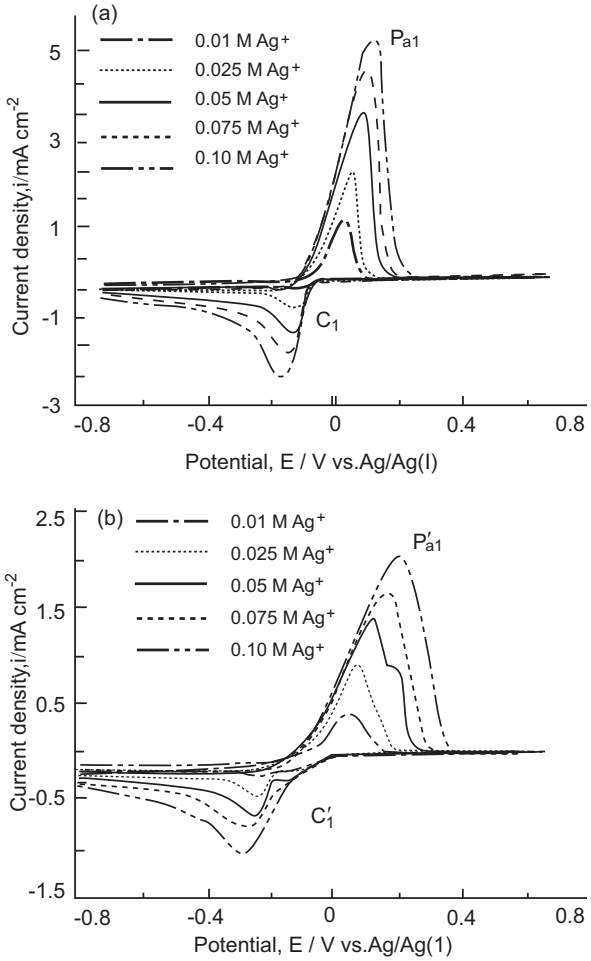

Fig. 3. Effect of $AgNO_3$ concentrations on the cyclic voltammograms recorded on a platinum electrode in ChCl:2EG (a) and ChCl:2urea (b) ionic liquids at 30 °C with a scan rate of 10 mV/s.

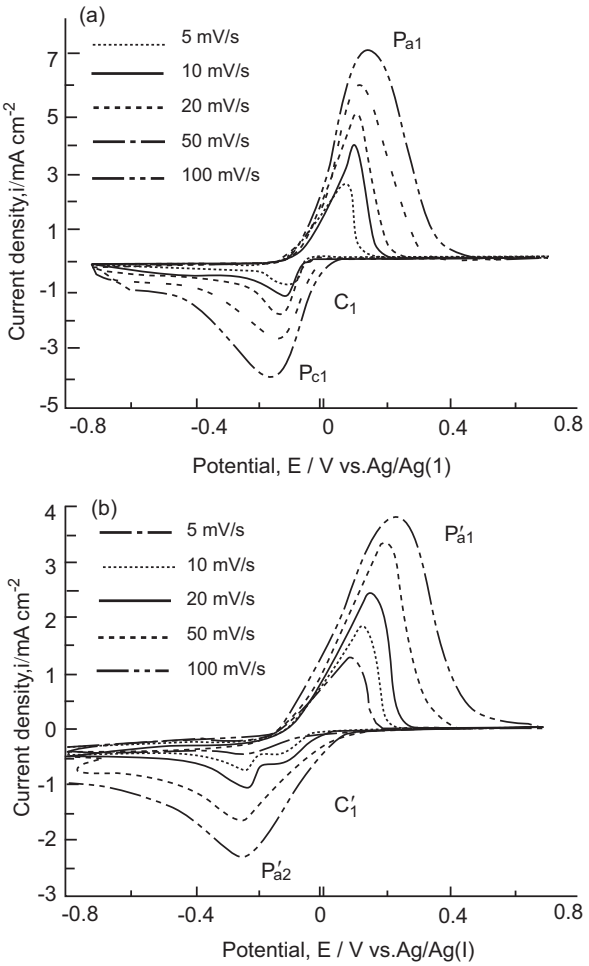

Fig. 4. Effect of scan rates on the cyclic voltammograms recorded on a platinum electrode in ChCl:2EG (a) and ChCl:2urea (b) ionic liquids containing 0.05 M $AgNO_3$ at 30 °C.

E_p is independent of the scan rate (ν), and the peak current density (i_p) is proportional to the square root of scan rate ($\nu^{1/2}$). In the present study (Fig. 4a), the cathodic peak potentials ($E_{p/c}$) are -0.135, -0.14, -0.141, -0.142 and -0.145 V for 5, 10, 20, 50 and 100 mV/s scan rates and the anodic peak potentials ($E_{p/c}$) are 0.095, 0.098, 0.10, 0.105 and 0.115 V for 5, 10, 20, 50 and 100 mV/s scan rates, respectively. In Fig. 4b, the cathodic peak potentials ($E_{p/c}$) are -0.223, -0.224, -0.225, -0.23 and -0.24 V for 5, 10, 20, 50 and 100 mV/s scan rates and the anodic peak potentials ($E_{p/a}$) are 0.13, 0.14, 0.15, 0.20 and 0.22 V for 5, 10, 20, 50 and 100 mV/s scan rates, respectively. It is evident from these results that the peak potentials for the reduction and oxidation waves of silver are almost independent of the scan rates indicating the systems are reversible in nature. Variations in peak current densities of C_1 and C'_1 with the square root of scan rate (i_p vs. $\nu^{1/2}$) are shown in Fig. 5. For a reversible system, the relationship between the cathodic peak current density i_p and the square root of the scan rate $V^{1/2}$ is given by Baird and Faulkner (1980):

$$i_p = (2.69\times10^5)\, n3^{/2}.A.D_{Ag(I)}{}^{1/2}.C_{Ag(I)*}.V^{1/2} \quad (3)$$

where:

$C_{Ag(I)*}$ = the concentration of silver ions in the bulk solution, D = the diffusion coefficient of silver ions, A = the surface area of the electrode, n = the number of electron transferred during reduction reaction and V the scan rate. The linear increases in the peak current densities of C_1 and C'_1 with the square root of scan rate, as shown in Fig. 5, indicate that the reduction processes of silver ions in both ChCl:2EG and ChCl:2urea based ionic liquids are controlled by diffusion.

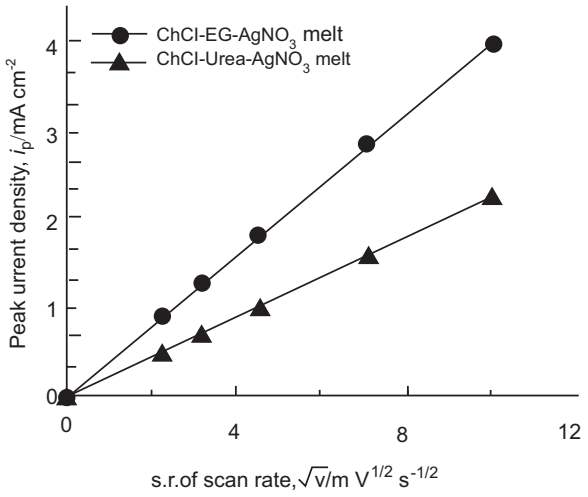

Fig. 5. Variations in cathodic peak current densities with the square root of scan rate for the reduction of silver ions in ethaline (a) and reline (b) containing 0.05 M $AgNO_3$.

Electroless deposition of silver from ethaline and reline. The camera images of electroless deposited silver layer obtained from both ethaline and reline based ionic liquids at different immersion time and different $AgNO_3$ concentrations are shown in Fig. 6. The deposits are smooth, shiny, and good adherence. The deposits are not peeling off by hand scratching. The scanning electron micrographs of silver electroless deposits obtained from 1:2:0.05 (mole ratio) ChCl:EG:$AgNO_3$ and ChCl: urea: $AgNO_3$ at 30 °C are shown in Fig. 7. The SEM images show that the surfaces are free from crack. Fig. 8a and 8b show the EDX profile for the SEM images of Figs 7a and 7b, respectively. Pure silver has been detected in the deposited layer by EDX analysis. There is no spectrum for residual chloride ions in the EDX profile indicate no incorporation of the ionic liquid in the deposits. Therefore, it is concluded that eutectic based ionic liquids of ChCl:2EG (ethaline) and ChCl:2urea (reline) can be used for the electroless deposition of bright metallic colour silver on a metallic substrate.

Electrodeposition of silver from ethaline and reline. Silver electrodeposition experiments have been carried out on steel and copper cathodes under constant potential and constant current methods from both EG and urea based ionic liquids at room temperature. All of the electrodeposits obtained on Pt and Cu substrates at the applied deposition potentials ranging from -0.20 to -0.40 V and the applied deposition current densities ranging from -1.0 to -5.0 A/m^2 appear to be smooth and silver metallic colour. There is no apparent rupture on the deposit surface and the deposits do not peeling off by hand scratching. However, the

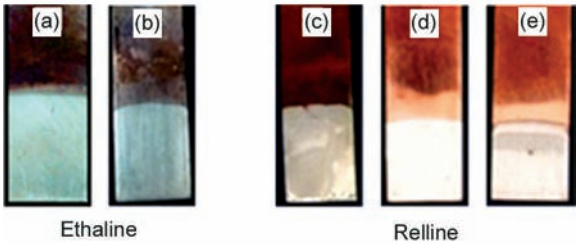

Fig. 6. Camera images of silver electroless deposits on copper substrates obtained from ethaline (a, b) and reline (c, d, e) containing 0.10 M $AgNO_3$ at 30 °C. Immersion time: a, b, c, 4 min; d, 2 min and e, 1 min.

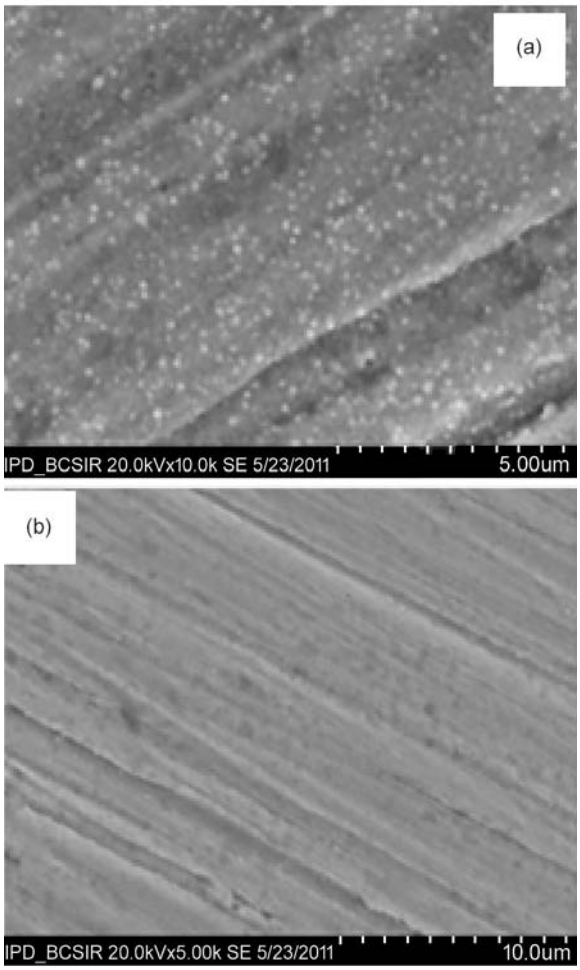

Fig. 7. SEM images of silver electroless deposits on Cu substrates obtained from mole ratios of 1:2:0.05 in ChCl:EG:$AgNO_3$ (a) and ChCl:urea:$AgNO_3$ (b) ionic liquids at 30 °C. Immersion time: (a) 3 min and (b) 5 min.

deposits obtained at the applied deposition potential of -0.60 V are not smooth due to high deposition over potential. The SEM images of the electrodeposited silver layer on copper cathodes under constant potential method from both EG and urea based ionic liquids are shown in Fig. 9. The electrodeposited crystals are angular and also nodular in shape and in the order of 1~3 μm in size. From SEM images it is clear that the crystal sizes in the electrodeposited thin films are bigger than the electroless deposited thin films. However, it is difficult to get thick coating in electroless method. The thickness of the deposited layers is approximately 4~6 μm, which has been controlled by adjusting the total charge applied.

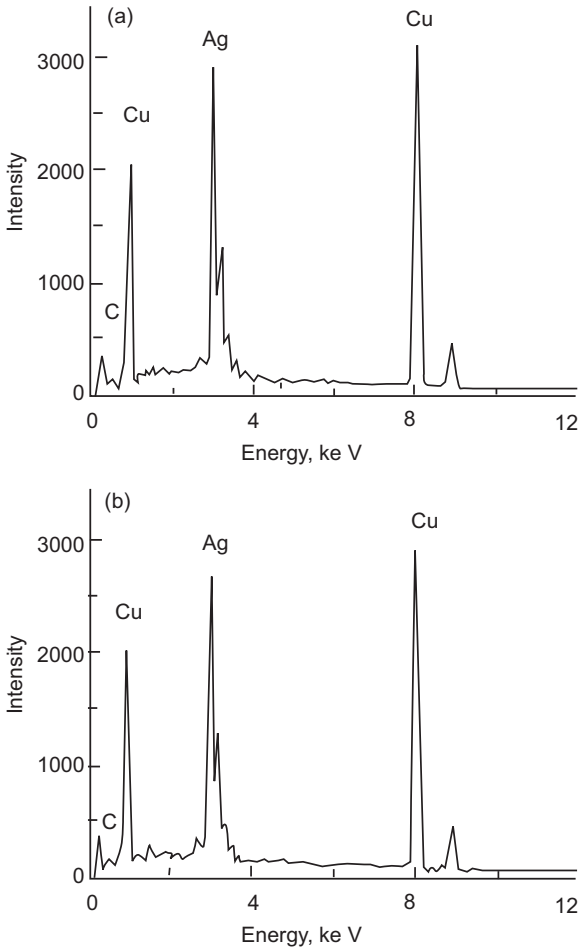

Fig. 8. EDX profile for the SEM images of Figs 7(a) and 7(b).

The acquired diffraction patterns for the deposits obtained from mole ratios of 1:2:0.05 in ChCl:urea:$AgNO_3$ ionic liquids at applied deposition potential of -0.25 V is shown in Fig. 10. The diffraction peaks at 2θ = 38.1°, 44.3°, 64.4°, and 77.4° are for Ag (111), Ag (200), Ag (220) and Ag (311), respectively. The diffraction peaks are very sharp, indicating the deposit has the crystalline structure. The current efficiency for the deposition of pure silver is about 99%. However, additional diffraction peaks at 2θ = 43.3°, 50.45°, and 74.1° corresponding to copper (substrate) are also observed in Fig. 10.

Conclusion

This work shows that the ionic liquids based on eutectic mixtures of choline chloride and hydrogen bond donors such as ethylene glycol or urea can be used as electrochemical solvents. Crack free smooth and bright metallic coloured silver can be electroless and electrolytic deposited onto steel and copper cathodes from ethaline and reline

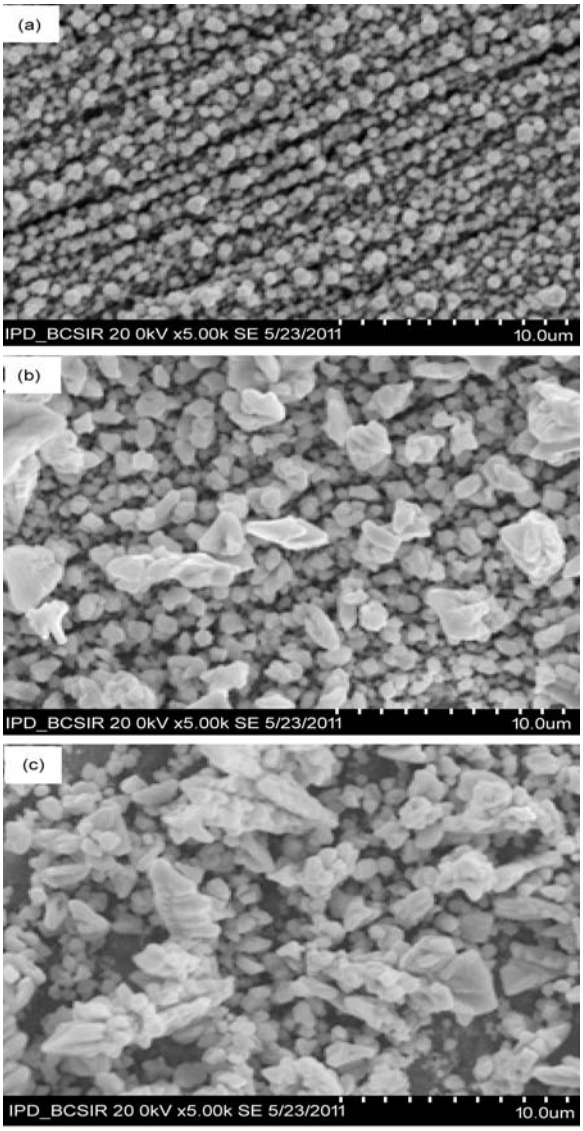

Fig. 9. SEM images of silver electroless deposits on Cu cathodes obtained from ethaline (a, c) and reline (b) ionic liquids containing 0.05 M $AgNO_3$ at 30 °C. Applied deposition potential: (a) -0.20 V, (b) -0.25 V and (c) -0.30 V.

based ionic liquids containing $AgNO_3$ at room temperature. The silver electrodeposits obtained at the applied deposition potentials up to -0.40 V and applied deposition current densities up to -5.0 A/m^2 are smooth and bright metallic colour.

Acknowledgement

The authors gratefully acknowledge the Ministry of Science and Technology, Government of the People's Republic of Bangladesh for financial support to carry out this work. Part of the study has been presented at the 6th Japan-China joint seminar on Marine Corrosion and Control, held at Tokyo Institute of Technology, Tokyo, Japan on 2nd March, 2012.

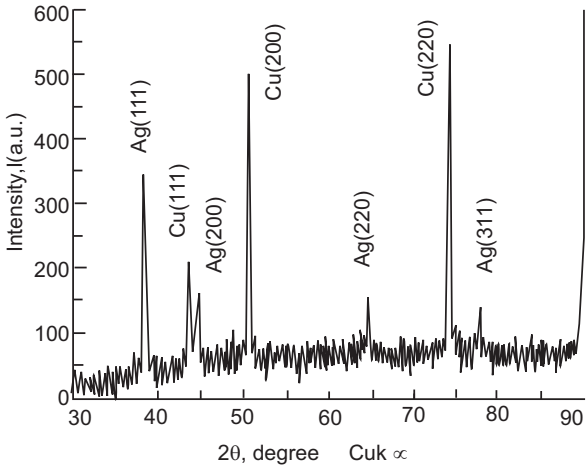

Fig. 10. X-ray diffraction pattern of silver electrodeposit obtained on copper from mole ratios of 1:2: 0.05 in ChCl: urea: $AgNO_3$ ionic liquid at 30 °C and -0.25 V.

References

Abbott, A.P., Fulian, Q., Abood, H.M.A., Ali, M.R., Ryder, K.S. 2010. Double layer, diluent and anode effects upon the electrodeposition of aluminium from chloroaluminate based ionic liquids. *Physical Chemistry Chemical Physics,* **12:** 1862-1872.

Abbott, A.P., McKenzie, K.J. 2006. Application of ionic liquids to the electrodeposition of metals. *Physical Chemistry Chemical Physics,* **8:** 4265-4279.

Abbott, A.P., Capper, G., McKenzie, K.J., Glidle, A., Ryder, K.S. 2006a. Electropolishing of stainless steels in a choline chloride based ionic liquid: an electrochemical study with surface characterisation using SEM and atomic force microscopy. *Physical Chemistry Chemical Physics,* **8:** 4214-4221.

Abbott, A.P., Capper, G., McKenzie, K.J., Ryder, K.S. 2006b. Voltammetric and impedance studies of the electropolishing of type 316 stainless steel in choline chloride based ionic liquid. *Electrochimica Acta,* **51:** 4420-4425.

Abbott, A.P., Capper, G., Davies, D.L., Rasheed, R.K. 2004a. Ionic liquid analogues formed from hydrated metal salts. *Chemistry,* **10:** 3769-3774.

Abbott, A.P., Boothby, D., Capper, G., Davies, D.L.,

Rasheed, R.K. 2004b. Deep eutectic solvents formed between choline chloride and carboxylic acids: Versatile alternatives to ionic liquids. *Journal of American Chemical Society,* **126:** 9142-9147.

Abbott, A.P., Capper, G., Davies, D.L., Rasheed, R.K., Tambyrajah,V. 2003. Novel solvent properties of choline chloride/urea mixtures. *Chemical Communications,* **7:** 70-71.

Baird, A.J., Faulkner, L.R. 1980. *Electrochemical Methods: Fundamentals and Applications,* 218 pp., John Wiley & Sons, New York, USA.

Djokic, S.S. 2002. Electroless deposition of metals and alloys. In: *Modern Aspects of Electrochemistry,* B.E. Conway and R.E. White (eds.), vol. **1,** pp. 51-133, Springer, USA.

Endres, F. 2002. Ionic liquids: Solvents for the electrodeposition of metals and semiconductors. *Chemphyschem: A European Journal of Chemical Physics and Physical Chemistry,* **3:** 145-154.

Ohno, H. (ed.). 2005. *Electrochemical Aspects of Ionic Liquids,* 408 pp., John Wiley & Sons, New York, USA.

Shipley, C.R. 1961. US Patent 3, 011, 920.

Sun, J., MacFarlane, D.R., Forsyth, M. 2003. A new family of ionic liquids based on the 1-alkyl-2-methyl pyrrolinium cation. *Electrochimica Acta,* **48:** 1707-1711.

Pak. j. sci. ind. res. Ser. A: phys. sci. 2015 **58** (2) 74-78

An Assessment of Cleaning Amenability of Salt Range Coal Through Physical Cleaning Methods

Muhammad Shahzad*, Syed Muhammad Tariq, Mansoor Iqbal, Syed Mahmood Arshad and Shahab Saqib

Mining Engineering Department, University of Engineering & Technology, Lahore, Pakistan

(received November 12, 2013; revised May 13, 2014; accepted July 1, 2014)

Abstract. Representative coal samples from the eastern salt range (Modern Engineering and Kishor coal mines, Pakistan) and the central salt range (Punjmin coal mine, Pakistan) were collected and examined for their chemical composition. The chemical characteristics indicate that the salt range coal belongs to sub-bituminous category. Washability analysis on selected coal samples (6.70 × 0.212 mm) using zinc chloride solution with a specific gravity from 1.3 to 1.7 were executed. The results classify the central salt range coal as easily washable while, the Eastern salt range coal as moderately difficult to wash. Jigging, shaking table and spiral techniques were applied to check the cleaning amenability of the salt range coal through these techniques. Among these techniques, shaking table revealed the most promising results for all the three coals. Punjmin coal showed the maximum rejection of ash of 55% and that of total sulphur of 74% with a recovery of 46%.

Keywords: coal washability, physical processing, gravity concentration, salt range coal, coal cleaning

Introduction

Coal is black or dark black combustible rock that contains carbon, hydrogen, oxygen and smaller amounts of sulphur, nitrogen and other trace elements in chemical combination. It is the single largest source of energy for the world economy (Sanders *et al.,* 2002). Coal not only plays an important role in fulfilling the energy requirements of the world, but is also traded in huge volumes for use as a fuel in cement industry and many other industries like fertilizer, glass and ceramic, sugar and brick firing etc. It is also used as a source of domestic heating and as a source of production of coke which is extensively utilised as reducing agent in metallurgical processes (Nawaz *et al.,* 2009).

Chemical properties and heating value of coal have prime importance in the end use of coal. High ash and sulphur contents in coal create problems in terms of slagging and fouling, clinker formation and corrosion of equipment due to SO_2 production during combustion of coal in boilers. Presence of large amounts of ash in coal produce slag along walls of furnace and around burner regions which reduce the heat transfer to water wall and cause damage to the burners (Hatt, 1990; Hatt and Rimmer, 1989). The use of poor quality coal as an energy source also create environmental problems due to emission of harmful gases such as CO_2 and SO_2 which in turn, causes global warming and health problems (Oteyaka *et al.,* 2008).

Salt Range coal is characterised by large amount of mineral matter especially pyrite, which restricts its use in power generation and local industry. Most of the salt range coal is consumed in brick making sector for the benefit of construction industry. In order to use it in power generation, cement industry and other manufacturing industries, there is a need to clean it from impurities.

Washability analysis is generally required to assess the liability of coal for cleaning and for the design and optimisation of coal processing plants as well as for monitoring coal preparation plant performance (Callen *et al.,* 2008; 2002). Galvin (2006) reviewed various techniques available for acquiring coal washability data, including float-sink, water fluidisation, jigging, water pycnometry, displacement pycnometry, and *in-situ* measurement of partition curves. Image analysis and release analysis are also gaining inspiration in determining washability characteristics of fine coal (Adel and Wang, 2005).

Normally, sink-float tests are carried out in the laboratory on the representative coal samples to generate useful information relating to amenability of coal cleaning. Washability curves are usually drawn to anticipate the theoretical yield and ash contents of clean coal at different specific gravities (Majumdar and Barnwal, 2004). The

*Author for correspondence; E-mail: m.shahzad87@yahoo.com

basic coal washability technique, float-sink technique involve the use of dense medium (organic liquid, salt solution or suspension). Several issues need to be addressed while selecting a dense medium including occupational safety, health, recoverability, chemical interaction and economy (Galvin, 2006). Salt solutions such as zinc chloride offer noteworthy advantages in terms of toxicity, safety, health and environmental standards.

Today various physical cleaning techniques like gravity concentration, flotation, electric and magnetic separation and oil agglomeration, are in use for the beneficiation of coal (Chen, 1998). Among these, gravity concentration processes enjoy the advantages of being cheaper, simple in operation and convenient (Shahzad, 2012) and are used extensively for coal cleaning (Wills and Napier-Munn, 2006). Gravity concentration entails a variety of techniques such as water-only cyclone, dense medium separators, jigs, shaking tables and spirals etc.

Jigs are primarily used for coarser size particles, in which a bed of particles is pulsated with a current of water, resulting in the assortment of particles on the basis of different densities (Xie and Kawn, 2004). Peng *et al.* (2002) have enlisted various modern jigging units. They applied packed column jig for the cleaning of coal in the size range from 1.18 mm to 150 μm which produced a clean coal concentrate corresponded to 90-98 % ash rejection with combustible material recovery of 75-85%. Shaking tables operate within the size range of – 5 mm to 0.5 mm (Anastassakis, 2004) while spirals are normally applicable for cleaning 1 × 0.15 mm fraction of coal feed (Honaker *et al.,* 2007). Cicek *et al.* (2008) found shaking table efficient at 15% and higher ash ratios.

The aim of this study is to evaluate the cleaning amenability of coal of selected areas of salt range through washability analysis and gravity concentration techniques including jigging, shaking table and spiral.

Materials and Methods

Coal samples. Representative coal samples, which weighed above 50 kg each, were collected from three Pakistan coal mines: (i) Modern Engineering, (ii) Kishor and (iii) Punjmin. Modern Engineering and Kishor coal mines are located in the eastern salt range in the areas of Ara and Mahinwal-Basharat, respectively while Punjmin coal mine is situated in the area of Badhrar in the central salt range (Fig. 1). The head sample of each coal mine was crushed to minus 18 mm using laboratory scale Denver Jaw Crusher and mixed properly.

Equipment. Jigging tests were carried out by using laboratory scale Denver coal Baum jig while the tabling tests were performed on a Wilfley laboratory scale shaking table. Spiral tests were conducted on Humphrey coal spiral.

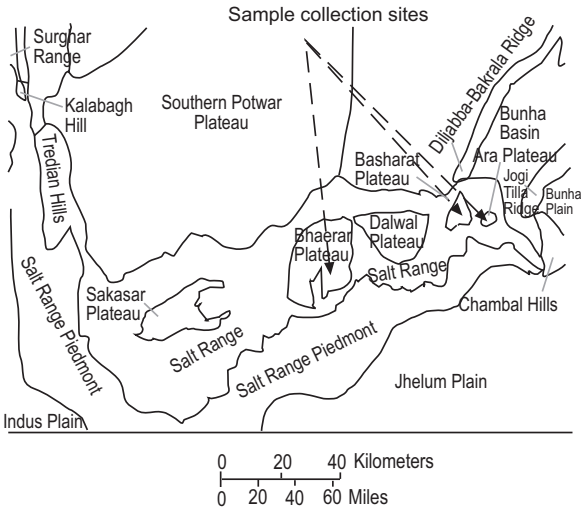

Fig. 1. Location map of sample collection mine sites: Modern Engineering coal mine (Ara), Kishor coal mine (Basharat) and Punjmin coal mine (Badhrar). (Source: Warwick, 2007).

Results and Discussion

Proximate analysis. One coal fraction of each coal mine was ground to - 0.150 mm using disc mill and proximate analysis (ASTM D 3173, 3174, 3175) were carried out on these powdered fractions. Total sulphur was determined by using Eschka method (ASTM E 775-87). Calorific values were determined by using Bomb calorimeter. The results of proximate analysis are presented in Table 1. These results categorize Modern Engineering and Punjmin coal to sub-bituminous C class, while Kishor coal to sub-

Table 1. Results of proximate analysis of Modern Engineers, Kishor and Punjmin coal

Properties	Modern Engineering coal	Kishor coal	Punjmin coal
Specific gravity	1.43	1.49	1.38
Moisture contents (%)	4.5	3.7	4.7
Volatile matter (%)	38.6	40.2	28.7
Ash contents (%)	25.0	25.5	26.0
Fixed carbon (%)	31.9	30.6	40.6
Sulphur contents (%)	4.139	5.071	9.336
Calorific value (Kcal/kg)	5266.00	5435.00	4753.00

bituminous B class (ASTM D 388). The results also show that all the three coals contain higher amounts of ash and sulphur in them.

Sink-and-float tests. A representative sample from each product with a particle size range from 0.670 to 0.212 mm was subjected to float-and-sink test. Zinc chloride solution was prepared and used as heavy medium with specific gravities of 1.4, 1.5, 1.6 and 1.7. The results of washability analysis for Modern Engineering, Kishor and Punjmin coals are presented in Fig. 2-4, respectively. Three other related curves, namely: clean coal curve for ash and sulphur and specific gravity/yield curve are also drawn along with primary washability curve for these three coals.

According to coal washability data established for Modern Engineering coal, clean coal with 16 % ash, 2.65 % sulphur and 70 % recovery can be obtained at a medium specific gravity of 1.57. Similarly, for Kishor coal, 17 % ash and 3.30 % sulphur can be acquired with theoretical clean coal recovery of 80 % at a specific gravity of 1.51. In case of Punjmin coal, the values of ash, sulphur and weight recovery of clean coal at a specific gravity of 1.54 were found to be 8, 2.40 and 70 %, respectively.

Generally, the ease or difficulty of washing of coal is judged by the shape of primary washability curve. The more the shape approximates the letter L, the easier the cleaning process will be (Lin *et al.,* 1999). According

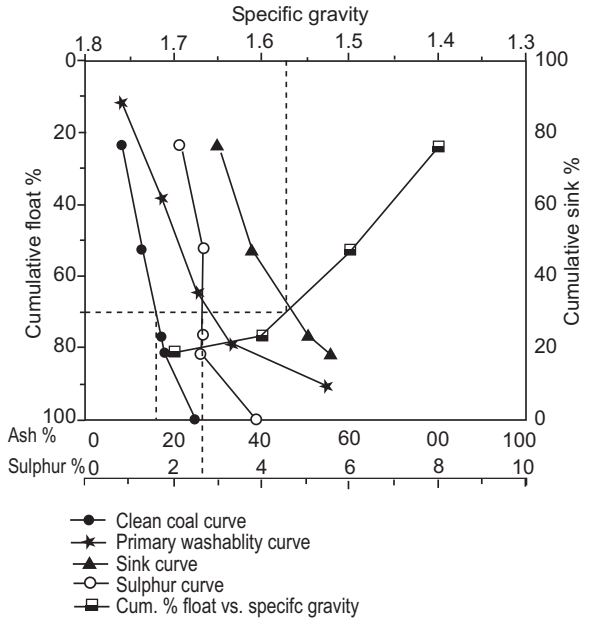

Fig. 2. Washability curves for Modern Engineering coal.

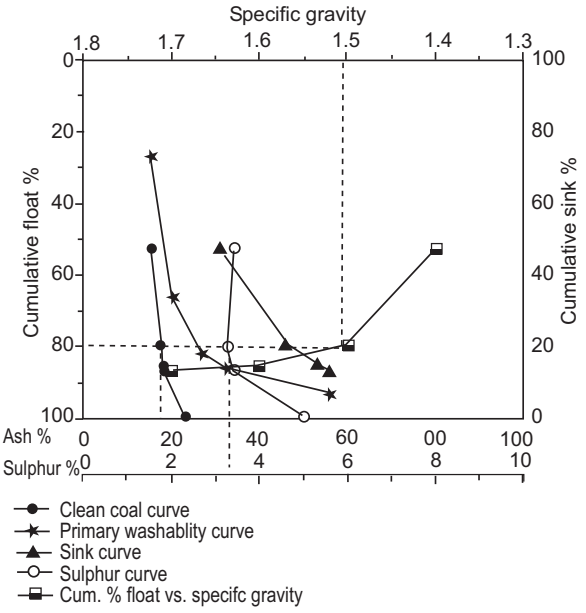

Fig. 3. Washability curves for Kishor coal.

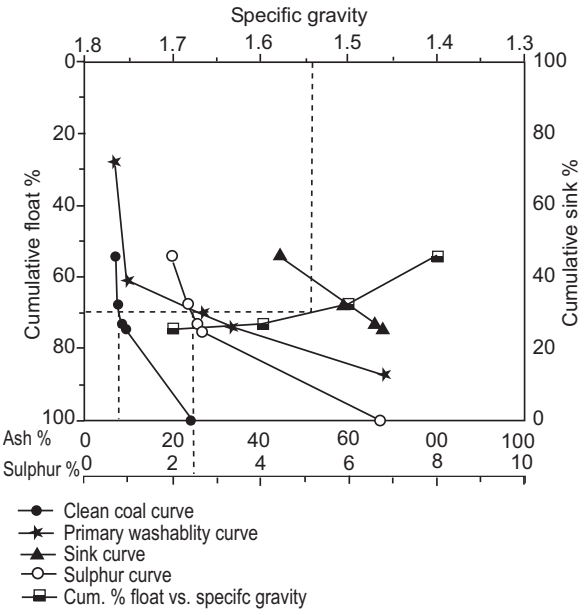

Fig. 4. Washability curves for Punjmin coal.

to washability curves drawn for salt range coal, Punjmin coal is found to be easily washable while Modern Engineering and Kishor coals can be classified as moderately cleanable coals.

Moreover, it is also shown by the clean coal curves for sulphur that most of the sulphur of Punjmin coal is associated with mineral matter, probably in the form of pyrite. In case of Modern Engineering and Kishor coals, it appears that a certain portion of sulphur is attached with

the mineral matter while, relatively larger portion of it is bound to organic material in the form of organic sulphur.

Gravity concentration tests. Gravity concentration techniques including jigging, shaking table and spiral were employed to check the cleaning susceptibility of the salt range coal. The feed size was kept in the range of -1.18 + 0.60 mm, - 0.833 + 0.295 mm and – 0.600 + 0.212 mm for jigging, shaking table and spiral, respectively. The solid concentration for the jigging and shaking table operation was kept at 35% while it was maintained at 40% for the spiral concentrator. Water flow rate for jig, shaking table and spiral was managed at 15, 8 and 20 gallon/min, respectively. The speed and stroke length of the shaking table was maintained at 260 strokes/min and 20 mm. The slope (length) and tilt (cross) of the shaking table were kept at 15 mm and 20 mm, respectively. The average values of ash, sulphur and weight recovery of the concentrate obtained from gravity concentration tests are presented in Table 2.

Table 2. Results of gravity concentration tests conducted on Modern Engineering, Kishor and Punjmin coal samples

Concentration techniques	Concentrate				Average recovery
	Average (%)		Rejection (%)		
	Ash	Sulphur	Ash	Sulphur	
Modern Engineers coal					
Jigging	17.7	2.781	29.2	32.82	31.89
Shaking table	16.8	2.621	32.8	36.67	45.43
Spiral	20.7	3.772	17.2	8.87	5.71
Kishor coal					
Jigging	22.3	4.951	12.55	2.36	64.03
Shaking table	20.7	4.337	18.82	14.47	74.58
Spiral	23.1	3.957	9.41	21.97	10.22
Punjmin coal					
Jigging	13.2	2.456	49.23	73.7	11.81
Shaking table	11.7	2.43	55	73.98	46.27
Spiral	14.9	2.369	42.69	74.63	10.67

In case of jigging tests, maximum rejection of ash of 49.23 % and that of sulphur 73.70 % was observed for Punjmin coal but recovery was very low. Modern Engineering and Kishor coal exhibit average weight recovery of 31.89 and 64.03 % with ash rejection of 29.20 and 12.55 % and elimination of sulphur of 32.82 % and 2.36 %, respectively.

The results of tabling tests revealed the elimination of ash 32.80, 18.82 and 55.0 % and that of sulphur 36.67, 14.47 and 73.98 % with average weight recovery of 45.43, 74.58 and 46.27 % for Modern Engineering, Kishor and Punjmin coal, respectively.

The results of spiral tests indicate that the recoveries for all the three coals remained very low. Punjmin coal showed maximum rejection of ash (42.7%) and that of sulphur (74.63%) while these values were less for Modern Engineering and Kishor coal.

Conclusion

Following conclusions can be drawn from this study:

1. Salt range coal contains higher amounts of ash and sulphur which make it unsuitable for use in cement industry and power generation.
2. Washability analysis revealed that the Eastern salt range coal (Modern Engineering and Kishor) was found to be moderately difficult to wash while the central salt range coal (Punjmin) was classified as easily washable coal.
3. Shaking table was found the most promising one among the three gravity concentration techniques (jig, shaking table, spiral) for all three coals for the rejection of ash.
4. Spiral was observed to be more efficient than shaking table and jig for the removal of sulphur for Kishor coal and Punjmin coal.
5. Punjmin coal can be used in local cement industry after cleaning through gravity concentration process. In order to use it for power generation, further cleaning of sulphur is required. For this purpose, a combination of shaking table and spiral may prove fruitful.
6. Modern Engineering and Kishor coal need more attention in terms of cleaning prior to their use in local cement industry. Special considerations with respect to their beneficiation are required for their use in power generation.

References

Adel, G.T., Wang, D. 2005. The assessment of fine coal cleanability. *Coal Preparation,* **25:** 129-140.

Anastassakis, G.N. 2004. Beneficiation of Greek lignites. *Coal Preparation,* **24:** 19-34.

ASTM, 2004. *Annual Book of ASTM Standards*, vol. 05.06. American Society for Testing and Materials, West Conshohocken, PA, Specifically, USA.

ASTM D 3173. Standard Test Method for Moisture in the Analysis Sample of Coal and Coke.

ASTM D 3174. Standard Test Method for Ash in the Analysis Sample of Coal and Coke.

ASTM D 3175. Standard Test Method for Volatile Matter in the Analysis Sample of Coal and Coke.

ASTM D 388. Classification of Coals by Rank.

ASTM E 775-87. Standard Test Methods for Total Sulphur in the Analysis Sample of Refuse-Derived Fuel.

Callen, A.M., Patel, B., Zhou, J., Galvin, K.P. 2008. Development of water-based methods for determining coal washability data. *International Journal of Coal Preparation and Utilization,* **28:** 33-50.

Callen, A.M., Pratten, S.J., Belcher, B.D., Lambert, N., Galvin, K.P. 2002. An alternative method for float-sink analysis of fine coal samples using water fluidization. *Coal Preparation,* **22:** 293-310.

Chen, X. 1998. Control of Surface Chemistry of Coal, Pyrite and Pyrrhotite. *M.Sc. Thesis,* Virginia Polytechnic Institute & State University, 118 pp.

Çiçek, T., Cöcen, I., Engin, V.T., Cengizler, H. 2008. An efficient process for recovery of fine coal from tailings of coal washing plants. *Energy Sources, Part A: Recovery, Utilization and Environmental Effects,* **30:** 1716-1728.

Galvin, K.P. 2006. Options for washability analysis – A literature review. *Coal Preparation,* **26:** 209-234.

Hatt, R.M. 1990. Fireside deposits in coal-fired utility boilers. *Progress in Energy and Combustion Science,* **16:** 235-241.

Hatt, R.M., Rimmer, S.M. 1989. Classification and sampling of deposits from coal-fired boilers. *Journal of Coal Quality,* **8:** 40-44.

Honaker, R.Q., Jain, M., Parekh, B.K., Saracoglu, M. 2007. Ultrafine coal cleaning using spiral concentrator. *Minerals Engineering,* **20:** 1315-1319.

Lin, C.L., Parga, J.R., Drelich, J., Miller, J.D. 1999. Characterization of washability of some mexican coals. *Coal Preparation,* **20:** 227-245.

Majumder, A.K., Barnwal, J.P. 2004. Development of a new coal washability index. *Minerals Engineering,* **17:** 93-96.

Nawaz, S., Butt, M.A., Sheikh, N., Hassan, M. 2009. Chemical, microscopic and XRD studies on Makerwal coal. *Journal of Faculty of Engineering and Technology,* **16:** 41-49.

Oteyaka, B., Yamik, A., Ucar, A., Sahbaz, O., Demir, U. 2008. The washability of lignites for clay removal. *Energy Sources,* **30:** 797-808.

Peng, F.F., Dai, Q., Yang, D.C. 2002. Analysis of packed column jig for fine coal separation. *Coal Preparation A Multimaterial Journal,***22:** 199-217.

Sanders, G.J., Ziaja, D., Kottmann, J. 2002. Cost-efficient beneficiation of coal by Rom Jigs and BATAC Jigs. *Coal Preparation A Multimaterial Journal,* **22:** 181-197.

Shahzad, M. 2012. Cleaning Susceptibility of Coal Deposits from Selected Areas of Salt Range. *M.Sc. Thesis,* Mining Engineering Department, University of Engineering & Technology, Lahore, Pakistan.

Warwick, P.D. 2007. Overview of the geography, geology, and structure of the Potwar regional framework assessment project study area, northern Pakistan. Chap. A, *U.S. Geological Survey Bulletin* 2078, P.D., Warwick, and B. R. Wardlaw, (eds.), Regional Northern Pakistan, pp. A1-A9.

Wills, B.A., Napier-Munn, T. 2006. *Mineral Processing Technology,* pp. 456, 7th edition, Elsevier Science & Technology Books, Amsterdam, The Netherlands.

Xie, J.X., Kawn, Y.L. 2004. Properties of jigging bed analyzed with high speed analyzer (Part 2). *Coal Preparation,* **24:** 285-295.

Pak. j. sci. ind. res. Ser. A: phys. sci. 2015 **58** (2) 79-89

Variability in Foliar Phenolic Composition of Several *Quercus* Species in Northern Mexico

Jorge Armando Arámbula-Salazar[a], Norma Almaraz-Abarca[b], José Javier Corral-Rivas[c]*, Eli Amanda Delgado-Alvarado[b], Raúl Díaz-Moreno[c] and Eusebio Montiel-Antuna[a]

[a]Facultad de Ciencias Forestales, Universidad Juárez del Estado de Durango, Río Papaloapan y Blvd. Durango s/n Col. Valle del Sur, Durango, Durango, Mexico, 34120

[b]Centro Interdisciplinario de Investigación para el Desarrollo Integral Regional, Instituto Politécnico Nacional Unidad Durango (CIIDIR-IPN-Durango), Sigma No. 119, Fraccionamiento 20 de Noviembre II, Durango, Mexico, 34220

[c]Instituto de Silvicultura e Industria de la Madera, Universidad Juárez del Estado de Durango, Blvd. del Guadiana # 501 Ciudad Universitaria, Durango, Mexico, 34160

(received December 30, 2013; revised June 2, 2014; accepted June 10, 2014)

Abstract. Quantitative and qualitative composition of the foliar phenolic compounds were investigated in 81 individual specimens of several white oak species (*Quercus* spp.). The trees were growing in twelve locations in Durango, Mexico. The phenol profiles were determined by HPLC-DAD and a Folin-Ciocateu procedure. The results revealed that: (i) the foliar phenol profiles of all species analysed were complex and formed by 6 to 30 compounds, (ii) the flavonols mostly quercetin glycoside, isorhamnetin glycoside, kaempferol glycoside and phenolic acids were the main identified compounds, (iii) there was a high intra and inter-specific variability in the foliar phenol profiles both at the quantitative and qualitative levels, and (iv) the foliar phenol profiles indicated a slight species-specific tendency for phenols to be accumulated, although this was not clearly distinguished. Significant differences ($P < 0.05$) in the content and composition of the foliar flavonoids between species were observed due to the large environmental and soil conditions variability between localities.

Keywords: *Quercus chihuahuensis*, *Quercus arizonica*, *Quercus grisea*, *Quercus undata*, *Quercus convallata*, foliar phenol profiles

Introduction

Quercus is the most important and largest genus of the Fagaceae family (Rodríguez and Romero, 2007). Two centres of diversity of *Quercus* are recognised i.e. around 125 species found in Southeast Asia and about 161 species in Mexico (Valencia, 2004). *Quercus* species after *Pinus*, constitute the second most important timber yielding group in Mexico. Approximately 86 of the Mexico's species are endemic (González-Rodríguez *et al*., 2004), and distributed mainly in the temperate mountainous regions (Rzedowski, 2006).

Phenolic compounds are ubiquitous secondary metabolites in plants. They cover a large group of biologically active ingredients (more than 8000 compounds) ranging from simple phenol molecules to polymeric structures with molecular mass of more than 3000 daltons (Marinova *et al*., 2005). The foliar phenolic composition of plants is important for several reasons, e.g., for inhibiting phytophagous insects and for attracting pollinators (Hadacek, 2002). The broad biological activity of phenolic compounds, e.g., as antioxidants (Falleh *et al*., 2011; Almaraz-Abarca *et al*., 2007; 2006) and antibacterial compounds (Bangou *et al*., 2011), has also led to studies of phenolic composition in many species of plants. However, the phenolic composition of a few *Quercus* species have been studied, mainly with the aim of determining their biological activity including *Q. robur* (Salminen *et al*., 2004), *Q. alba* (Miller *et al*., 1992), *Q. rubra* (Warren *et al*., 2002), *Q. miyagii* (Ishimaru *et al*., 1987), *Q. dentata* (Wang *et al*., 2010), *Q. cerris* L. (Romussi *et al*., 1988), *Q. mongolica* (Ishimaru *et al*., 1988), *Q. suber* and *Q. pubescens* (Romussi *et al*., 1991), *Q. incana* (Iftikhar *et al*., 2009), *Q. ilex* (Karioti *et al*., 2011), *Q. acutissima* (Yeon *et al*., 2011), *Q. infectoria* (Gurpreet *et al*., 2008), *Q. petraea* (Meyer *et al*., 2009), *Q. salicina* (Jung-Il *et al*., 2008), *Q. coccifera* (Karageorgou and Manetas, 2006), *Q. sideroxyla*, *Q. eduardii*, and *Q. resinosa*

*Author for correspondence; E-mail: jcorral@ujed.mx

(Rivas-Arreola *et al*., 2010). These species represents around 4% of the 531 species that are included in this genus (Borazan and Babaç, 2003).

Flavonoids represent the most common and widely distributed group of plant-food phenolics, and their contents and compositions are associated with the antioxidant properties of different fruits and vegetables (Harborne and Williams, 2000). Flavonoid profiles have been used as significant taxonomic markers for establishing a system of classifying several plant species (Almaraz-Abarca *et al*., 2006; Emerenciano *et al*., 2001; Fiasson *et al*., 1997; Abdala and Seeligmann, 1995). These chemical markers were found to be rather species-specific (Almaraz-Abarca *et al*., 2006; Míka, 2005). Changes in phenolic composition caused by environmental factors influence directly the quality of the plant material for potential uses (Santos *et al*., 2006).

The aim of the present study was to investigate the variability in foliar phenolic composition of the following eight *Quercus* species that are among the most abundant species in the temperate forests of Durango, Mexico: *Q. arizonica s.l*., *Q. chihuahuensis*, *Q. grisea*, *Q. undata*, *Q. convallata*, *Q*. aff. *convallata*, *Q. arizonica* intro. *coccolobifolia*, and *Q. arizonica* aff. *transmontana*. Quantitatively and qualitatively intra- and inter-specific variability in phenolic compounds were studied and their taxonomical significance was verified.

Materials and Methods

Plant material. The foliar phenol composition of individual specimens of *Q. arizonica s.l*., *Q. chihuahuensis*, *Q. grisea*, *Q. undata*, *Q. convallata*, *Q*. aff. *convallata*, *Q. arizonica* intro. *coccolobifolia*, and *Q. arizonica* aff. *transmontana* was analysed. The phenol composition was interpreted considering prior to morphological identification of the samples. Ecogeographic and soil information were also recorded when sampling (Table 1). Foliar samples were collected from individuals growing under variable ecological conditions. Leaves from 6 to 7 adult individuals of healthy appearance were collected in all cases. A total of 81 specimens were sampled at 12 locations. Authentication of each specimen sampled was done at the CIIDIR Herbarium in Durango City, Mexico.

Phenol extraction. Each sample was analysed individually and 2 g of dried and grounded leaves of each sample were macerated with 40 mL 60% methanol (v/v) in darkness and at room temperature for 24 h. The extracts were centrifuged (8000 rpm) for 10 min at room temperature. The supernatants were separated and pellets re-extracted in 7 mL 60% methanol (v/v) in darkness and at room temperature for 2 h. The extracts were centrifuged under the same conditions. Similar supernatants were combined to form the total extracts, and these were concentrated to dryness by rotary evaporation and then re-dissolved in 3 mL methanol. Aliquots were removed for determination of the phenol content and HPLC-DAD analysis.

Total phenol contents. The amount of total phenols in the methanol foliar extracts of each sample of *Quercus* was determined by the Folin-Ciocalteu method (Lozoya-Saldaña *et al.,* 2007). The following values were obtained from the standard curve for gallic acid (32-260 µg/mL vs. absorbance): $A_{760\,nm} = -0.011 + 0.0004$ (gallic acid) and correlation coefficient, r = 0.9989. Absorbance values were recorded at 760 nm after 120 min of incubation at darkness. Total phenol contents were expressed as mg of gallic acid equivalents GAE/g dry weight (Dw).

Analysis by HPLC/DAD. The individual HPLC-DAD phenol profiles were obtained following the method described by Campos and Markham (2007). Extracts (20 µL) were analysed in a Perkin Elmer Series 200 HPLC system, with a Perkin Elmer Brownlee analytical C18 column (4.6×250 mm, 5 µ) and a gradient of acidified water and acetonitrile. The flow rate was 0.8 mL/min. Standard chromatograms were plotted at 280 and 340 nm. Spectral data for all peaks were accumulated in the range of 200-400 nm using a diode-array detector (DAD) (Perkin Elmer Series 200). The structural information on each resolved compound was obtained by direct comparison of retention times (RT) and UV spectra with those of standards (quercetin, quercitrin, naringenin, hesperidin, epicatechin, phthalic acid, vanillic acid, gallic acid and trans-cinnamic acid) and according to the data compiled by Mabry *et al*. (1970) and Campos and Markham (2007). Quantitative determination of the major flavonoids was made from a stock solution of quercetin, which was prepared (120, 250, and 500 µg/mL)

Table 1. Collection sites for *Quercus* species and hybrids

Individuals	Reference number: Species	Eco-geographic information (location, latitude N, longitude W, altitude (masl), average temperature (°C), annual precipitation (mm), soil type, date
1-6	36286: *Q. chihuahuensis*, 36319: *Q .chihuahuensis* × *grisea*, 36315: *Q. chihuahuensis*, 36316: *Q. chihuahuensis*, 36321: *Q. chihuahuensis* and 36327: *Q. chihuahuensis*	Site I: 35 Km Durango-Mazatlán Highway, 23°56'08.5", 104°51'58.3", 2270, 13, 733, eutric regosol, May 2008
7-13	36387: *Q. arizonica s.l*., 36515: *Q. arizonica* intro. *grisea*, 36385: *Q. arizonica* intro. *grisea*, 36419: *Q. grisea*, 36426: *Q. arizonica s.l*., 36396: *Q. arizonica s.l.* and 36466: *Q. grisea s.l.*	Site II: 29 Km Durango-Mazatlán Highway, 23°57'12.4", 104°51'01.5", 2207, 14, 711, 2207, entisoil, May 2008
14-20	36410: *Q. chihuahuensis*, 36403: *Q. undata*, 36400: *Q. chihuahuensis*, 36401: *Q. chihuahuensis*, 36404: *Q. undata*, 36402: *Q. chihuahuensis* and 36394: *Q. undata*	Site III: 13 Km Durango-Mazatlán Highway, 23°59'11.4", 104°44'53.7", 2082, 16, 644, leptosol, May 2008
21-27	36760: *Q. arizonica s.l*., 36739: *Q. arizonica s.l*., 36737: *Q. arizonia s.l*., 36736: *Q. arizonica s.l*., 36743: *Q. arizonica s.l*., 36725: *Q. arizonica s.l.* and 36726: *Q. arizonica s.l*	Site IV: 187 Km Tepehuanes-Guanaceví Road, 25°28'25.4", 105°47'51.5, 2167, 14, 632, eutric regosol, Jun 2008
28-33	36762: *Q. grisea*, 36730: *Q. arizonica s.l*., 36784: *Q. aff.arizonica*, 36783: *Q. aff. arizonica*, 36741: *Q. arizonica s.l.* and 36742: *Q. arizonica s.l.*	Site V: 191 Km Tepehuanes-Guanaceví Road, 25°29'31.4", 105°47'11.2", 2079, 15, 606, eutric regosol, Jun 2008
34-40	36727: *Q. arizonica s.l*., 36728: *Q. arizonica s.l*., 36750: *Q. arizonica s.l*., 36780: *Q. arizonica s.l*., 36781: *Q. arizonica s.l*., 36761: *Q. grisea* and 36782: *Q. arizonica s.l.*	Site VI: 193 Km Tepehuanes-Guanaceví Road, 25°30'11.6", 105°47'14.6", 2098, 15, 611, eutric regosol, Jun 2008
41-47	38820: *Q.* aff. *convallata,* 38821: *Q.* aff. *convallata,* 38822: *Q*. aff. *convallata,* 38823: *Q*. aff. *convallata* intro. *arizonica,* 38824: *Q*. aff. *convallata,* 38825: *Q*. aff. *convallata* and 38826: *Q*. aff. *convallata*	Site VII: 6 Km El Tecuán-Regocijo Road, 23°52'37.2", 105°00'58.7", 2168, 13, 765, regosol, Jun 2008
48-54	38827: *Q.* aff. *convallata,* 38828: *Q.* aff. *convallata,* 38829: *Q. convallata* introgresión *arizonica,* 38830: *Q. convallata,* 38831: *Q. convallata,* 38832: *Q. convallata* and 38833: *Q. convallata*	Site VIII: 8 Km El Tecuán-Regocijo Road, 23°51'41.9", 105°00'12.9", 2188, 13, 773, district regosol, Jun 2008
55-61	38834: *Q.* aff. *convallata,* 38835: *Q.* aff. *convallata,* 38836: *Q. arizonica* x *convallata,* 38837: *Q*. aff.*convallata,* 38838: *Q. arizonica s.l,* 38839: *Q. arizonica s.l.,*and 38840: *Q*. aff. *arizonica* x *convallata*	Site IX: 10 Km El Tecuán-Regocijo Road, 23°50'54.4", 105°00'01.6", 2172, 13, 777, district regosol, Jun 2008
62-68	36734: *Q. arizonica* intro. *coccolobifolia,* 36733: *Q. arizonica s.l.* intro. *coccolobifolia,* 36825: *Q. arizonica* aff. *transmontana,* 36836: *Q. arizonica* aff. *transmontana,* 36837: *Q. arizonica s.l.,* 36834: *Q. arizonica* aff. *Transmontana* and 36838: *Q. arizonica s.l.*	Site X: 39 Km Durango-Mezquital, 23°46'35.6", 104°25'23.7", 2098, 16, 602, leptosol, Jun 2008
69-75	36860: *Q. arizonica s.l.,* 36845: *Q. arizonica s.l.,* 36816: *Q. arizonica* intro. *coccolobifolia,* 36788: *Q. arizonica s.l.,* 36858: *Q. arizonica* aff. *transmontana,* 36859: *Q. arizonica* intro. *coccolobifolia* and 36843: *Q.* aff. *arizonica* x *coccolobifolia*	Site XI: 41 Km Durango-Mezquital, 23°45'45.3", 104°25'05.9", 2043, 16, 588, leptosol, Jun 2008
76-81	36830: *Q. arizonica* aff. *transmontana,* 36835: *Q. arizonica* x *coccolobifolia,* 36831: *Q. arizonica* intro. *coccolobifolia,* 36735: *Q. arizonica* intro. *coccolobifolia,* 36829: *Q. arizonica* intro. *coccolobifolia and* 36832: *Q. arizonica* intro. *coccolobifolia*	Site XII: 36 Km Durango-Mezquital Highway, 23°47'01.4", 104°25'33.2", 2061, 16, 593, calcium afisol, Jun 2008

for construction of the calibration curve ($A_{280\ nm}$ = 413389 + 25881[quercetin], r = 0.9999) by plotting the standard concentrations against the peak area in the HPLC chromatograms. The concentration of each individual compound was expressed in µg of quercetin equivalents (EQ quercetin µg/g Dw) (here 395.9 µg/g Dw).

Data analysis. The individual phenol profiles comprised of all compounds detected in the respective HPLC-DAD chromatograms. Each compound was treated as a single chemical character and assessed in a binary matrix coded by 1 (presence) or 0 (absence) in each population. A dendrogram obtained from a cluster analysis (Ward´s method) based on chemical marker data was calculated

using PAST 1.43 (Hammer *et al*., 2001). Because phenolic contents were not normally distributed, the non-parametric Kruskal-Wallis test was used to evaluate intra and inter-specific variability of these compounds either at the quantitative or the qualitative levels (Kruskal and Wallis, 1952). The test was performed with the NPAR1WAY procedure of SAS/ETS® (SAS Institute Inc., 2004).

Results and Discussion

***Quercus* foliar phenolic compounds.** A total of 73 compounds were determined by HPLC-DAD analysis of the leaves of the species under study (Table 2). The analysis revealed 20 phenolic acids and 53 flavonoids. The flavonoids present in the foliar tissues included 34 flavonols, 5 flavones, 4 dihydroflavonoids and 10 un-identified flavonoids. The flavonols included seven quercetin derivatives, four myricetin derivatives, seven kaempferol derivatives and two isorhamnetin derivatives. The flavones included two tricitin derivatives and one luteolin derivative. Compounds f 13 (quercetin glycoside), f 31 (isorhamnetin glycoside) and f 37 (kaempferol glycoside) were the most abundant phenolic compounds. The results of the present study are consistent with those

Table 2. Retention time and λ_{max} of the phenolic compounds present in the foliar tissues of the analysed *Quercus* species

Compound	Identification	Retention time (min)*	λ_{max} (nm)
f01	Fl	36.40±0.00	255, 360
f02	Fl	37.87±0.00	255, 360
f03	U	41.83±0.00	280, 360
f04	Qg	44.18±0.00	255, 299 sh, 350
f05	Fl	63.12±0.17	255, 370
f06	Fl	67.72±0.27	250, 301sh, 370
f07	Fl	68.50±0.31	255, 367
f08	Fl	68.46±0.22	265, 285sh, 355
f09	Fl	69.59±0.31	255, 360
f10	Qg	69.97±0.00	255, 294 sh, 355
f11	Lg	70.07±0.00	265, 295 sh, 360
f12	U	70.27±0.44	265, 290 sh, 355
f13	Qg	70.65±0.27	252, 290 sh, 350
f14	Mg	70.81±0.00	253, 265 sh, 299 sh, 353
f15	U	71.50±0.36	253, 270 sh, 360
f16	Qg	72.60±0.26	255, 300 sh, 360
f17	Df	72.56±0.30	280
f18	Td	72.91±0.01	266, 293 sh, 350
f19	U	72.97±0.00	265, 350
f20	U	73.43±0.26	266, 297 sh, 353
f21	Fl	74.43±0.25	254, 305 sh, 364
f22	Kg	74.76±0.13	260, 350
f23	U	74.82±0.16	267, 285sh, 360
f24	Qg	75.27±0.21	256, 300 sh, 357
f25	Mg	75.66±0.33	255, 297 sh, 352
f26	Fl	75.17±0.00	267, 360
f27	Tg	75.66±0.22	250, 262 sh, 353
f28	Fl	75.66±0.00	250, 360
f29	Qg	76.44±0.39	256, 266 sh, 292sh, 356
f30	U	76.43±0.18	270, 357
f31	Ig	76.56±0.36	255, 267 sh, 355
f32	Ig	77.18±0.00	255, 267sh, 355
f33	U	77.50±0.36	267, 285 sh, 356
f34	Df	77.74±0.09	281
f35	Fl	78.93±0.05	266, 296 sh, 351
f36	U	78.72±0.21	255, 269 sh, 355
f37	Kg	78.74±0.32	265, 350
f38	Fl	80.13±0.15	267, 350
f39	Kg	80.62±0.36	266, 351
f40	U	80.43±0.00	270, 287 sh, 361
f41	Kg	81.45±0.42	265, 295 sh, 349
f42	Df	81.02±0.00	278
f43	Mg	81.07±0.00	255, 267 sh, 297sh, 354
f44	Mg	82.06±0.03	256, 300 sh, 351
f45	Qg	82.48±0.37	256, 267 sh, 300 sh, 351
f46	Kg	82.15±0.25	265, 351
f47	Kg	83.89±0.04	266, 350
f48	Df	88.25±0.31	281
f49	Ca	89.50±0.00	287, 311
f50	F	89.47±0.00	266, 294sh, 314
f51	Pa	93.46±0.07	267, 316
f52	Pa	96.95±0.00	267, 311
f53	Fl	101.37±0.00	266, 364
f54	Fl	103.08±0.01	256, 370
f55	Kg	103.10±0.12	264, 364
f56	Pa	104.66±0.42	266, 314
f57	F	105.63±0.00	266, 297 sh, 313
f58	Pa	108.57±0.21	267, 314
f59	Pa	109.31±0.24	267, 312
f60	Pa	110.35±0.34	267, 311
f61	Pa	111.37±0.26	267, 312
f62	Pa	112.40±0.29	267, 314
f63	Pa	113.30±0.25	266, 311
f64	Pa	114.11±0.05	266, 311
f65	Pa	115.47±0.06	266, 311
f66	Pa	116.60±0.30	268, 311
f67	Pa	117.50±0.32	267, 312
f68	Pa	118.52±0.34	267, 312
f69	Pa	119.52±0.33	266, 313
f70	Pa	120.42±0.26	267, 315
f71	Pa	121.53±0.04	267, 313
f72	Pa	122.35±0.21	266, 314
f73	Pa	123.52±0.39	266, 311

*Retention times are mean values and standard deviations for 1-81 independent samples; Ca = cinnamic acid; Df = dihydraflavonoid; F = flavone; Fl = flavonel; Ig = isorhamnetin glycoside; Kg = kaempferol glycoside; Lg = lutheolin glycoside; Mg = myricetin glycoside; Pa = phenolic acid; Qg = quercetin glycoside; Td = tricitin derivative; Tg = tricin glycoside; U = unidentified.

continued next column →

reported by Karioti *et al.* (2011) who also identified kaempferol glycosides, isorhamnetin glycosides and quercetin glycosides as the most abundant phenolic compounds in extracts of *Quercus ilex* trichomes. Rivas-Arreola *et al.* (2010) and Wang *et al.* (2010) also identified kaempferol glycosides and quercetin glycosides as the most abundant phenolic compounds in other species of *Quercus*. The most complex foliar phenol profile was that of *Q. chihuahuensis*, which included 30 phenols. The least complex profile was that of *Q. arizonica* intro. *coccolobifolia*, with 6 phenols.

Total phenolic contents. Table 3 shows the average total foliar phenolic contents of the species of *Quercus* analysed. According to the non-parametric Kruskal-Wallis test, the total phenol contents varied significantly among *Quercus* species (H = 28.48, P = 0.0002) (Table 4). A comparison among groups of individuals belonging to the same *Quercus* species and that were growing in different sites showed that locality also affected phenol contents of the (H = 62.69, P<0.0001), suggesting variation in phenolic compounds within tree species and localised environmental control of levels of these compounds. As an example phenol contents of *Q. arizonica s.l.* which was recorded in sites II, II, IV, V, VI, IX, X and XI varied significantly in 6 of the 7 pair comparisons tested using the individuals of site II as the reference group. These results could be explained by the effect of site variability in soil composition, temperature, and rainfall (Borges *et al*., 2013; Gobbo-Neto and Lopes, 2007; Monteiro *et al*., 2006). The lowest average level (196.85 mg/g Dw) was estimated for individuals of *Q. convallata* (site IX) and the highest average level (399.61 mg/g Dw) for *Q. arizonica s.l.* (site IV).

Table 3. Average total foliar phenolic contents (gallic acid equivalents) of *Quercus grisea, Q. arizonica s.l., Q. chihuahuensis, Q. undata, Q. arizonica* intro. *coccolobifolia, Q. arizonica* aff. *transmontana, Q.* aff. *convallata*, and *Q. convallata*

Site	Tree species	No. of individuals	Average total concentration
I	*Q. chihuahuensis*	5	369.74
II	*Q. arizonica s.l.*	3	340.00
II	*Q. grisea*	1	367.50
III	*Q. chihuahuensis*	4	280.30
III	*Q. undata*	3	299.97
IV	*Q. arizonica s.l.*	7	399.61
V	*Q. arizonica s.l.*	3	313.73
V	*Q. grisea*	1	311.20
VI	*Q. arizonica s.l.*	6	295.62
VI	*Q. grisea*	1	281.20
VII	*Q.* aff. *convallata*	6	259.97
VIII	*Q.* aff. *convallata*	2	198.75
VIII	*Q. convallata*	4	198.73
IX	*Q.* aff. *convallata*	3	208.73
IX	*Q. arizonica s.l.*	2	196.85
X	*Q. arizonica* aff. *transmontana*	3	239.97
X	*Q. arizonica intro coccolobifolia*	1	255.00
X	*Q. arizonica s.l.*	2	232.45
XI	*Q. arizonica* aff. *transmontana*	1	213.70
XI	*Q. arizonica intro coccolobifolia*	2	210.00
XI	*Q. arizonica s.l.*	3	221.23
XII	*Q. arizonica* aff. *transmontana*	1	247.50
XII	*Q. arizonica intro coccolobifolia*	4	273.75

Results of the non parametric Kruskal-Wallis test among studied *Quercus* species are shown in Table 4. Significant differences (P<0.05) between foliar phenol levels were observed in 16 of 28 pair comparisons. The foliar phenol contents were highest in *Quercus arizonica s.l.* and *Q. chihuahuensis* and lowest in *Q. arizonica* aff. *transmontana, Q. convallata* and *Q.* aff. *convallata*. The foliar phenol contents estimated for the species of *Quercus* analysed in the present study are similar to the levels reported by Karageorgou and Mantas (2006), who estimated levels ranging from 50 to 550 mg/g Dw in the leaves of *Q. coccifera* L., and by Rivas-Arreola *et al*. (2010), who estimated levels ranging from 227 to 537 mg/g Dw in the leaves of another species of *Quercus.*

Individual phenolic concentration. The relative concentrations of the individual phenolic compounds detected in each sample are shown in Table 5. The Kruskal-Wallis test revealed statistically significant differences between the relative concentrations of phenolic compounds in several samples (Table 6). The maximum concentration observed was that of compound f 08 (385.86 µg/g Dw) in *Q. chihuahuensis* (sample 1), and the lowest concentration was that of compound f 72 (37.21 µg/g Dw) in *Q. arizonica* intro. *coccolobifolia* (sample 71).

As shown in Table 6, highly significant differences were observed in the mean relative concentrations of

Table 4. Results of the Kruskal-Wallis test for paired comparisons of foliar phenol contents in the analysed *Quercus* species

Pairs of species compared (mean score in brackets)	H	*Pr*> H
Q. chihuahuensis (19.38) – Q. arizonica s.l. (17.51)	0.22	0.636
Q. chihuahuensis (6.61) – Q. grisea (6.16)	0.03	0.853
Q. chihuahuensis (6.88) – Q. undata (5.33)	0.42	0.516
Q. chihuahuensis (15.27) – Q. aff. *convallata (6.59)*	10.68	0.001**
Q. chihuahuensis (9.00) – Q. convallata (2.50)	7.73	0.005**
Q. chihuahuensis (11.16) – Q. arizonica intro. *coccolobifolia (5.07)*	6.46	0.011*
Q. chihuahuensis (10.0) – Q. arizonica aff. *transmontana (3.0)*	9.00	0.002**
Q. arizonica s.l. (14.94) – Q. grisea (15.50)	0.01	0.914
Q. arizonica s.l. (15.15) – Q. undata (13.66)	0.08	0.774
Q. arizonica s.l. (22.46) – Q. aff. *convallata (10.81)*	8.95	0.002**
Q. arizonica s.l. (17.26) – Q. convallata (4.00)	7.88	0.0050**
Q. arizonica s.l. (18.75) – Q. arizonica intro. *coccolobifolia (10.50)*	4.02	0.044*
Q. arizonica s.l. (17.46) – Q. arizonica aff. *transmontana (8.40)*	4.17	0.041*
Q. grisea (4.0) – Q. undata (3.0)	0.483	0.486
Q. grisea (12.83) – Q. aff. *convallata (6.04)*	6.21	0.012*
Q. grisea (6.00) – Q. convallata (2.50)	5.58	0.0323*
Q. grisea (8.33) – Q. arizonica intro. *coccolobifolia (4.28)*	3.75	0.0527
Q. grisea (7.0) – Q. arizonica aff. *transmontana (3.0)*	5.00	0.025*
Q. undata (12.50) – Q. aff. *convallata (6.13)*	5.47	0.0193*
Q. undata (6.00) – Q. convallata (2.50)	4.66	0.030*
Q. undata (8.33) – Q. arizonica intro. *coccolobifolia (4.28)*	3.77	0.052
Q. undata (7.0) – Q. arizonica aff. *transmontana (3.0)*	5.06	0.0245*
Q. aff. *convallata (9.27) – Q. convallata (4.50)*	3.34	0.067
Q. aff. *convallata (8.45) – Q. arizonica* intro. *coccolobifolia (11.14)*	1.08	0.297
Q. aff. *convallata (8.31) – Q. arizonica* aff. *transmontana (8.90)*	0.051	0.820
Q. convallata (3.25) – Q. arizonica intro. *coccolobifolia (7.57)*	4.34	0.037*
Q. convallata (3.00) – Q. arizonica aff. *transmontana (6.60)*	3.93	0.047*
Q. arizonica intro. *coccolobifolia (7.35) – Q. arizonica* aff. *transmontana (5.30)*	0.95	0.329

*significant differences; **highly significant differences.

phenols between the following pairs of *Quercus* species: *Q.* aff. *convallata* and *Q. arizonica s.l.; Q.* aff. *convallata* and *Q. chihuahuensis*; *Q. arizonica* intro. *coccolobifolia* and *Q. convallata*; *Q. chihuahuensis* and *Q. convallata.* The tree species *Quercus grisea, Q. chihuahuensis, Q. arizonica s.l.* and *Q. undata* accumulated the highest relative concentrations of phenols, whereas *Q.* aff. *convallata* and *Q. arizonica* aff. *transmontana* accumulated the lowest levels.

In summary, phenolic concentrations of studied white oak tree species varied greatly among, species, individuals, and sites. This is in agreement with previous studies on phenolic contents. Significant variation in phenolic concentrations has been reported among tissue types in an individual, among sites, and between species (Van Alstyne *et al*., 1999, Rivas-Arreola *et al*., 2010). The results indicate that *Quercus* species contain larger amounts of phenol compounds than most of the other plants. Rivas-Arreola *et al.* (2010) reported phenolic contents of 537 mg/g, 331 mg/g and 227 mg/g in dried leaves of *Quercus sideroxyla*, *Quercus eduardii* and *Quercus resinosa*, respectively. Amarowicz *et al.* (2004) reported phenolic contents of 55.4, 58, and 67.6 mg/g in dried seeds of red bean (*Phaseolus vulgaris*), red lentil (*Lens culinaris*) and green lentil (*Lens culinaris*), respectively. Marinova *et al.* (2005) reported total phenolic contents of 3.03, 4.29, 3.55 and 6.70 mg/g in fruits of plum (*Prunus domestica*), sour cherry (*Prunus cerasus*), blackberry (*Rubus coesins*) and blueberry (*Vaccinium myrtilus*), respectively.

Cluster analysis. The results of the cluster analysis of the foliar phenol profiles of the individuals analysed

Table 5. Relative concentrations of the individual phenolic compounds identified in the leaves of the *Quercus* species under study (quercetin equivalents)

Compound	Relative concentration (µg/g Dw)							
	Q. grisea	*Q. arizonica s.l.*	*Q. chihuahuensis*	*Q. undata*	*Q. arizonica* intro. *coccolobifolia*	*Q. arizonica* aff. *transmontana*	*Q.* aff. *convallata*	*Q. convallata*
f05	71.2	76	-	-	-	-	-	69.6
f06	323.84	302.12	285	306.42	98.18	96.59	-	80.76
f07	-	-	-	-	152.55	-	-	-
f08	300.88	-	385.86	-	212.20	-	203.49	-
f09	-	344.43	-	-	167.86	-	-	69.28
f12	362.64	336.15	-	-	66.51	-	-	
f13	-	214.73	330.37	-	-	-	66.51	67.30
f15	-	289.64	145.29	-	120.35	120.35	-	-
f17	227.24	306.95	-	-	216.16	-	-	-
f20	-	-	-	-	100.29	-	-	-
f21	-	309.59	-	318.30	184.09	193.72	184.09	179.73
f22	-	160.73	146.22	142.52	-	-	-	-
f23	-	193.19	-	-	-	187.65	180.13	-
f24	-	-	-	102.14	-	100.55	71.26	60.96
f25	-	-	-	-	-	-	146.74	-
f27	-	145.69	-	-	-	-	95.80	62.55
f29	213.78	239.91	-	-	148.85	-	-	-
f31	-	306.95	174.98	-	-	-	128.46	58.59
f34	-	313.02	-	-	-	-	-	-
f36	-	139.35	124.31	-	-	63.34	-	-
f37	-	153.41	146.87	-	72.84	101.54	55.42	-
f39	-	64.13	-	-	59.38	58.59	46.71	-
f45	-	-	-	-	-	-	43.81	-
f46	-	-	-	70.47	-	63.34	58.85	50.41
f55	-	67.46	-	-	-	-	-	-
f58	-	69.10	66.51	-	-	-	-	-
f59	71.26	84.72	99.76	-	-	-	-	-
f60	-	67.3	72.05	-	-	-	-	-
f61	57.8	61.36	82.34	-	-	-	-	-
f62	-	-	59.38	-	-	52.25	45.92	-
f63	-	62.81	-	-	46.71	-	-	-
f65	-	62.29	-	-	-	53.05	-	-
f66	62.55	84.19	-	67.30	-	55.42	49.48	-
f67	57	-	67.30	-	-	-	-	-
f68	-	62.55	-	49.09	-	-	-	-
f69	-	58.59	-	-	44.73	-	-	-
f70	-	57.14	-	-	-	-	-	42.75
f72	-	45.76	-	-	37.21	-	-	-
f73	-	43.15	-	-	-	-	-	-

are shown in Fig. 1. Two main groups can be distinguished: group I, formed by subgroups A and B, and group II, by subgroups C, D, E, F. Clade I excluded samples from sites 2, 4, 5, 6, and 12, which mainly included specimens of *Quercus arizonica s.l.* and *Q. arizonica* intro. *coccolobifolia*. Clade II excluded samples from site 9, which comprised samples of *Q.* aff. *convallata* and *Q. arizonica s. l.* All subgroups were heterogeneous, except subgroup C, which included three samples of the same taxa, *Q. arizonica* intro. *coccolobifolia* from site 12. A third of the samples of *Q. chihuahuensis* were grouped in subgroup A, from

Table 6. Results of the Kruskal-Wallis test for paired comparisons of samples to assess differences in the relative concentrations of phenolic compound in the leaves of the *Quercus* species under study

Pairs of species compared	H	Pr > H
Q. aff.*convallata (33.07) –Q. arizonica* intro. *coccolobifolia (41.87)*	3.02	0.0821
Q. aff. *convallata (59.51) –Q. arizonica s.l. (80.84)*	7.65	0.0057**
Q. aff. *convallata (30.25) –Q. arizonica* aff. *transmontana (34.55)*	0.72	0.3936
Q. aff. *convallata (32.61) –Q. chihuahuensis (48.41)*	9.32	0.0023**
Q. aff. *convallata (31.54) –Q. convallata (27.62)*	0.59	0.4418
Q. aff. *convallata (25.32) –Q. grisea (38.68)*	6.11	0.0134*
Q. aff. *convallata (26.62) –Q. undata (33.50)*	1.62	0.2029
Q. arizonica intro. *coccolobifolia (65.89) –Q. arizonica s.l. (66.66)*	0.00	0.9246
Q. arizonica intro. *coccolobifolia (25.12) –Q. arizonica* aff. *transmontana (20.97)*	1.04	0.3057
Q. arizonica intro. *coccolobifolia (29.37) –Q. chihuahuensis (33.25)*	0.70	0.3999
Q. arizonica intro. *coccolobifolia (26.48) –Q. convallata (15.53)*	7.4	0.0065**
Q. arizonica intro. *coccolobifolia (18.71) –Q. grisea (23.27)*	1.26	0.2611
Q. arizonica intro. *coccolobifolia (20.35) –Q. undata (19.09)*	0.09	0.7549
Q. arizonica s.l. (62.66) –Q. arizonica aff. *transmontana (54.75)*	0.76	0.3803
Q. arizonica s.l. (66.19) –Q. chihuahuensis (79.61)	2.89	0.0891
Q. arizonica s.l. (63.65) –Q. convallata (39.96)	6.43	0.0112*
Q. arizonica s.l. (57.14) –Q. grisea (66.09)	0.71	0.3973
Q. arizonica s.l. (57.75) –Q. undata (60.36)	0.06	0.8047
Q. arizonica aff. *transmontana (20.36) –Q. chihuahuensis (29.75)*	4.51	0.0335*
Q. arizonica aff. *transmontana (20.36) –Q. convallata (29.75)*	4.57	0.0324*
Q. arizonica aff. *transmontana (13.27) –Q. grisea (17.81)*	1.94	0.1634
Q. arizonica aff. *transmontana (14.55) –Q. undata (15.72)*	0.12	0.7191
Q. chihuahuensis (30.57) –Q. convallata (14.71)	12.87	0.0003**
Q. chihuahuensis (23.26) –Q. grisea (22.18)	0.05	0.8121
Q. chihuahuensis (24.45) –Q. undata (18.50)	1.71	0.1910
Q. convallata (10.87) –Q. grisea (18.54)	6.09	0.0136*
Q. convallata (11.40) –Q. undata (17.77)	4.20	0.0404*
Q. grisea (12.22) –Q. undata (10.77)	0.27	0.5988

*significant difference; **highly significant difference.

sites 1 and 3. Subgroup B mainly comprised samples of *Q.* aff. *convalata* from sites 7, 8 and 9, and *Q. arizonica s.l.* from sites 9 and 10. Subgroup D comprised samples of *Q. arizonica s.l.* from sites 2, 4, 5 and 6. Subgroup E included the samples of *Q. arizonica* intro. *coccolobifolia* from sites 10 and 11, and subgroup F included two samples of the same taxa *Q. arizonica* intro. g*risea* from site 2 and *Q. arizonica s.l.* from site 4. Despite the species-specific tendency reported for phenol profiles (Almaraz-Abarca *et al*., 2006; Veit *et al*., 1995), the species of *Quercus* analysed in the present study were not clearly distinguished by their phenol profiles.

Conclusion

The phenols synthesised by foliar tissues of the species of *Quercus* analysed here are diverse and some of the profiles are complex (e.g., that of *Q. chihuahuensis*). The compounds are produced in different ways and can reach very high concentrations. The variability in the phenol composition and the amounts of those compounds in the leaves hampered identification of some trends in the patterns of accumulation. This is the first report on the quantitative and qualitative composition of foliar phenolic compounds in selected *Quercus* tree species of Mexico. Further chemo-taxonomic studies including the analysis of terpenoid profiles in other types of tissues may yield more conclusive results.

Acknowledgement

The authors are grateful to Socorro González Elizondo for help with taxonomical identification of the samples. One of the authors is grateful to the Comisión de Fomento

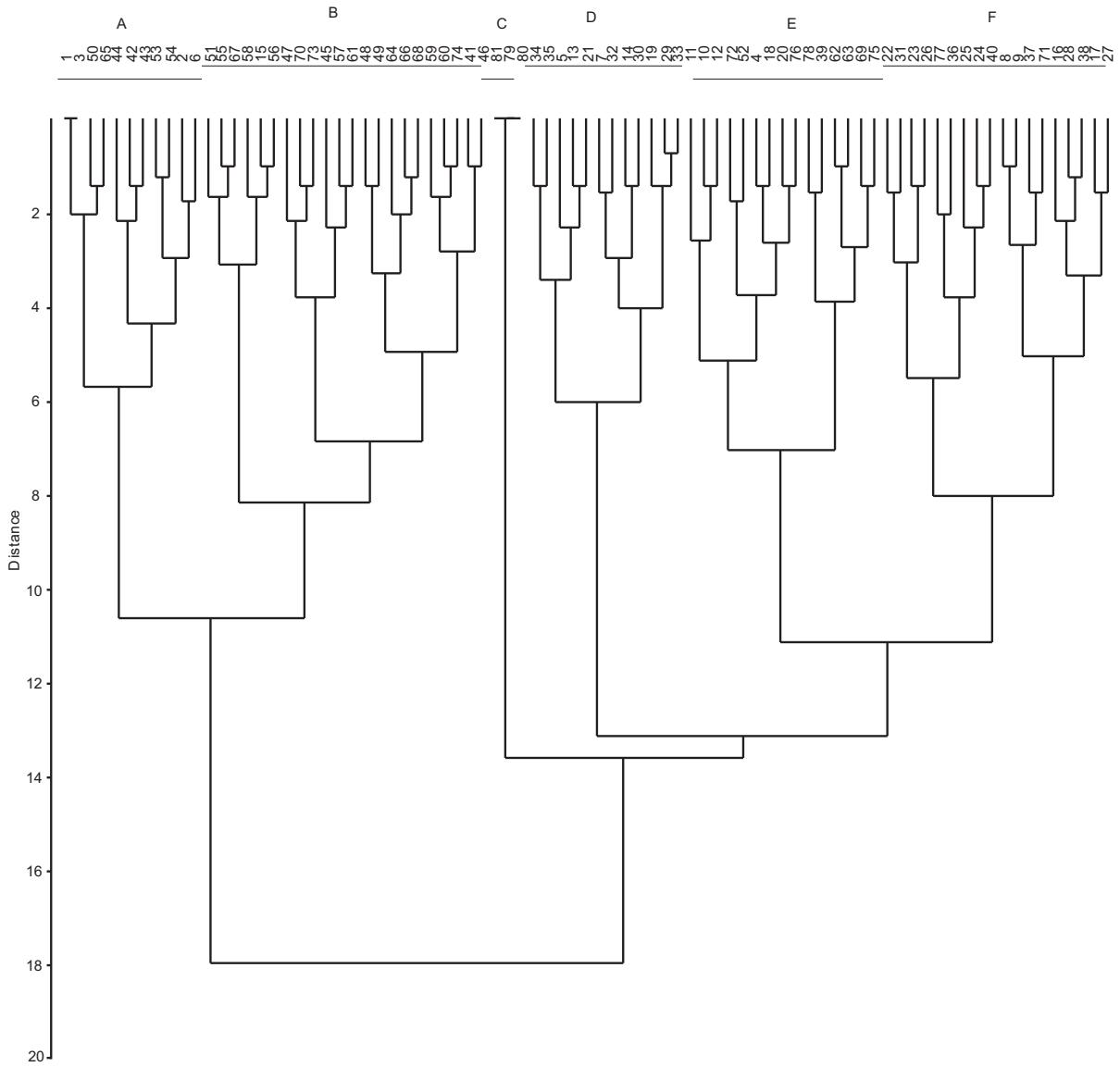

Fig. 1. Results of cluster analysis comparing foliar phenol profiles of 81 specimens of *Quercus arizonica s.l., Q. chihuahuensis, Q. grisea, Q. undata, Q. arizonica intro. coccolobifolia, Q. arizonica* aff. *transmontana, Q. convallata* and *Q.* aff. *convallata*. The numbers of the samples correspond to those shown in Table 1.

a las Actividades Académicas del Instituto Politécnico Nacional (COFAA IPN) for research funding. We are also grateful to two anonymous reviewers for their guidance in correcting the manuscript.

References

Abdala, L.R., Seeligmann, P. 1995. Flavonoids in *Tagetes zipaquirensis* and their chemosystematic significance. *Biochemical Systematics and Ecology*, **23:** 871-872.

Almaraz-Abarca, N., Campos, M.G., Delgado-Alvarado, A., Ávila-Reyes, J.A., Naranjo-Jiménez, N., Herrera-Corral, J., Tomatas, A.F., Almeida, A.J., Vieira, A. 2007. Fenoles del polen de *Stenocactus, echinocereus y Mammillaria* (Cactaceae). *Polibotánica*, **23:** 37-55.

Almaraz-Abarca, N., González-Elizondo, M.S., Tena-Flores, J.A., Ávila-Reyes, J.A., Herrera-Corral, J., Naranjo-Jiménez, N., 2006. Foliar flavonoids distinguish *Pinus leiophylla* and *Pinus chihuahuana* (Confierales: Pinaceae). *Proceedings of the Biological Society of Washington*, **119:** 426-436.

Amarowicz, R., Troszyñska, A., Barylko-Pikielna, N., Shahidi, F. 2004. Polyphenolics extracts from legume seeds: correlations between total antioxidant activity, total phenolics content, tannins content and astringency. *Journal of Food Lipids*, **11:** 278-286.

Bangou, M.J., Almaraz-Abarca, N., Méda, N.T.R., Zeba, B., Kiendrebéogo, M., Millogo-Rasolodimby, J., Nacoulma, O.G. 2011. Polyphenolic composition of *Lantana camara* and *Lippia chevalieri*, and their antioxidant and antimicrobial activities. *International Journal of Phytomedicine*, **4:** 115-124.

Borazan, A., Babaç, M.T. 2003. Morphometric leaf variation in oaks (*Quercus*) of Bolu, Turkey. *Annales Botanici Fennici*, **40:** 233-242.

Borges, L.L., Alves, S.F., Sampaio, B.L., Conceição, E.C., Bara, M.T.F., Paula, J.R. 2013. Environmental factors affecting the concentration of phenolic compounds in Myrcia tomentosa leaves. *Brazilian Journal of Pharmacognosy*, **23:** 230-238.

Campos, M.G., Markham, K.R. 2007. *Structure Information from HPLC and on-line Measured Absortion Spectra-flavone, Flavonols and Phenolic Acids*. 118 pp., Coimbra University Press, Portugal.

Emerenciano, V.P., Militão, J.S.L.T., Campos, C.C., Romoff, P., Kaplan, M.A.C., Zambon, M., Brant, A.J.C. 2001. Flavonoids as chemotaxonomic markers for Asteraceae. *Biochemical Systematrics and Ecology*, **29:** 947-957.

Falleh, H., Ksouri, R., Medini, F., Guyot, S., Abdelly, C., Magné, C. 2011. Antioxidant activity and phenolic composition of the medicinal and edible halophyte *Mesembryanthemum edule* L. *Industrial Crops and Products*, **34:** 1066-1071.

Fiasson, J., Gluchoff-Fiasson, L.K., Dahlgren, G. 1997. Flavonoid patterns in European *Ranunculus* L. subgenus *Batrachium* (Ranunculaceae). *Biochemical Systematics and Ecology*, **25:** 327-333.

Gobbo-Neto, L., Lopes, N.P. 2007. Plantas medicinais: fatores de influência no conteúdo de metabólitos secundários. *Quim Nova*, **30:** 374-381.

González-Rodríguez, A., Arias, D.M., Valencia, S., Oyama, K. 2004. Morphological and RAPD analysis of hybridization between *Quercus affinis* and *Quercus laurina* (Fagaceae), two Mexican red oaks. *American Journal of Botany*, **91:** 401-409.

Gurpreet, K., Mohammad, A., Sarwar, A.M. 2008. *Quercus infectoria* galls possess antioxidant activity and abrogates oxidative stress-induced functional alterations in murine macrophages. *Chemico-Biological Interactions*, **171:** 272-282.

Hadacek, F. 2002. Secondary metabolites as plant traits: current assessment and future perspectives. *Critical Reviews in Plant Science*, **21:** 273-322.

Hammer, O., Harper, D.A.T., Ryan, P.D. 2001. PAST: Paleontological statistics software for education and data analysis. *Paleontologia Electronica*, **4:** 1-9.

Harborne, J.B., Williams, C.A. 2000. Advance in flavonoid research since 1992. *Phytochemistry*, **55:** 481-504.

Iftikhar, B., Perveen, S., Malik, S., Sultana, N., Arayne, S., Muhammad, P. 2009. Structural determination of quercusides A and B, new flavonoid flucosides from *Quercus incana*, by 1D and 2D NMR. *Spectroscopy Magnetic Resonance in Chemistry*, **47:** 605-608.

Ishimaru, K., Ishimatsu, M., Nonaka, G-I., Mihashi, K., Iwase, Y., Nishioka, I. 1988. Tannins and related compounds. LXXI. Isolation and characterization of mongolicins A and B, novel flavono-ellagitannins from *Quercus mongolica* var. grosseserrata. *Chemical & Pharmaceutical Bulletin*, **36:** 3312-3318.

Ishimaru, K., Nonaka, G.I., Nishioka, I. 1987. Flavan-3-ol and procyanidin glycosides from *Quercus miyagii*. *Phytochemistry*, **26:** 1167-1170.

Jung-Il, K., Ho-Hyun, K., Sungun, K., Kyoung-Tae, L., In-Hye, H., Wan-Kyunn, W. 2008. Antioxidative compounds from *Quercus salicina* blume stem. *Archives of Pharmacal Research*, **31:** 274-278.

Karageorgou, P., Manetas, Y. 2006. The importance of being red when young: anthocyanins and the protection of young leaves of *Quercus coccifera* from insect herbivory and excess light. *Tree Physiology*, **26:** 613-621.

Karioti, A., Tooulakou, G., Bilia, A.R., Psaras, G.K., Karabourniotis, G., Skaltsa, H. 2011. Erinea formation on *Quercus ilex* leaves: Anatomical, physiological and chemical responses of leaf trichomes against mite attack. *Phytochemistry*, **72:** 230-237.

Kruskal, W.H., Wallis, A.W. 1952. Use of ranks in one-criterion variance analysis. *Journal of American Statistical Association*, **47:** 583-621

Lozoya-Saldaña, H., Rivera-Hinojosa, R., Colinas-León, M.T. 2007. Fenoles, peroxidasas y fenilalanina amonio-liasa: su relación con la resistencia genética de clones de papa (*Solanun tuberosum* L.) contra el tizón tardío (Phytophthora infestans Mont. De Bary). *Agrociencia*, **41:** 479-489.

Mabry, T.J., Markham, K.M., Thomas, M.B. 1970. *The*

Systematic Identification of Flavonoids. 354 pp. Springer-Verlag, New York, USA.

Marinova, D., Ribarova, F., Atanassova, D. 2005. Total phenolics and total flavonoids in Bulgarian fruits and vegetables. *Journal of the University of Chemical Technology and Metallurgy*, **40:** 255-260.

Meyer, S., Louis, J., Moise, N., Piolot, T., Baudin, X., Cerovic, Z.G. 2009. Developmental changes in spatial distribution of in vivo fluorescence and epidermal UV absorbance over *Quercus petraea* leaves. *Annals of Botany*, **104:** 621-633.

Míka, V., Kubáò, V., Klejdus, B., Odstrèilová, V., Nerušil, P. 2005. Phenolic compounds as chemical markers of low taxonomic levels in the family Poaceae. *Plant Soil Environment*, **51:** 506-512.

Miller, D.P., Howell, G.S., Michaelis, C.S., Dickmann, D.I. 1992. The content of phenolic acid and aldehide flavor components of white oak as affected by site and species. *American Journal of Enology and Viticulture*, **43:** 333-338.

Monteiro, J.M., Albuquerque, U.P., Lins Neto E.M.F., Araújo, E.L, Albuquerque, M.M, Amorim E.L.C. 2006. The effects of seasonal climate changes in the Caatinga on tannin level. *Brazilian Journal of Pharmacognosy*, **16:** 338-344.

Rivas-Arreola, M.J., Rocha-Guzmán, N.E., Gallegos-Infante, J.A., González-Laredo, R.F., Rosales-Castro, M., Bacon, J.R., Rong (Tsao) Cao, Proulx, A., Intriago-Ortega, P. 2010. Antioxidant activity of oak (*Quercus*) leaves infusions against free radicals and their cardioprotective potential. *Pakistan Journal of Biological Sciences*, **13:** 537-545.

Rodríguez, I., Romero, S. 2007. Arquitectura foliar de diez especies de encino (*Quercus, Fagaceae*) de México. *Acta Botánica Mexicana*, **81:** 9-34.

Romussi, G., Parodi, B., Caviglioli, G. 1991. Flavonoid glycosides from *Quercus pubescens* Willd., *Quercus cerris* L. and *Quercus ilex* L. 14. Contents of Cupuliferae. *Pharmazie*, **46:** 679.

Romussi, G., Bignardi, G., Pizza, C. 1988. Constituents of cupuliferae, XII. Minor acylated flavonoids from *Quercus cerris* L. *European Journal of Organic Chemistry*, **10:** 989-991.

Rzedowski, J. 2006. *Vegetación de México*. 504 pp. 1ª Edición Digital. Comisión Nacional para el conocimiento y Uso de la biodiversidad. México.

Salminen, J.P., Roslin, T., Karonen, M., Sinkkonen, J., Pihlaja, K., Pulkkinen, P. 2004. Seasonal variation in the content of hidrolizable tannins, flavonoid glycosides, and proanthocyanidins in oak leaves. *Journal of Chemical Ecology*, **30:** 1693-1711.

Santos, S.C., Costa W.F., Batista, F., Santos, L.R., Ferri P.H, Ferreira, H.D, Seraphin J.C. 2006. Seasonal variation tannins in barks of barbatimao. *Brazilian Journal of Pharmacognosy*, **16:** 552-556.

Valencia, A.S. 2004. Diversidad del género Quercus (Fagaceae) en México. *Boletín de la Sociedad Botánica de México*, **75:** 33-53.

Van Alstyne, K.L., McCarthy III, J.J., Hustead C.L., Kearns L.J. 1999. Pholorotannin allocation among tissues of Northeastern Pacific kelps and rockweeds. *Journal of Phycology*, **35:** 483-492.

Veit, M., Beckert, C., Höhne, C., Bauer, K., Geiger, H. 1995. Interspecific and intraspecific variation of phenolics in the genus *Equisetum* subgenus *Equisetum*. *Phytochemistry*, **38:** 881-891.

Wang, L.L., Jiang, M.X., Xu, S.X., Sun, Q.S., Zeng, G.Y., Zhou, Y.J. 2010.Two acylated flavonoid glycosides from the leaves of *Quercus dentata*. *Natural Product Communications*, **5:** 1597-1599.

Warren, J.M., Bassman, J.H., Mattinson, D.S., Fellman, J.K., Edwards, G.E., Robberecht, R. 2002. Alteration of foliar flavonoid chemistry induced by enhanced UV-B radiation in field ground *Pinus ponderosa*, *Quercus rubra* and *Pseudotsuga menziessi*. *Journal of Photochemistry and Photobiology B: Biology*, **66:** 125-133.

Yeon, S.L., Jin Kyu, K., Young Soo, B., Moo-Ho, W., Il-Jun, K., Soon Sung, L. 2011. Inhibitory effect of glucodistylin from the bark of *Quercus acutissima* on human recombinant aldose reductase and sorbitol accumulation. *Archives of Pharmacal Research*, **34:** 211-215.

Pak. j. sci. ind. res. Ser. A: phys. sci. 2015 **58** (2) 90-98

Automated Method for Delineating Watershed, Drainage Pattern and Calculation of Flow Accumulation in Punjab Province using Digital Elevation Model

Umair bin Zamir* and Jamil Hassan Kazmi
Department of Geography, University of Karachi, Karachi-75270, Pakistan

(receivd November 26, 2013; revised June 1, 2014; accepted June 25, 2014)

Abstract. Delineation of the watershed and drainage is among the prior requirement of any organised hydrological study. Delineating watershed is important for elucidating the geo-hydrological conditions of any geographical space. This study aims to explore the vitality of Digital Elevation Model (DEM) data in calculating the flow accumulation, flow length, drainage pattern and watershed basin delineation of Punjab as well as elevational profiling district wise and delineating the catchment density. The potential hydrological system developed is based on 1 arc second Aster GDEM data. Depression less DEM is developed by filling process. Furthermore flow accumulation, drainage pattern and watershed is demarcated on the basis of derived stream channels. This study presents the effectiveness of DEM data for hydrological studies and introduces a better method of water management in Punjab province of Pakistan.

Keywords: DEM, watershed, flow accumulation, drainage pattern

Introduction

The advent of satellite technology and access to a variety of remote sensing and GIS data types increases the prospects of understanding the terrain of geographical space with remarkable accuracy. GIS and remote sensing offers the combination of apparatus to speed up the decision and helps in enumerating more precise results.

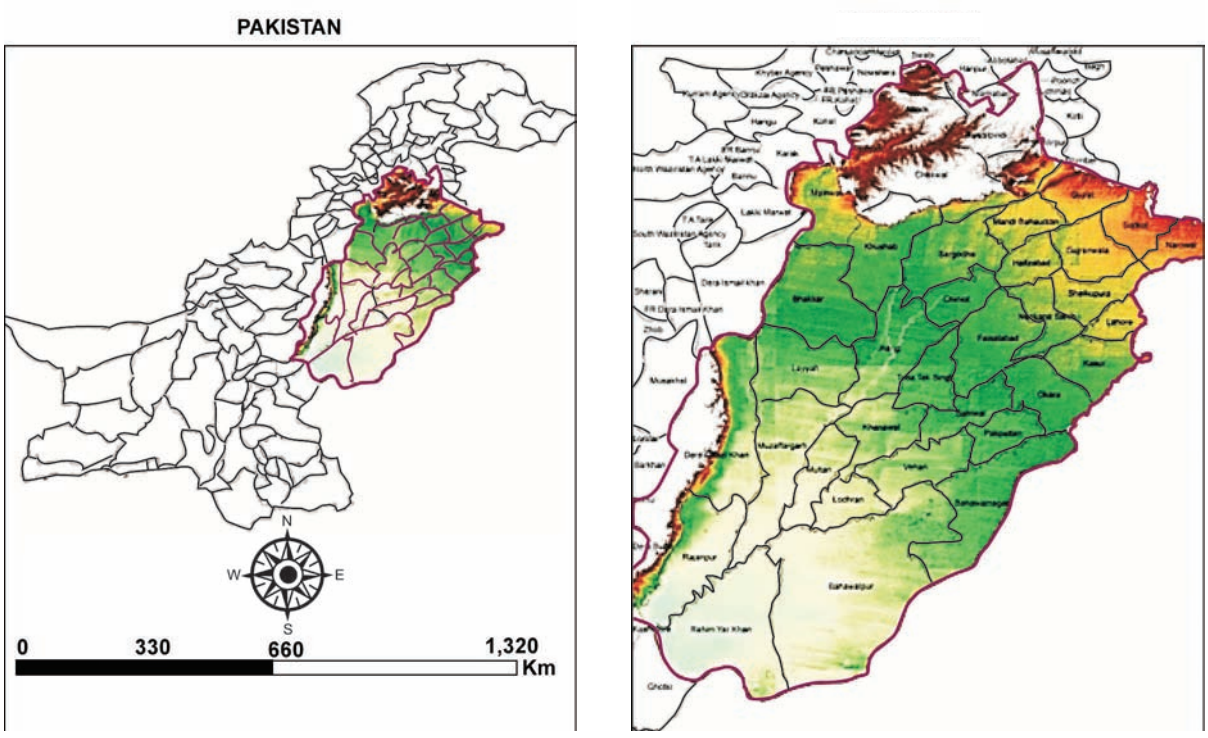

Fig. 1. Study area (Punjab province).

*Author for correspondence; E-mail: binzamir@hotmail.com

Hydrological risks and jeopardies can easily be cut and dried and tactics formulated to alleviate the loss and increases the decision making abilities. Geographic Infor-mation System (GIS) and Remote Sensing (RS) is an authoritative combination of technology, which is helpful in hydrological modeling, monitoring and mitigation. By using the Digital Elevation Model (DEM) automated and accurate watershed delineation and development of drainage network is possible, which is comparatively less time consuming, more accurate and provide easily calculable measurements than traditional manual techniques. GIS and RS have the aptitude to perform watershed management and help in developing high accuracy oriented hydrological mapping which promotes the Spatial Decision Support System (SDSS).

Materials and Methods

Study area. Various techniques are used for getting the desired objectives; methodological framework is classified into six stages (Fig. 2).

Data acquisition. The major data was obtained on request, from the United States Geological Survey (USGS). Most of the files were downloaded from there by assigning the Keyhole Markup Language (KML), file for the study area and by uploading it. Digital Elevation Model (DEM) raster scenes of the study area were selected and downloaded.

DEM reconditioning. DEM data obtained is not perfect for using until it is reconditioned. Sinks and Peaks (Fig. 3) are among the common resolution errors, therefore it is required to fill the sinks for proper delineation of watershed and streams. Filling of DEM helps in avoiding discontinuity of the derived drainage network. The fill function in ArcGIS recapitulates until Z limits are filled (Tarboton *et al*., 1991).

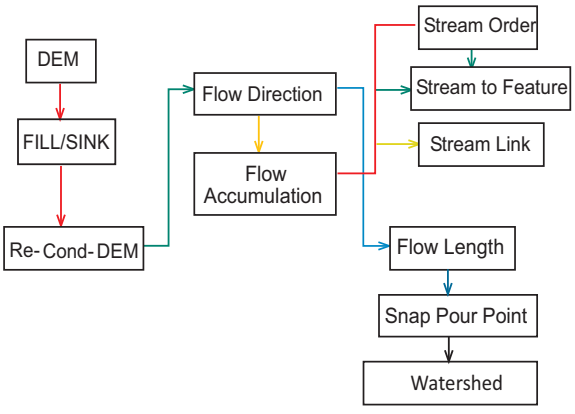

Fig. 2. Methodological framework (steps for delineating watershed).

Calculating flow direction. Flow direction is calculated by directing steepest lineage obtained from each cell value (Fig. 4). The calculation is made as Change in z-value/distance* 100. All distances calculated are focusing cell centres. In case of cell extent is 1 then the distance between two orthogonal cells is 1, while if two cells flow towards each other are considered as sinks and have ill-defined flow direction (Jenson and Domingue, 1988).

Calculating flow accumulation. Flow accumulation is calculated by using flow accumulation tool in which cell values are designated as weightage flowing into each downslope cell in the output (Fig. 5). Cells of high

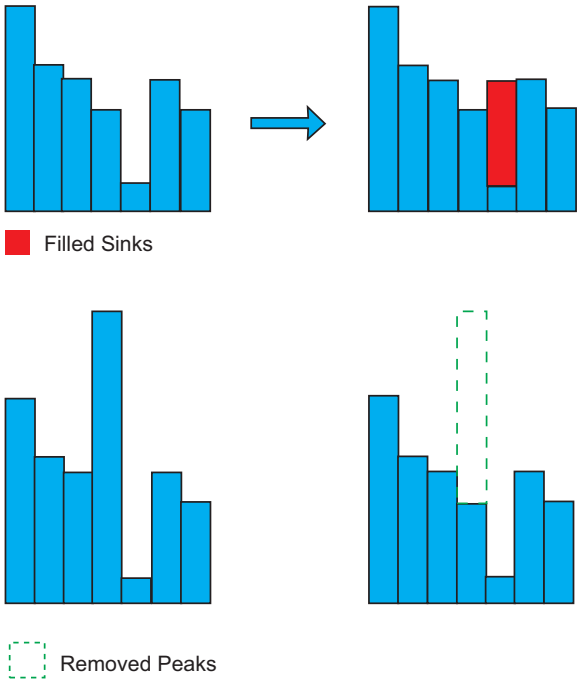

Fig. 3. Profile view of fill.

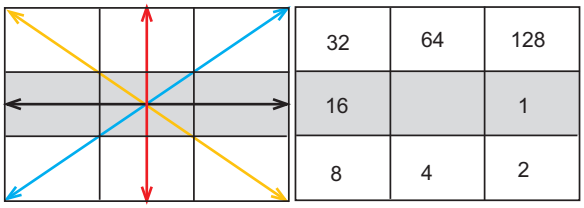

Fig. 4. Flow direction.

flow accumulation identifying areas of concentrated flow, cells with 0 accumulation values identified as ridges. Extracted flow accumulation used to create a stream network which requires to assign threshold, setnull (flowacc < 100, 1) (Tarboton *et al*., 1991).

Identifying stream network. The output obtained from flow accumulation was further used for the identification of stream network, by applying the threshold using map algebra to the flow accumulation raster a stream network is outlined.

0	0	0	0	0	0
0	1	1	2	2	0
0	3	7	5	4	0
0	0	0	15	0	1
0	0	0	1	20	0
0	2	4	8	30	2

Fig. 5. Flow accumulation grid.

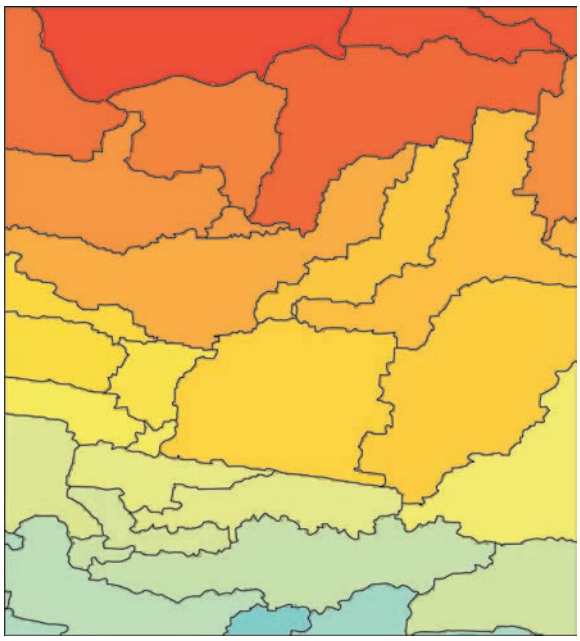

Fig. 6. Watershed.

Delineating watershed. The final objective of this study is delineating watershed. Watershed is the upslope area which is playing its role in providing flow to given location, this type of zone is also referred as the catchment. For this to achieve flow direction raster is used in ArcGIS watershed function to determine the contributing areas (Fig. 6). In this study, flow accumulation threshold with specific pour point is used to delineate the watershed.

Results and Discussion

Advancement in Geographical Information System (GIS) and Remote Sensing (RS) in terms of availability of data and the advent of new tools increases the efficiency typically in hydrological studies which lead towards minimizing the expenses of acquisition of data as well as reduces the time and effort in performing the task with accuracy. Combo aid of GIS and RS helps in addressing the water resource issues and helps in investigating and modeling the solution of the issues. From the last two decades information acquisition paradigm rapidly shifted towards digital representations of topography (Martz and Garbrecht, 1992; Moore *et al*., 1991; Jenson and Domingue, 1988; Mark, 1984). The automated method was applied to the district of Punjab, Pakistan in order to demarcate the watershed, drainage pattern and flow accumulation (Fig. 7). In addition, elevation based characteristics are also extracted district wise (Table 1). By using 1 arc-second Aster GDEM Digital Elevation Model data statistical variational maps are developed representing the different district wise elevation characteristics (Fig. 8). This will be helpful in modeling the different hydrological studies. Furthermore, extracted elevation data is used in order to get the flow direction share district wise (Table 2) which helps in developing the flow accumulation probability plot district wise categorizes the Punjab in low, moderate and high accumulation probability zone (Fig. 9). Muzafargarh, Rajanpur are at high probability of accumulation, and Jhang, Multan, Rahimyarkhan and Bhawalpur are in the moderate accumulation category, while the remaining districts are in the low accumulation zone. Furthermore, the catchment area is delineated (Fig. 10) which is overlaid on the district boundaries of Punjab so that the catchment density district wise is calculated using polygon in polygon analysis (Fig. 11). It represents the east and the

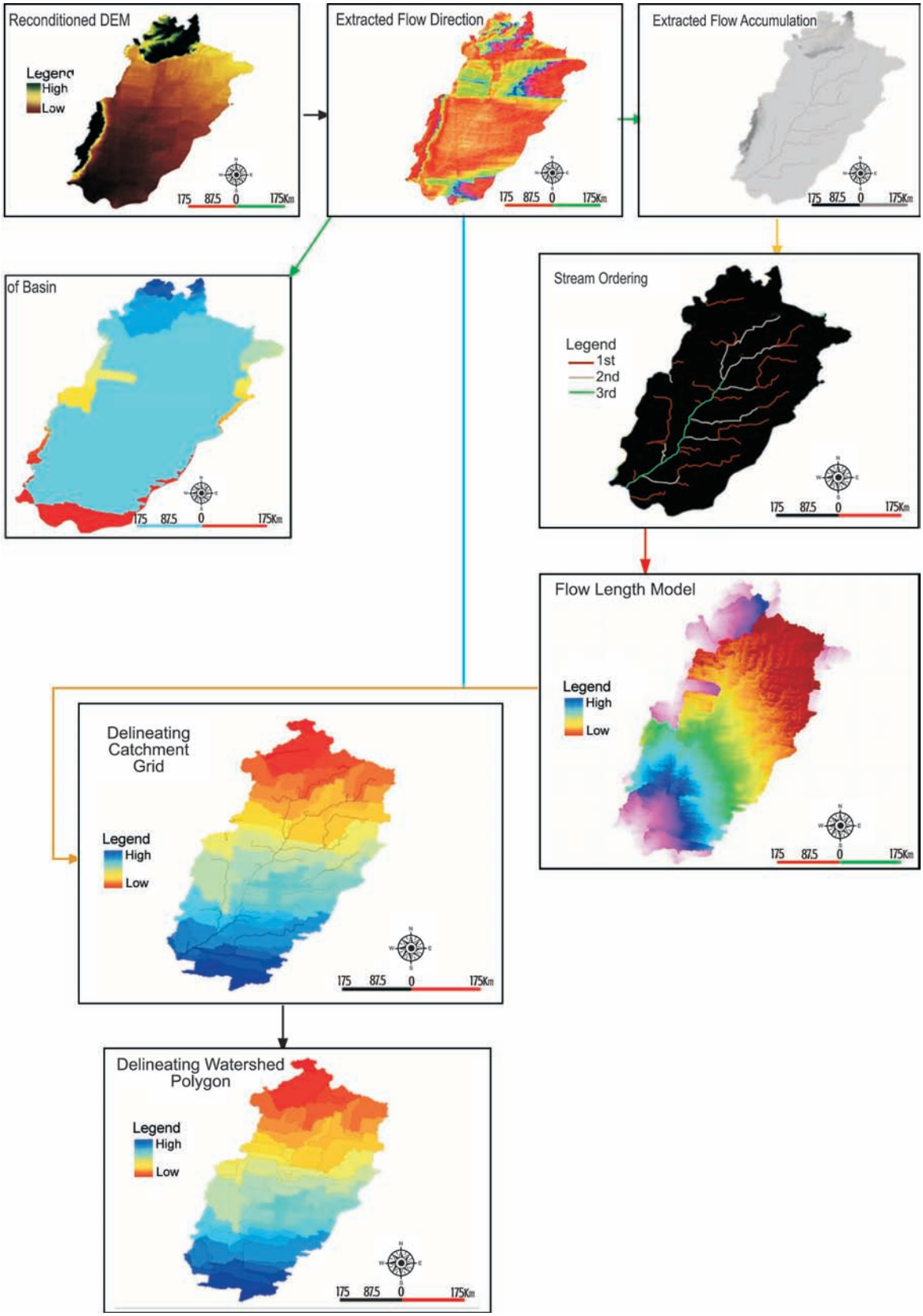

Fig. 7. Delineated results (steps from reconditioning to watershed delineation).

Table 1. Elevation based characteristics of Punjab districts

Id	District names	Zone_ code	Count	Area	Min	Max	Range	Mean	STD	SUM	Vari- ety	Majo- rity	Mino- rity	Median
2	Attock	2	9232	0.64111100000	214	961	747	395.38300000000	79.06030000000	3650180.00000000000	457	361	221	392
21	Bahawalnagar	21	11553	0.80229200000	120	179	59	146.81800000000	9.76701000000	1696190.00000000000	60	146	172	147
27	Bahawalpur	27	31825	2.21007000000	79	170	91	112.31200000000	14.46050000000	3574330.00000000000	90	112	79	112
18	Bhakkar	18	11158	0.77486100000	125	197	72	169.69400000000	11.53430000000	1893450.00000000000	62	163	195	168
10	Chakwal	10	9079	0.63048600000	236	1211	975	492.65500000000	136.21600000000	4472820.00000000000	675	481	237	472
36	Chiniot	36	3696	0.25666700000	136	199	63	167.88200000000	8.47456000000	620493.00000000000	55	161	145	168
29	Dera Ghazi Khan	29	22912	1.59111000000	66	2213	2147	462.14500000000	408.29200000000	10588700.00000000000	1793	109	69	283
19	Faisalabad	19	7966	0.55319400000	146	198	52	172.26500000000	9.75735000000	1372260.00000000000	53	176	146	174
8	Gujranwala	8	4987	0.34631900000	189	242	53	217.34400000000	9.60113000000	1083900.00000000000	52	224	189	221
9	Gujrat	9	4336	0.30111100000	203	376	173	250.73900000000	30.17700000000	1087200.00000000000	159	222	203	244
11	Hafizabad	11	3236	0.22472200000	177	219	42	197.18800000000	7.33245000000	638099.00000000000	42	199	177	198
22	Jhang	22	8338	0.57902800000	110	178	68	149.14000000000	14.48910000000	1243530.00000000000	68	161	177	153
13	Jhelum	13	4846	0.33652800000	179	818	639	307.19300000000	108.29700000000	1488660.00000000000	464	193	179	275
12	Kasur	12	5347	0.37131900000	157	211	54	185.96400000000	9.59967000000	994347.00000000000	55	179	211	186
33	Khanewal	33	5798	0.40263900000	105	158	53	130.37500000000	8.99953000000	755914.00000000000	52	128	105	129
16	Khushab	16	9006	0.62541700000	132	1408	1276	296.04900000000	236.95900000000	2666210.00000000000	759	177	143	180
6	Lahore	6	2340	0.16250000000	187	218	31	205.92600000000	4.80421000000	481867.00000000000	31	210	187	206
26	Layyah	26	8518	0.59152800000	118	170	52	138.98500000000	10.28370000000	1183880.00000000000	52	133	170	136
32	Lodhran	32	3903	0.27104200000	101	126	25	111.83000000000	4.41416000000	436472.00000000000	26	109	101	112
1	Mainwali	1	7814	0.54263900000	163	1390	1227	282.13600000000	150.93800000000	2204610.00000000000	675	185	163	212
14	Mandi Bahauddin	14	3696	0.25666700000	182	255	73	207.91800000000	9.07886000000	768466.00000000000	55	205	182	206
31	Multan	31	4944	0.34333300000	93	132	39	111.43700000000	8.98876000000	550946.00000000000	38	101	95	109
34	Muzaffargarh	34	11132	0.77305600000	77	142	65	113.62300000000	11.46190000000	1264860.00000000000	58	122	140	116
35	Nankana Sahib	35	3756	0.26083300000	163	209	46	189.24800000000	7.14245000000	710816.00000000000	47	193	208	190
4	Narowal	4	3096	0.21500000000	215	319	104	251.47200000000	20.14980000000	778557.00000000000	100	241	311	247
15	Okara	15	5929	0.41173600000	152	192	40	168.59100000000	6.45099000000	999577.00000000000	40	167	189	168
23	Pakpattan	23	3667	0.25465300000	132	168	36	151.79700000000	4.51015000000	556638.00000000000	33	151	139	151
20	Rahim Yar Khan	20	16184	1.12389000000	61	146	85	86.98670000000	13.63170000000	1407790.00000000000	84	78	146	84
28	Rajanpur	28	9675	0.67187500000	41	245	204	106.13800000000	29.24170000000	1026880.00000000000	188	94	41	100
3	Rawalpindi	3	6761	0.46951400000	318	2189	1871	598.83400000000	308.62100000000	4048720.00000000000	1122	485	318	494
25	Sahiwal	25	4331	0.30076400000	126	173	47	154.20700000000	9.53589000000	667872.00000000000	48	159	126	156
17	Sargodha	17	8048	0.55888900000	140	271	131	181.14100000000	12.00780000000	1457820.00000000000	72	184	143	183
7	Sheikupura	7	4413	0.30645800000	150	228	78	204.75700000000	7.74245000000	903593.00000000000	55	208	150	205
5	Sialkot	5	3945	0.27395800000	215	289	74	240.92400000000	12.45880000000	950445.00000000000	73	230	216	237
24	Toba Tek Singh	24	4426	0.30736100000	127	183	56	153.59800000000	9.95932000000	679825.00000000000	57	150	127	151
30	Vehari	30	5898	0.40958300000	111	156	45	129.09500000000	7.90672000000	761402.00000000000	46	131	153	130

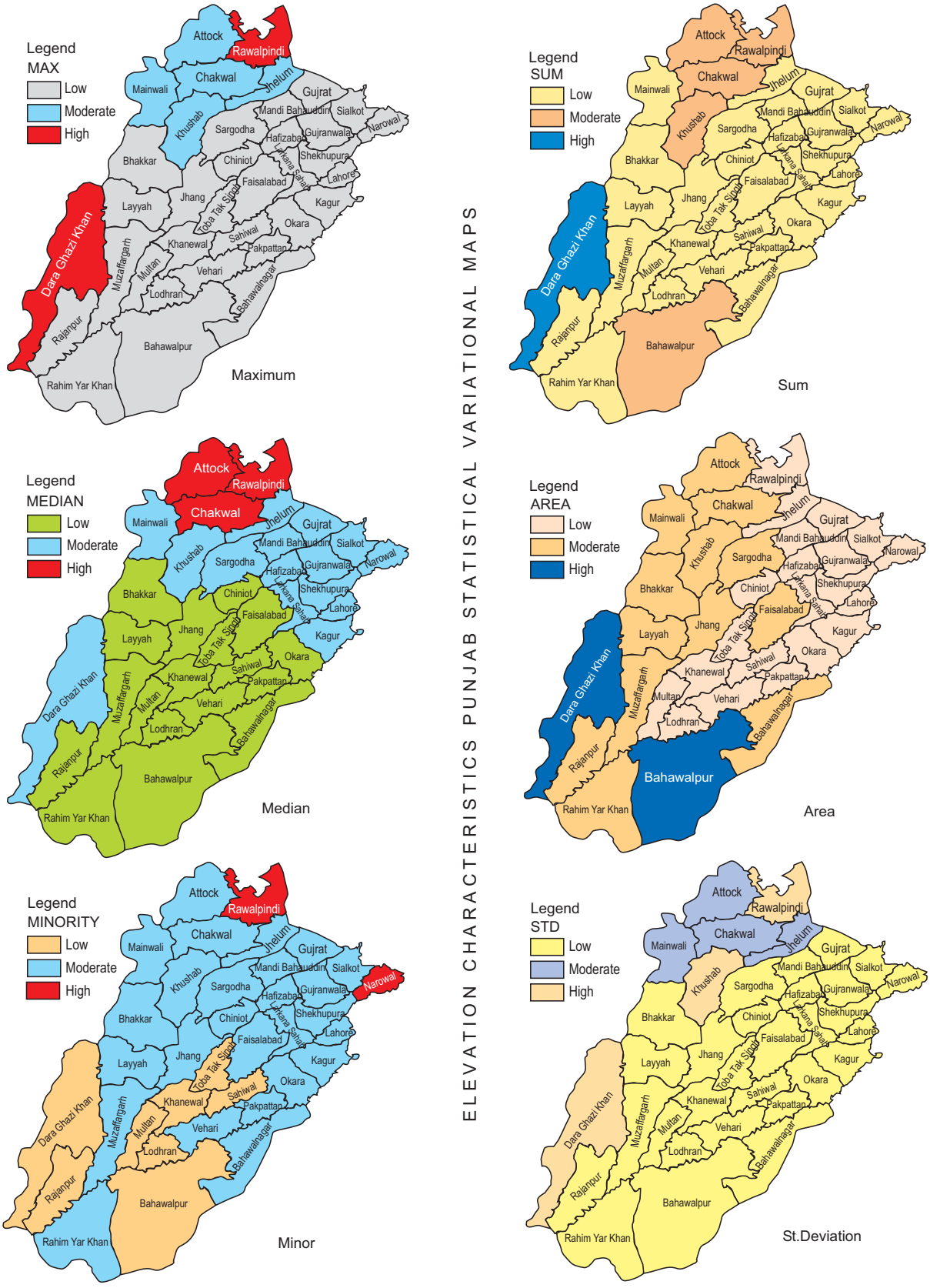

Fig. 8. Statistical variational map of Punjab district.

Table 2. Flow direction district-wise share of Punjab province

Id	District names	Zone_ code	Count	Area	Min	Max	Range	Mean	STD	SUM	Variety	Majority	Minority	Median
1	Mainwali	1	7814	0.54263900000	1	128	127	22.29640000000	32.25450000000	174224.00000000000	8	4	128	8
2	Attock	2	9232	0.64111100000	1	128	127	26.70220000000	31.25220000000	246515.00000000000	8	4	128	16
3	Rawalpindi	3	6761	0.46951400000	1	128	127	23.19110000000	32.91480000000	156795.00000000000	8	4	128	8
4	Narowal	4	3096	0.21500000000	1	128	127	11.91760000000	20.35740000000	36897.00000000000	8	4	128	4
5	Sialkot	5	3945	0.27395800000	1	128	127	19.91360000000	25.28990000000	78559.00000000000	8	16	128	16
6	Lahore	6	2340	0.16250000000	1	128	127	23.38590000000	29.65760000000	54723.00000000000	8	4	128	8
7	Sheikupura	7	4413	0.30645800000	1	128	127	18.88240000000	26.05810000000	83328.00000000000	8	4	128	8
8	Gujranwala	8	4987	0.34631900000	1	128	127	18.72070000000	25.66160000000	93360.00000000000	8	4	128	8
9	Gujrat	9	4336	0.30111100000	1	128	127	14.91470000000	22.08070000000	64670.00000000000	8	4	128	8
10	Chakwal	10	9079	0.63048600000	1	128	127	38.66110000000	38.92780000000	351004.00000000000	8	64	2	32
11	Hafizabad	11	3236	0.22472200000	1	128	127	20.91500000000	25.55000000000	67681.00000000000	8	16	128	16
12	Kasur	12	5347	0.37131900000	1	128	127	19.78380000000	26.70510000000	105784.00000000000	8	4	128	8
13	Jhelum	13	4846	0.33652800000	1	128	127	19.27450000000	33.62220000000	93404.00000000000	8	4	32	4
14	Mandi Bahauddin	14	3696	0.25666700000	1	128	127	19.76730000000	27.98950000000	73060.00000000000	8	4	128	8
15	Okara	15	5929	0.41173600000	1	128	127	19.19620000000	24.08820000000	113814.00000000000	8	16	128	16
16	Khushab	16	9006	0.62541700000	1	128	127	20.64830000000	33.50930000000	185959.00000000000	8	4	32	4
17	Sargodha	17	8048	0.55888900000	1	128	127	19.25390000000	26.43180000000	154955.00000000000	8	4	128	8
18	Bhakkar	18	11158	0.77486100000	1	128	127	22.08860000000	31.08660000000	246465.00000000000	8	4	128	8
19	Faisalabad	19	7966	0.55319400000	1	128	127	19.03380000000	25.88000000000	151623.00000000000	8	4	128	8
20	Rahim Yar Khan	20	16184	1.12389000000	1	128	127	26.25290000000	29.21340000000	424877.00000000000	8	16	2	16
21	Bahawalnagar	21	11553	0.80229200000	1	128	127	25.77060000000	27.91050000000	297728.00000000000	8	16	128	16
22	Jhang	22	8338	0.57902800000	1	128	127	22.50190000000	30.07520000000	187621.00000000000	8	16	128	8
23	Pakpattan	23	3667	0.25465300000	1	128	127	20.49880000000	25.02570000000	75169.00000000000	8	16	128	16
24	Toba Tek Singh	24	4426	0.30736100000	1	128	127	23.30770000000	26.06130000000	103160.00000000000	8	16	128	16
25	Sahiwal	25	4331	0.30076400000	1	128	127	20.98080000000	28.70750000000	90868.00000000000	8	4	128	8
26	Layyah	26	8518	0.59152800000	1	128	127	18.06180000000	28.09710000000	153850.00000000000	8	4	128	4
27	Bahawalpur	27	31825	2.21007000000	1	128	127	27.54080000000	29.27220000000	876487.00000000000	8	16	2	16
28	Rajanpur	28	9675	0.67187500000	1	128	127	18.29560000000	34.30310000000	177010.00000000000	8	4	32	4
29	Dera Ghazi Khan	29	22912	1.59111000000	1	128	127	23.49490000000	40.61880000000	538315.00000000000	8	1	32	4
30	Vehari	30	5898	0.40958300000	1	128	127	21.65170000000	25.75390000000	127702.00000000000	8	16	128	16
31	Multan	31	4944	0.34333300000	1	128	127	20.47920000000	24.57400000000	101249.00000000000	8	16	128	16
32	Lodhran	32	3903	0.27104200000	1	128	127	22.78610000000	23.85220000000	88934.00000000000	8	16	128	16
33	Khanewal	33	5798	0.40263900000	1	128	127	23.05420000000	27.99380000000	133668.00000000000	8	16	128	16
34	Muzaffargarh	34	11132	0.77305600000	1	128	127	19.72010000000	30.87410000000	219524.00000000000	8	4	32	4
35	Nankana Sahib	35	3756	0.26083300000	1	128	127	18.41450000000	23.37880000000	69165.00000000000	8	16	128	8
36	Chiniot	36	3696	0.25666700000	1	128	127	22.34060000000	27.15510000000	82571.00000000000	8	16	128	16

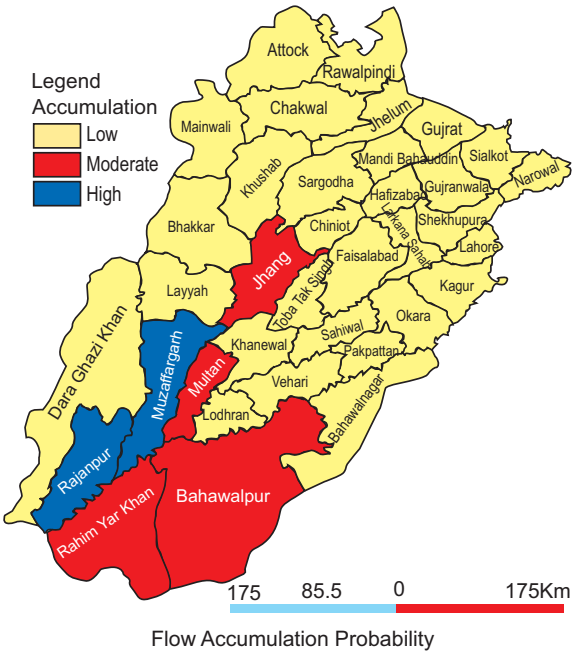

Fig. 9. Flow accumulation - district.

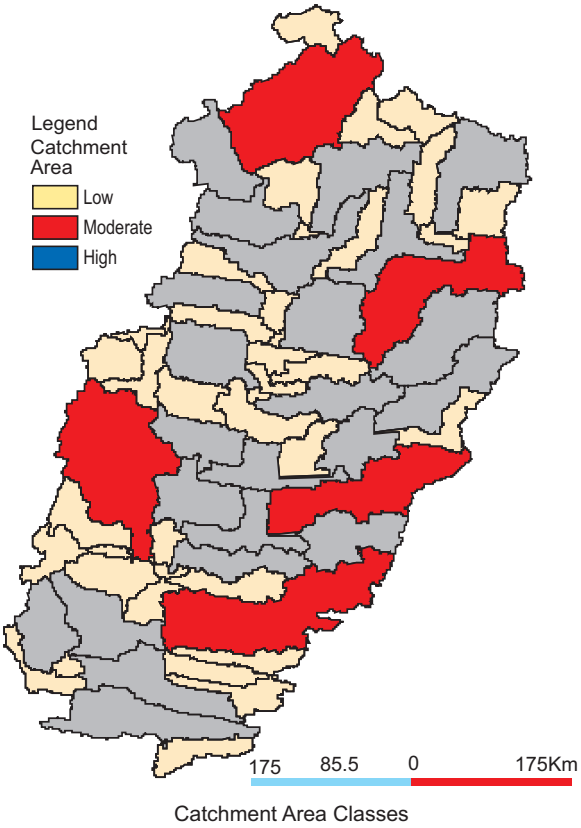

Fig. 10. Catchment zones.

westernmost districts of Punjab Bhawalpur and Dera Ghazi Khan is having a high catchment density encircling the 15 and 10 catchment polygon count respectively, (Table 3). While the Chakwal, Layyah, Kushab, Sargodha, Jhang, Bhakkar, Faisalabad districts are in moderate category and the remaining districts like Khanewal, Lodhran, Vehari, Pakpatan, Sahiwal, Okara, Toba tek Singh, Kasur, Nankana sahib, Hfizabad,

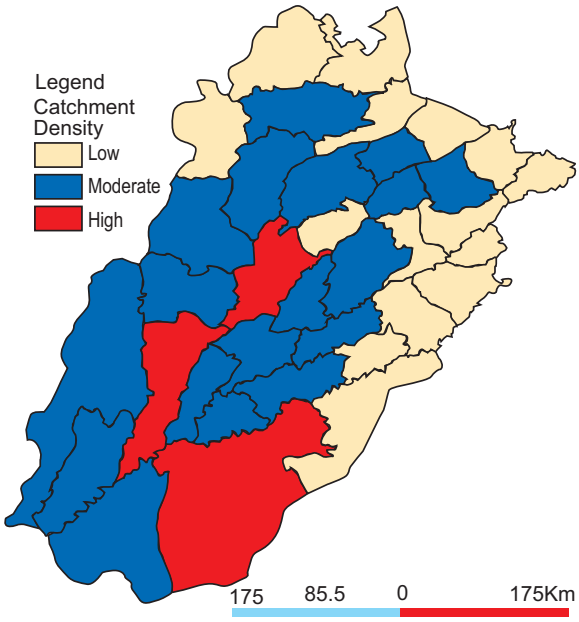

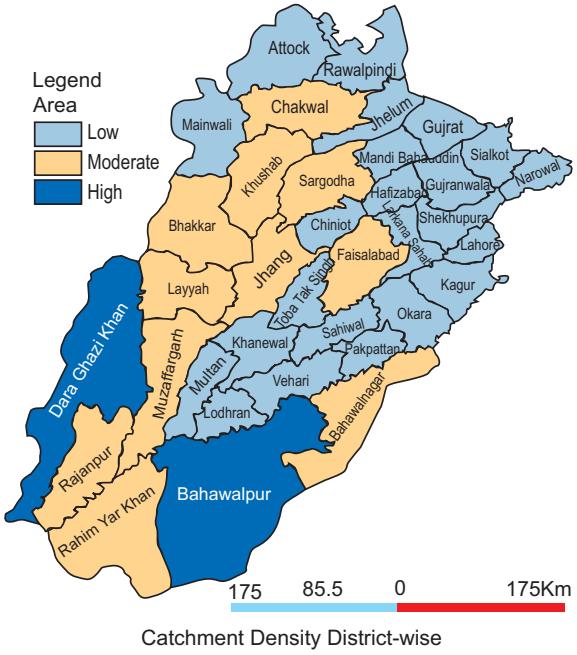

Fig. 11. Catchment density - district wise.

Table 3. Catchment Density and Counts

Id	Name	Province	Cat_Dis_Ar	Cat_Dis_Co
1	Mainwali	Punjab	4778780687	3
2	Attock	Punjab	3901439487	2
3	Rawalpindi	Punjab	2089692611	4
4	Narowal	Punjab	0	0
5	Sialkot	Punjab	1589225322	2
6	Lahore	Punjab	823028890	2
7	Sheikupura	Punjab	2603449112	4
8	Gujranwala	Punjab	3305395712	6
9	Gujrat	Punjab	3006925737	4
10	Chakwal	Punjab	6547563755	6
11	Hafizabad	Punjab	2362742972	6
12	Kasur	Punjab	2717603804	3
13	Jhelum	Punjab	3270190343	3
14	Mandi Bahauddin	Punjab	2687784067	6
15	Okara	Punjab	4070488303	5
16	Khushab	Punjab	6557651414	9
17	Sargodha	Punjab	5865371647	8
18	Bhakkar	Punjab	6797850003	8
19	Faisalabad	Punjab	5858808069	6
20	Rahim Yar Khan	Punjab	9913077272	10
21	Bahawalnagar	Punjab	7829835559	4
22	Jhang	Punjab	6119635818	14
23	Pakpattan	Punjab	2721978337	4
24	Toba Tek Singh	Punjab	3270587698	6
25	Sahiwal	Punjab	3205987304	7
26	Layyah	Punjab	6129910485	8
27	Bahawalpur	Punjab	22758088164	15
28	Rajanpur	Punjab	7239180864	10
29	Dera Ghazi Khan	Punjab	15165159536	10
30	Vehari	Punjab	4382527642	7
31	Multan	Punjab	3671622565	8
32	Lodhran	Punjab	2915417722	6
33	Khanewal	Punjab	4295591785	8
34	Muzaffargarh	Punjab	8266040301	15
35	Nankana Sahib	Punjab	2767148666	3
36	Chiniot	Punjab	2703181366	5

Chiniot, Gujranwala, Mandi bhauddin, Jehlum districts etc are in the low catchment density zone.

Conclusion

It is concluded that, GIS and Remote Sensing play a vital function in calculating and delineating the watershed, calculation of flow statistics, flow paths, stream network, drainage dynamics etc. It holds enough potential to address different hydrological associated issues. Development of watershed model using DEM and Hydrological tools provided in ArcGIS leading towards the accurate hydrological modeling as compared to the manual techniques or it is obvious that digital methods overcome the flaws of manual representation therefore, globally catchment geometric properties are preferably extracted by digital means. It is mandatory for the developing countries especially agro-based economic countries, like Pakistan to adopt such technological advancement for the better management of water and other resources. This study helps in understanding the usefulness of DEM data for hydrological studies and leads to derive a better technique of water management in Punjab province of Pakistan. Further calibration, adjustment and validation would give more precise results and enhance the possibilities for watershed and drainage pattern assessment. In the time to come, it will be indispensable to carry on this subject area to receive the optimal solutions for watershed management in the field region.

References

Jenson, S.K., Domingue, J.O. 1988. Extracting topographic structure from digital elevation data for geographic information system analysis. *Photogrammetric Engineering and Remote Sensing*, **54:** 1593-1600.

Mark, 1984. Link length distributions in drainage networks with lakes. *Water Resources Research*, **20:** 457-462.

Martz, L.W., Garbrecht, J. 1992. Numerical definition of drainage network and sub-catchment areas from digital elevation models. *Computers & Geosciences*, **18:** 747-761.

Moore, I.D., Grayson, R.B., Ladson, A.R. 1991. Digital terrain modelling: A review of hydrological, geomorphological and biological applications. *Hydrological Processes*, **5:** 3-30.

Tarboton, D.G., Bras, R.L., Rodriguez–Iturbe, I. 1991. On the extraction of channel networks from digital elevation data. *Hydrological Processes*, **5:** 81-100.

Pak. j. sci. ind. res. Ser. A: phys. sci. 2015 **58** (2) 99-105

DSC Cure Kinetics of an Unsaturated Polyester Resin Using Empirical Kinetic Model

Iram Abdullah

Pak-Korea Garment Technology Institute, SFDAC Building, ST # 2/30, Korangi Industrial Area, Korangi, Karachi, Pakistan

(received May 25, 2013; revised February 15, 2014; accepted February 20, 2014)

Abstract. In this paper, the kinetics of curing of unsaturated polyester resin initiated with benzoyl peroxide was studied. In case of unsaturated polyester (UP) resin, isothermal test alone could not predict correctly the curing time of UP resin. Therefore, isothermal kinetic analysis through isoconventional adjustment was used to correctly predict the curing time and temperature of UP resin. Isothermal kinetic analysis through isoconversional adjustment indicated that 97% of UP resin cures in 33 min at 120 °C. Curing of UP resin through microwaves was also studied and found that 67% of UP resin cures in 1 min at 120 °C. The crosslinking reaction of UP resin is so fast at 120 °C that it becomes impossible to predict correctly the curing time of UP resin using isothermal test and the burial of C=C bonds in microgels makes it impossible to be fully cured by microwaves at 120 °C. The rheological behaviour of unsaturated polyester resin was also studied to observe the change in viscosity with respect to time and temperature.

Keywords: isothermal kinetic, unsaturated polyester resin, microwave curing, rheology

Introduction

The unsaturated polyester (UP) resin is the thermosetting material used for composite applications such as the preparation of structural parts of automobiles, building materials, coating materials, electrical parts, etc. The thermosetting resins generally contain reactant groups. The composition of these reactant groups influences not only the curing rate but also the final mechanical properties of the material. Therefore, their processing requires an understanding of the reaction kinetics of polymerisation during cure. The curing is a highly exothermal reaction and can be monitored by thermal analysis as the differential scanning calorimetry (DSC). Such kinetic studies allow us to determine how much, how fast and at which temperature range heat is released. Furthermore, it gives fundamental data on reaction rate and degree on conversion of reactants which is required to fully cure resin in composite moulding techniques (Bu *et al.,* 2014; Vargas *et al.,* 2012; Wuzella *et al.,*2011; Jankoviæ, 2010).

In DSC, it is common to assume that the evolution of exchanged heat is strictly proportional to the rate of the global chemical reaction (Martine *et al.,* 1997), at any instant, as follows:

$$dH/dt = \Delta H_R [d\alpha/dt] \quad (1)$$

Author for correspondence; E-mail: i_tayyab@hotmail.com

Where:

dH/dt = the heat generated by time unit or heat flow, dα/dt = the rate of reaction, and

ΔHr = the heat of reaction obtained as the area of the DSC thermogram.

Therefore, it is possible to evaluate the reaction rate dá/dt at time t, and degree of conversion α reached at time t, by mean of the following expression:

$$d\alpha/dt = 1/\Delta H_R [dH/dt], \alpha = \Delta H_t/\Delta H_R \quad (2)$$

Where:

ΔH_t = the heat released up to the time t, and it can be obtained by integration of calorimetric signal dH/dt up to time t.

The unsaturated polyester resin is generally a co-polymer of anhydride with diols. The double bond of unsaturated polyesters reacts with a monomer, usually, resulting in a 3-D cross-linked structure (Fink, 2013). The exothermic heat generated during the curing of resin is proportional to the number of double bonds that have reacted with styrene in the system. The maximum conversion is reached when all the double bonds of polyester that can react have reacted with the styrene. Since, the reaction rate is directly proportional to rate of heat generation dH/dt, the reaction rate and degree of conversion can be evaluated by expression (2).

The purpose of this study was to stimulate the process of curing of UP resin by means of DSC calorimetry. Non-isothermal experiments were made at different heating rates; the experimental curves were fitted using an empirical kinetic model. This model gave good theoretical predictions with experimental results. These predictions were then correlated with actual microwave curing of UP resin.

In general kinetic model relates the rate of reaction $d\alpha/dt$ to some function of α and T. It is commonly accepted in the kinetic analysis of chemical reactions by thermal analysis that any chemical process of reaction will obey of rate law of the form (Martin *et al.,* 1997; Salla and Ramix, 1994):

$$d\alpha/dt = k(T)\, f(\alpha) \quad \text{..... (3)}$$

Where:

the functional dependence upon α is separated from the dependence upon T. Here, k(T) = the rate constant which is given by an Arrhenius type equation depends on temperature

$$k = k_0 \exp [-E/RT] \quad \text{..... (4)}$$

Where:

A = the Arrhenius frequency factor, E = the activation energy, R = the universal gas constant and T is the curing temperature.

Thus for one reaction, using a multiple linear regression, it is possible to determine the kinetic parameters for DSC exothermic peak obtained from either isothermal or non-isothermal measurements. When the process is isothermal the temperature constant, but in non-isothermal process temperature usually increases according to a constant heating $\beta = dT/dt$ ($T = T_0 + \beta t$). The isothermal rate expression obtained in isothermal measurements is theoretically more precise than non-isothermal rate expression. However, non-isothermal DSC measurement is in general less time consuming than isothermal DSC measurement and thus more attractive than isothermal measurement.

In isothermal DSC measurement, it is not necessary to know the equation for $f(\alpha)$, which may vary during the curing process. Applying the iso-conversional adjustment (Martin *et al.,* 1997; Salla and Ramix, 1995;1994), given by the expression $\ln t = A + E/RT$, (α = ct) at a series of temperatures, it is possible to determine the activation energy at different degree of conversion from the slope of this linear relationship and thus to see how the reaction process evolves. Using this method activation energy is obtained which depends upon the degree of conversion. On the other hand when non-isothermal experiments are performed, the function $f(\alpha)$ has to be specified. With regard to $f(\alpha)$, auto-catalysed mechanism of reaction is used to characterise the curing of thermosetting resin. The auto-catalysed function of $f(\alpha)$ is given by the expression:

$$f(\alpha)^m (1-\alpha)^n \quad \text{..... (5)}$$

Where:

m and n are the orders of reaction; therefore the experimental data will be fitting according the next expression:

$$d\alpha/dt\ Ae^{[-E/RT]}\alpha^m (1-\alpha)^n \quad \text{..... (6)}$$

The constants A, E, m and n are the kinetic parameters that must be determined. This expression can be written in logarithmic form:

$$\ln (d\alpha/dt) = \ln A - E/RT + m\ln + n\ln (1-\alpha) \quad \text{..... (7)}$$

Materials and Methods

Materials and colorimetric instrumentation. Norpol 420-100 resin system used in this study was supplied by Rachold Chemicals. This resin system contains 75% polyester resin and 25% styrene with no added accelerator. Benzoyl peroxide was used as 1% by the weight of resin as an initiator.

Calorimetric measurements. The calorimetric measurements were carried out using TA Instruments Thermal Analyst DSC Standard Cell.

All DSC measurements were performed in a hermetic aluminium pans. A standard sample was prepared by mixing 10 g of UP resin with a fixed portion of initiator (100: 1). The required amount of sample 20 mg was weighted into a sample pan which was then sealed and placed in the DSC for each measurement. After each run, weight of the sample was determined to check any weight loss due to evaporation of styrene monomer. No considerable weight loss was observed.

Results and Discussion

The dynamic scan was performed from-50 °C to 300 °C using nitrogen atmosphere at 50 mL/min and a heating rate of 10 °C/ min. Figure 1 shows the typical dynamic thermogram for curing polyester resin in temperature range -50 °C to 300 °C. Several UP resin samples were tested at heating rate 10 °C/min and the peak temperature position observed was in the range 113 °C-117 °C. The heat of reaction estimated from area under the curve was 230 J/g.

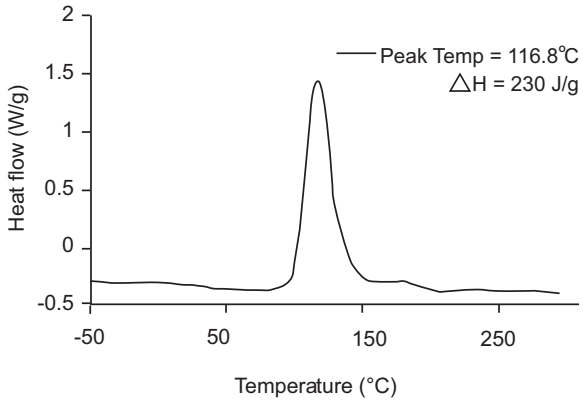

Fig. 1. Typical dynamic thermogram for curing of unsaturated polyester resin in temperature range –50 to 300 °C.

Figure 1 also shows two peaks for trace; the first is greater in area than the second peak. First peak is about 80 % of the total area; which starts at lower temperature as the free radicals are produced to initiate the polymerisation reaction. The second peak appears at high temperature when the DSC trace suggests that curing of PU resin is completed. Avella *et al.,* (1985) suggested that the first peak indicates the copoly-merisation of styrene with polyester unsaturation, while the second peak indicates the homo-polymerisation of styrene. This is arguable since in the absence of initiator UP resin polymerises in the temperature range of 180 °C-210 °C. Furthermore, pure polystyrene polymerises in the temperature range of 140 °C-310 °C (Severini and Gallo, 1985; Horic *et al.,* 1969, Lewis *et al.,* 1948). Due to the complexity of the reaction; only the first peak is used to determine the heat of reaction, peak temperature and later degree of cure.

Figure 2 shows the isothermal thermogram of UP resin cured in DSC at a temperature 120 °C in nitrogen atmosphere (50 mL/min). The curing time given was 60 min. The reaction enthalpy measured was 23.4 J/g and the resin sample was fully cured in 15 min. Re-test (Fig. 3) confirms that the UP resin is fully cured considering the first peak. 188.9 °C is the peak temperature of second peak which shows that sum of residual heat and iso-thermal heat (23.4 J/g) is much lower than the dynamic heat (230 J/g). This indicates that either the isothermal heat or the residual heat is not correct, since their sum should be equal to dynamic heat. Several authors attributed that part of heat that cannot be registered isothermally by the calorimeter is that which is lost during the stabilisation of calorimeter. Cure kinetics were therefore, determined by mean of an empirical (autocatalytic) model.

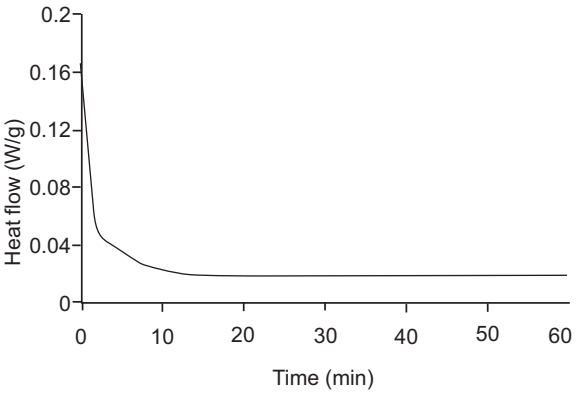

Fig. 2. Isothermal thermogram of unsaturated polyester resin at 120 °C for 60 min.

The isothermal cure in DSC was performed at temperatures range 90 °C–120 °C as shown in Fig. 4. The required properties i.e. the degree of conversion and the reaction rate dα/dt as time or temperature functions were evaluated

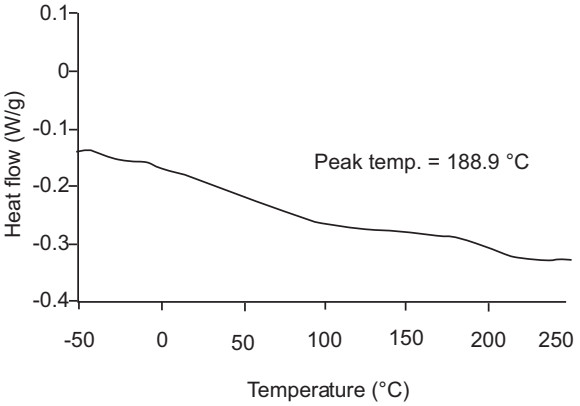

Fig. 3. Re-ramp of isothermal unsaturated polyester resin at temperature range –50 to 300 °C.

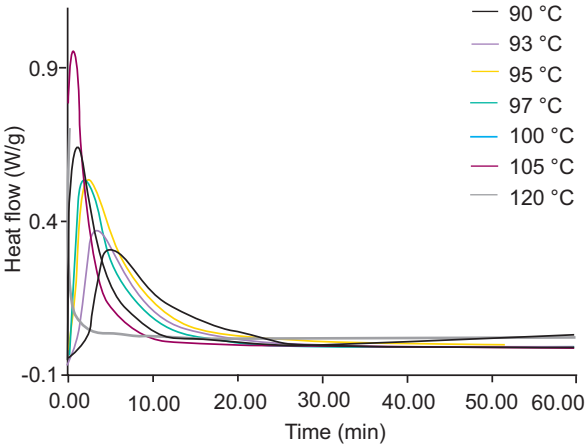

Fig. 4. Isothermal thermograms of unsaturated polyester resin at different temperatures.

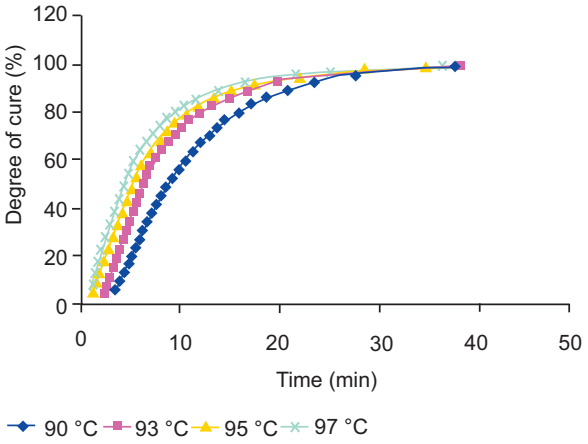

Fig. 5. Degree of conversion against curing time at temperatures 90, 93, 95and 97 °C.

for 90, 93, 95 and 97 °C as shown in Fig. 5 by using equation 2.

Salla and Ramix (1995) established that the isothermal kinetic analysis through isoconventional adjustment is the best method that offers the most accurate results for unsaturated polyester resin cure kinetics. Derivation of isoconventional adjustment lnt = A + E/RT as established by Salla and Ramix (1994) is substituting the Arrhenius equation 3 into the rate equation 4 recording and integrating between curing time t = 0 where α = 0 and time t with degree of conversion, and taking logarithms, the degree of conversion is ln t = A + E/RT, where A takes the following value:

$$A = \ln [f d\alpha / f(\alpha)] - \ln k_0 \quad \text{..... (8)}$$

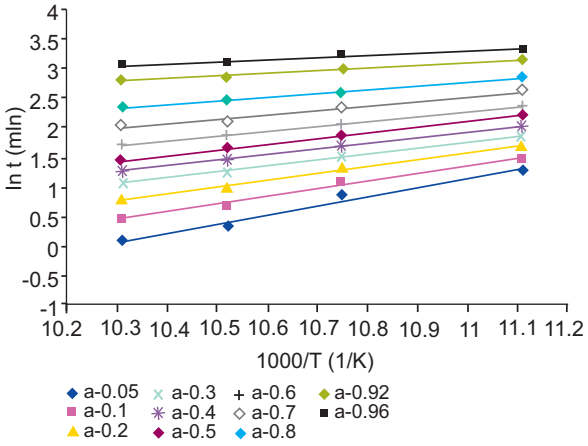

Fig. 6. . Correlation of logarithms of time against the inverse of temperature for different degree of conversion according to ln t = A + E/RT.

According to equation 8 the linear relationship ln t against T at different temperatures is shown in Fig. 6. The activation energy E and constant A can be determined from the slope and intercept line least square fitted to data. Curing times at 120 °C was determined by extra plotting the straight line shown in Fig. 6. At 120 °C (1/T = 8.3 according to ln t = A + E/RT) series of points along ln t at different degrees of conversions were noted, by taking anti-log of ln t, time was also determined at different degrees of conversion which is plotted against the degree of conversion in Fig. 7. According to this prediction 95 % of UP resin must take 33 min to fully cure, while according to isothermal DSC run UP resin will take 60 min at 120 °C to be fully cured (see Fig. 2).

Degree of cure. 1 mL of UP resin samples were cured for different intervals of time with microwave radiation using a solid state amplifier having frequency range 2.3-2.7 GHz and maximum power 30W. The network analyzer was used as microwave signal source. Figure 8 shows the

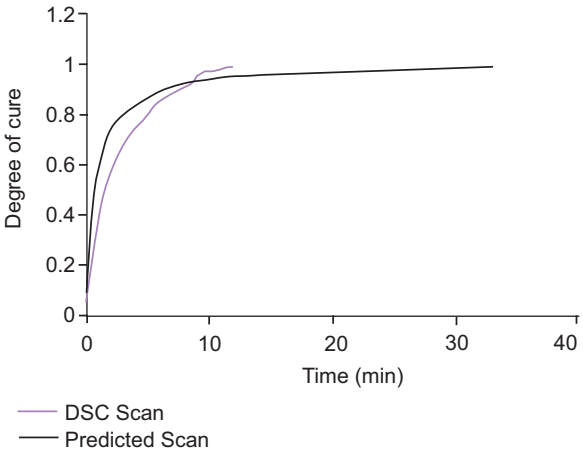

Fig. 7. Degree of conversion against time.

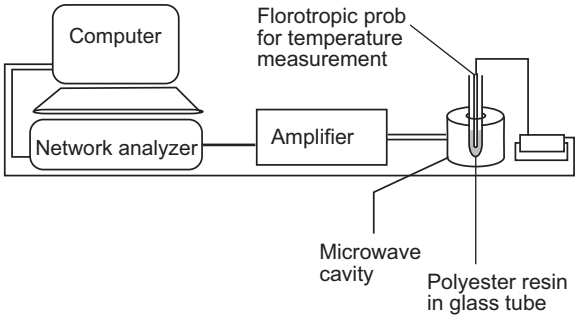

Fig. 8. Systematic diagram of microwave curing apparatus.

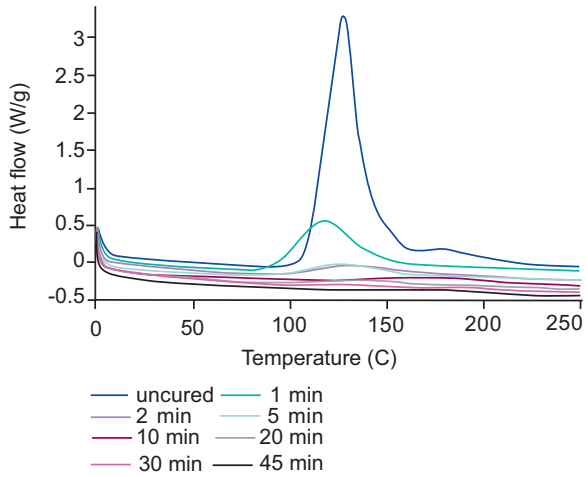

Fig. 9. DSC thermograms of UP resin cured at different time intervals in microwave at 120 °C.

systematic diagram of microwave processing. Figure 9 shows the DSC thermograms of microwaved samples cured for temperature range of -50 °C to 300 °C at a heating rate of 20 °C/min. The degree of conversion at each temperature was determined by using the following expression

$$\alpha = 1 - (\Delta H_t / \Delta H_{dyn}) \quad \text{.....} \quad (9)$$

Where:

ΔH_t = the heat released during the time t and ΔH_{dyn} = total heat released i.e. the heat of reaction for uncured resin at the same rate of heating. Figure 10 shows the degree of conversion against time for microwave cured UP resin and it indicates that 67% resin is cured in 1 min. In microwave heating polymer molecules are heated directly due to the relaxation of the polarisation of dipoles along the electric field. The carboxylic (HO_2C-) segments of fumaric residues are the most dielectrically active polar groups. The induced polymer polarisation in the network structure will increase the molecular mobility which resulted in the acceleration of the curing reaction during early stages of the process. After 15 min the conversion occurred slowly because it might be possible that the remaining C=C bonds are buried in the microgel structure. Thus the full conversion may not be achieved even at high temperature (Hanemann *et al.,* 2010; Huang and Chen, 1993; 1992; Jacobs and Jones, 1992; Yang and Lee, 1988; Tinga and Nelson, 1973).

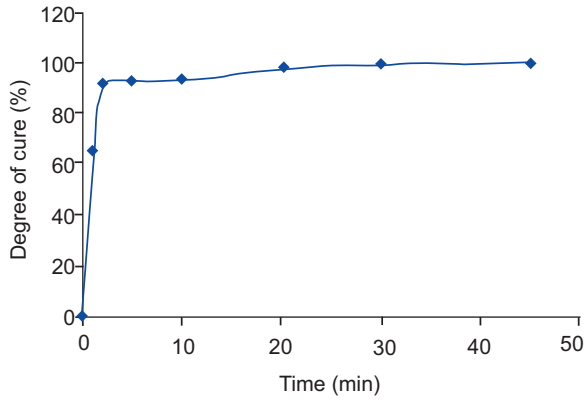

Fig. 10. Degree of conversion against time for microwave cured UP resin.

Rheological characterisation of UP resin. It is fundamental to determine the viscosity-temperature relationship of resins used for Resin Transfer Moulding processing. The rate of advance of flow front is coupled inversely to the resin viscosity. The parameter of interest is the time in which the viscosity of resin rises to a value where further impregnation and wetting of fibre reinforcement is impractical. Rheometers determine the change in viscosity by determining the torsional resistance of the resin at preset shearing rate. Test is terminated once the torque achieves a certain threshold in order to avoid damage. The Rheological characterization of UP resin was carried out with parallel plate rheometer; Rheometric Scientific RMS 800, using 50 mm parallel plates and the gap between plates was set 0.5 mm. The test was undertaken with a set frequency of 1Hz and shear strain of 2.5%.

Figure 11 indicates the rheological changes for a mixture of UP resin and 1% Benzyl peroxide catalyst. But it does not show any changes in G', G" and viscosity after 200 sec because the reaction at 120 ºC was so fast that the resin

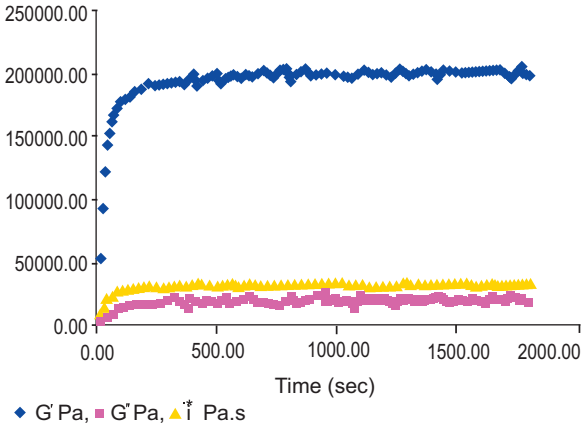

Fig. 11. Changes in steady viscosity (i), dynamic modulus G' and loss modulus G" with time at temperature 120 °C.

cured during the stabilisation of instrument. However, the maximum value of G" corresponding to the time can be seen, after which G' remains constant. Gelation is defined as the point at which the curing system transforms suddenly from viscous liquid to an elastic gel (Yang and Lee, 1988). Tung and Dynes, suggested that, the time at which the crossover of G' and G" occurs during isothermal curing can be taken as gel point (Tung and Dynes, 1982). Winter and Chambon also took this as gelation time, though indicating that for many systems the gel point may not be equal to the one calculated at G' = G" (Whiter and Chambon, 1987). A well-accepted indicator for occurrence of gelation is a rapid increase in viscosity. An accepted method to define gel point is when viscosity reaches a value of either 10^4 or 10^3 Pa.s. In this study, the gel point appears to be somewhat earlier than those determined from 10^4 or 10^3 Pa.s. In case of UP resin, these major changes in rheological properties occur at the beginning of the curing reaction i.e. for conversions lower than 5% in different manner to epoxy resin. The change in viscosity with time is shown in Fig. 12, which was recorded by raising the temperature

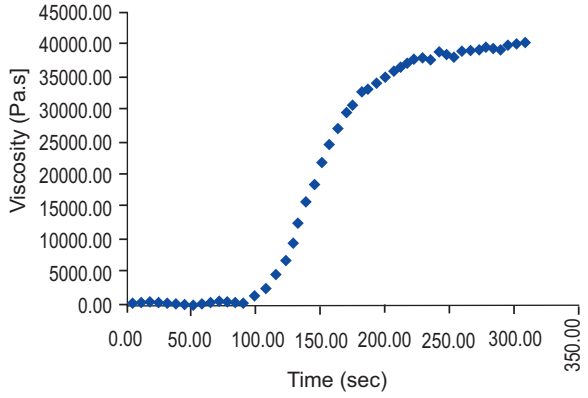

Fig. 12. Change in viscosity with time at 120 °C.

of hot plates from 90 °C to 120 °C. It can be seen that in case of unsaturated polyester resin the gel point reached before 10^4 Pa.s and crosslinking took place in approximately 100 sec.

Conclusion

The curing process of unsaturated polyester resin initiated with benzoyl peroxide was studied by differential scanning calorimetry (DSC). The kinetic analysis was performed by mean of an empirical model. The isothermal and non-isothermal DSC runs were performed to determine the time and temperature required to cure the UP resin. The isothermal test predicted that UP resin cured at temperature range of 90 °C-120 °C. However, the time predicted by non-isothermal test seemed to be incorrect since the sum of residual heat and isothermal heat was not equal to the dynamic heat which indicated that the heat was lost during the stabilisation of calorimeter. The time require to cure the UP resin was then predicted using the isothermal kinetic analysis through isoconversional adjustment which indicated that 95% of UP resin will cure in 33 min at 120 °C. The curing of UP resin using microwaves at different interval of time however, indicated that 67% of UP resin cures in 1 min. The crosslinking reaction of UP resin at 120 °C using microwaves was so fast that it was impossible to fully cure the resin due to burial of C=C bonds in the microgel structure. In rheological study of UP resin; curing also took place during the stabilisation of equipment at 120 °C which further confirmed that UP resin crosslink in 100 sec at 120 °C.

Acknowledgements

The Material Science Center, UMIST, Manchester is gratefully acknowledged for technical support.

References

Avella, M., Martuscelli, E., Mazzola, M. 1985. Kinetic study of the cure reaction of unsaturated polyester resins. *Journal of Thermal Analysis and Calorimetry,* **30:** 1359-1366.

Bu, Z., Hu, J., Li, B. 2014. Novel silicon-modified phenolic novolac resins: Non-isothermal curing kinetics, and mechanical and thermal properties of their biofiber-reinforced composites. *Thermochimica Acta,* **575:** 244-253.

Fink, J.K. 2013. Unsaturated polyester resins. In: *Reactive Polymers Fundamentals and Applications,* pp. 1-48, 2nd edition, William Andrew Publishing, New York, USA.

Hanemann, T., Schumacher, B., Haußelt, J. 2010. Polymerization conditions influence on the thermomechanical and dielectric properties of unsaturated polyester–styrene-copolymers. *Microelectronic Engineering,* **87:** 15-19.

Horic, K., Mita, I., Kambe, H. 1969. Calorimetric investigation of polymerization reactions. II. Copolymerization of diethyl fumarate with styrene. *Journal of Polymer Science: Part-A Polymer Chemistry,* **7:** 2561- 2567.

Huang, Y.J., Chen, C.J. 1993. Curing of unsaturated polyester resin: Effect of co-monomer Composition.

III-Medium Temperature Reaction. *Journal of Applied Polymer Science,* **48:** 151- 165.

Huang, Y.J., Chen, C.J. 1992. Curing of unsaturated polyester resin: Effect of co-monomer composition, II-High Temperature Reaction. *Journal of Applied Polymer Science,* **47:** 1533-1549.

Jacobs, P.M., Jones, F.R. 1992. The influence of heterogeneous crosslink density on the thermo-mechanism and hydrothermal properties of unsaturated polyester resin: I-Thermo-mechanical Response. *Polymer,* **33:** 1418- 1422.

Jankoviæ, B. 2010. The Kinetic analysis of isothermal curing reaction of an unsaturated polyester resin: Estimation of the density distribution function of the apparent activation energy. *Chemical Engineering Journal,* **162:** 331-340.

Lewis, F.M., Walling, C., Cummings, W., Briggs, E.R., Mayo, F.R. 1948. Copolymerization. IV. Effects of temperature and solvents on monomer reactivity ratios. *Journal of American Chemical Society,* **70:** 1519-1523.

Martin, J.L., Cadenato, A., Salla, J.M. 1997. Comparative Studies on the non-isothermal DSC curing kinetics of an unsaturated polyester resin using free radicals and empirical models. *Thermochimica Acta,* **306:** 115-126.

Salla, J.M., Ramix, X. 1995. Effect of the inhibitor on the curing of an unsaturated polyester resin. *Polymer,* **36:** 3511- 3521.

Salla, J.M., Ramix, X. 1994. A kinetic study of the effect of three catalytic systems on the curing of an unsaturated polyester resin. *Journal of Applied Polymer Sciences,* **51:** 453-462.

Severini, F., Gallo, R.J. 1985. Differential scanning calorimetry study of the thermal decomposition of peroxides in the absence of a solvent. *Journal of Thermal Analysis and Calorimetry,* **30:** 841-847.

Tinga, W. R., Nelson, S.O. 1973. Measurement of microwave dielectric properties materials. *Journal of Microwave Power,* **8:** 23-65.

Tung, C.Y.M., Dynes, P.J. 1982. Relationship between viscoelastic properties and gelation in thermosetting systems. *Journal of Applied Polymer Science,* **27:** 569-574.

Vargas, M.A., Sachsenheimer, K., Guthausen, G. 2012. In-situ investigation of the curing of polyester resin. *Polymer Testing,* **31:** 127-135.

Whiter, H.H., Chambon, F. 1987. Analysis of linear viscoelasticity of a crosslinking polymer at the gel point. *Journal of Rheology,* **30:** 367-383.

Wuzella, G., Kandelbauer, A., Mahendran, A.R., Teischinger, A. 2011. Thermochemical and isoconversional kinetic analysis of a polyester-epoxy hybrid powder coating resin for wood based panel finishing. *Progress in Organic Coating,* **70:** 186-191.

Yang, Y.S., Lee, L. 1988. Microstructure formation in the cure of unsaturated polyester resin. *Polymer,* **29:** 1793-1800.

Pak. j. sci. ind. res. Ser. A: phys. sci. 2015 **58** (2) 106-110

Amenability of Carboxylic Acids Adsorption on Surface of Activated Carbon

Tayyba Aftab, Naeem Abbas*, Muhammad Irfan, Farah Deeba, Naz Imtiaz and Rauf Ahmad Khan

Centre for Environment Protection Studies, PCSIR Laboratories Complex, Ferozepur Road, Lahore - 54600, Pakistan

(receivd December 11, 2013; revised July 11, 2014; accepted July 18, 2014)

Abstract. The objective of the present study was to investigate the adsorption of benzoic acid (BA), valeric acid (VA), propionic acid (PA) and butyric acid (BUA) from aqueous solutions at different dosing rate on the surface of activated carbon. Different trials were taken in order to determine the interaction between the carbon surface and adsorbent species. The residual concentration of acids was calculated by the titrimetric method. Maximum adsorption capacity was found to be 93.37% at dosing rate of 8.75 g for BUA and minimum adsorption capacity was measured as 41.47% at dosing rate of 0.69 g for VA. Keeping the same contact time and mass of activated carbon (2.8 g), the adsorption capacity increases with increasing dosing rate.

Keywords: activated carbon, benzoic acid, titrimetric method, adsorption capacity, dose rate

Introduction

Carboxylic acids are used in various industries for the production of polymers, pharmaceuticals, solvents, and food additives. Propionic acid is an important member of carboxylic acid family: used as intermediate for the production of other chemicals, a preservative for both animal feed and food for human consumption, especially polymers and artificial flavourings (Bertleff *et al*., 2005). Butyric acid is widely used as an animal feed supplement due to its ability to reduce pathogenic bacterial colonisation. Butyric acid has a powerful odour. It has also been used as a fishing bait additive. Valeric acid has been widely used in perfumes and cosmetics industries due to its pleasant odour.

Benzoic acid (BA) is one of the most important additives in the food industry. Many countries such as China, Japan, and the European Union have banned the usage of BA as a food additive due to its toxic nature. BA is also used in the formation of many compounds and produced exclusively by the liquid phase oxidation of toluene. It can be detected in industrial sewage, which could affect the human health (Xin *et al*., 2011). Therefore, the removal of carboxylic acid in water brings much public attention (Dong *et al*., 2006). Adsorption behaviour of acidic compounds with different adsorbents like activated carbons, montmorillonites, mesoporous silicas, soils and bentonites has been investigated by many earlier researchers (Yan *et al*., 2007; Ayranci and Duman, 2006).

*Author for correspondence; E-mail: naeemchemist@gmail.com

Activated carbon is one of the oldest and the most widely used adsorbents for the adsorption of organic compounds. It has been utilised in powder or granular form. These forms have been the primary adsorbent materials for many adsorption studies on organic compounds (Ania *et al*., 2002; Abe *et al*., 2000). Many studies have reported the adsorption of acid on surface of activated carbon (Dina *et al*., 2012). The adsorption behaviour of activated carbon from adsorbate solutions is affected by both the surface and the solution properties (Haghseresht *et al*., 2002). Presence of surface functional groups such as carboxyl, lactone, phenol, carbonyl, ether, pyrone and chromene gives activated carbon an acid-base character (Rodriguez-Reinoso and Molina-Sabio, 1998). Surface charge density is also an important factor in determining the adsorption characteristics of activated carbon.

Various surface structures and chemistry are expected to play a role during the adsorption process. Carboxylic acids are used in various industries for the production of various types of compounds; hence, these are present in wastewater generated in these industries. Thus, it is important to remove these compounds by a suitable and economic process before discharge of these wastewaters. The objective of the present study was to investigate the adsorption behaviours by use of activated carbon (AC) for the removal of benzoic acid (BA), valeric acid (VA), butyric acid (BUA) and propionic acid (PA) from aqueous solutions by changing their initial concentration.

The performance of activated carbon is evaluated by using different dosing rate of carboxylic acids.

Materials and Methods

Benzoic acid, valeric acid, butyric acid and propionic acid were obtained from Merck, whereas phenolphthalein and sodium hydroxide were reagent grade. Activated carbon was applied in powdered form in batch experiment which had been purchased from BDH chemicals. The characteristic of activated carbon before experiment was summarized in Table 1.

Table 1. Characteristics of activated carbon

Parameters	Results
pH	6.8 ± 0.05
Moisture content (%)	11 ± 0.10
Bulk density (g/cm^3)	0.317 ± 0.02
Tap density (g/cm^3)	0.672 ± 0.04
Surface area (BET) (m^2/g)	980 ± 1.45
Pore volume (g/cm^3)	1.43 ± 0.05
Porosity (%)	75.74 ± 1.05
Particle size (mm)	3.7 ± 0.02

Batch equilibrium experiments. All experiments were carried out in a reagent bottle with same amount of carbon (2.8 g) added in it. The carboxylic acids used were propionic, butyric, valeric and benzoic acids. The stock solution of each acid was prepared (i.e., 4, 16, 24, 40, 50, 70, 80 and 100%) by keeping its volume 50 mL with double distilled water. For adsorption of acids on activated carbon, same amount of carbon was (2.8 g) added in each bottle and placed for 30-45 min at 30 °C in a shake machine to reach 95% equilibrium. Then the solution was filtered off over a measuring cylinder. After discarding the first 5 mL of the filtrate, 25 mL was taken in Erlenmeyer flask for titration. Phenolphthalein (4 drops) was added and titrated with standard sodium hydroxide solution.

The adsorbed quantities of acid, X, were obtained by subtracting the residual concentration at equilibrium α_e, from the initial concentration, α_o Thus,

$$X = \alpha_o - \alpha_e \quad (1)$$

and Q_e the quantity of carboxylic acid adsorbed (adsorption capacity) per gram of adsorbent of mass m, V is volume. It can be expressed as:

$$Q_e = \frac{\alpha_o - \alpha_e}{\alpha_o} V \quad (2)$$

Results and Discussion

Adsorption of benzoic acid (BA). Results reveal that by increasing dosing rate, the adsorption of acid on activated carbon also increases. The concentration of acids provides necessary driving force to overcome the resistance to the mass transfer of adsorbate between aqueous and the solid phases. Moreover, the increase of concentration enhances the interaction between adsorbate and the adsorbent. Table 2 shows that keeping constant mass of carbon as 2.8 g and increasing dosing rate of benzoic acid from 0.09 g to 2.60 g, adsorption capacity of carbon increases from 2.22% to 91.30%. From Fig. 1 it is clear that the adsorption capacity was increased gradually up to dosing rate of 1.83 g then increased sharply at dosing rate of 2.6 g and became linear after it. The value of X/m and C_{eq} also increased gradually by increasing concentration of BA.

Table 2. Adsorption of benzoic acid on activated carbon

S. no.	m (g)	Dilution (%)	α_o (g)	NaOH (mL)	C_e (mole/L)	α_e (g)	$X=\alpha_o-\alpha_e$ (g)	X/m (g)	C_{eq} (g)	Q_e mg/g
1.	2.8	4	0.09	0.06	0.003	0.002	0.088	0.032	0.0094	2.22
2.	2.8	16	0.42	1.19	0.010	0.038	0.383	0.136	0.0735	9.00
3.	2.8	24	0.71	2.45	0.015	0.089	0.621	0.222	0.0675	12.35
4.	2.8	40	0.93	6.43	0.032	0.173	0.757	0.270	0.1185	18.60
5.	2.8	50	1.41	8.15	0.046	0.222	1.188	0.424	0.1084	26.66
6.	2.8	70	1.62	9.52	0.081	0.400	1.221	0.436	0.1857	24.62
7.	2.8	80	1.83	10.62	0.112	0.570	1.260	0.450	0.2488	31.14
8.	2.8	100	2.60	11.94	0.241	1.91	0.69	0.226	1.0663	91.30

m = weight of activated carbon (g); α_o = amount of carboxylic acid added to the bottle (g); C_e = concentration of carboxylic acid left in solution at equilibrium (mole/L); α_e = amount of carboxylic acid left in solution at equilibrium in the bottle (g); X = amount of carboxylic acid adsorbed (g); Q_e = adsorption capacity of acids (mg/g).

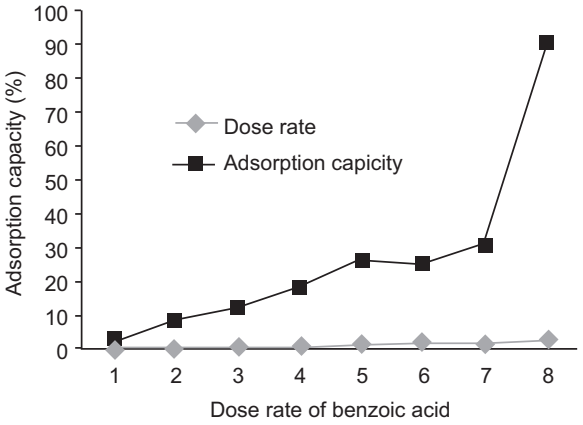

Fig. 1. Effect of dose rate on adsorption capacity of benzoic acid.

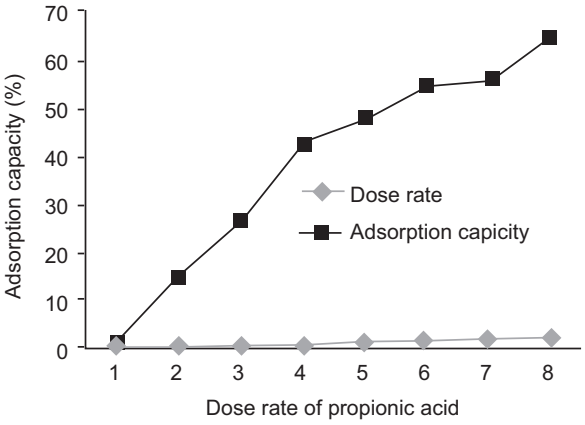

Fig. 2. Effect of dose rate on adsorption capacity of propionic acid.

Adsorption of propionic acid (PA). Adsorption of propionic acid from the aqueous solution on the surface of activated carbon was increased by increasing dosing rate as shown in Fig. 2. The adsorption capacity was increased from 1.69% up to 65.28% by increasing dosing rate of propanoic acid from 0.059 g up to 1.472 g. The value of X/m ranging from 0.021 to 0.148 and C_{eq} values from 0.018 to 1.411 are presented in Table 3.

Adsorption of valeric (VA) and butyric acid (BUA). The adsorption of valeric acid molecule with linear structure has more surface area as compared to its branched structure. More fatty acid get adsorbed with chain parallel to surface due to high affinity (Kipling, 1965).

The adsorption capacity of valeric acid increased sharply up to dosing rate of 0.692 g from 0.082 g as shown in Fig. 3. The value of X/m ranges from 0.029 to 0.446 and C_{eq} values from 0.007 to 0.313. Adsorption capacity was decreased at 0.820 g and then increased gradually up to 2.05 g as shown in Table 4. With butyric acid, adsorption capacity was sharply increased up to 93.37% with dosing rate of 8.75 g then became linear after it

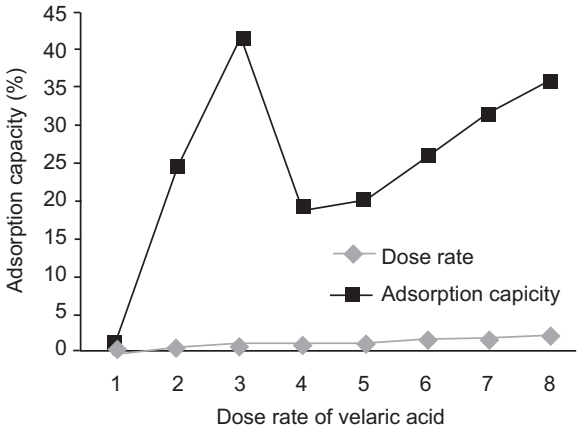

Fig. 3. Effect of dose rate on adsorption capacity of valeric acid.

Table 3. Adsorption of propionic acid on activated carbon

S. no.	m (g)	Dilution (%)	α_o (g)	NaOH (mL)	C_e (mole/L)	α_e (g)	$X=\alpha_o-\alpha_e$ (g)	X/m (g)	C_{eq} (g)	Q_e mg/g
1.	2.8	4	0.059	0.10	0.0003	0.0015	0.058	0.021	0.018	1.69
2.	2.8	16	0.236	2.40	0.0095	0.035	0.201	0.068	0.140	14.83
3.	2.8	24	0.354	6.40	0.094	0.094	0.260	0.099	0.256	26.55
4.	2.8	40	0.589	15.70	0.230	0.230	0.339	0.129	0.482	42.95
5.	2.8	50	0.736	24.0	0.352	0.352	0.334	0.145	0.652	47.82
6.	2.8	70	1.031	39.0	0.572	0.572	0.459	0.172	0.900	54.51
7.	2.8	80	1.178	45.0	0.660	0.660	0.518	0.173	1.031	56.02
8.	2.8	100	1.472	65.5	0.961	0.961	0.511	0.184	1.411	65.28

m = weight of activated carbon (g); α_o = amount of carboxylic acid added to the bottle (g); C_e = concentration of carboxylic acid left in solution at equilibrium (mole/L); α_e = amount of carboxylic acid left in solution at equilibrium in the bottle (g); X = amount of carboxylic acid adsorbed (g); Q_e = adsorption capacity of acids (mg/g).

Table 4. Adsorption of valeric acid on activated carbon

S. no.	m (g)	Dilution (%)	α_o (g)	NaOH (mL)	C_e (mole/L)	α_e (g)	$X=\alpha_o-\alpha_e$ (g)	X/m (g)	C_{eq} (g)	Q_e mg/g
1.	2.8	4	0.082	0.05	0.0002	0.001	0.081	0.029	0.007	1.22
2.	2.8	16	0.382	2.05	0.008	0.041	0.287	0.102	0.078	24.86
3.	2.8	24	0.692	4.35	0.017	0.087	0.405	0.143	0.119	41.47
4.	2.8	40	0.820	7.65	0.030	0.155	0.665	0.238	0.126	18.90
5.	2.8	50	1.025	10.20	0.040	0.206	0.819	0.292	0.137	20.09
6.	2.8	70	1.435	18.45	0.073	0.373	1.062	0.379	0.193	25.99
7.	2.8	80	1.640	25.70	0.102	0.520	1.120	0.400	0.255	31.70
8.	2.8	100	2.05	36.95	0.146	0.745	1.305	0.466	0.313	36.34

m = weight of activated carbon (g); α_o = amount of carboxylic acid added to the bottle (g); C_e = concentration of carboxylic acid left in solution at equilibrium (mole/L); α_e = amount of carboxylic acid left in solution at equilibrium in the bottle (g); X = amount of carboxylic acid adsorbed (g); Q_e = adsorption capacity of acids (mg/g).

Table 5. Adsorption of butyric acid on activated carbon

S. no.	m (g)	Dilution (%)	α_o (g)	NaOH (mL)	C_e (mole/L)	α_e (g)	$X=\alpha_o-\alpha_e$ (g)	X/m (g)	C_{eq} (g)	Q_e mg/g
1.	2.8	4	0.07	0.05	0.0002	0.002	0.068	0.024	0.0082	2.85
2.	2.8	16	0.280	3.05	0.0121	0.0532	0.2268	0.081	0.1493	19.28
3.	2.8	24	0.420	5.75	0.0228	0.1003	0.3197	0.114	0.200	24.04
4.	2.8	40	0.700	12.85	0.0509	0.224	0.476	0.170	0.2994	32.00
5.	2.8	50	8.75	16.90	0.0670	0.295	0.580	0.207	0.3236	93.37
6.	2.8	70	12.25	29.15	0.1155	0.508	0.717	0.256	0.4512	94.14
7.	2.8	80	14.00	31.25	0.1397	0.615	0.785	0.280	0.4989	94.39
8.	2.8	100	17.5	50.35	0.1996	0.878	0.872	0.311	0.6418	95.01

m = weight of activated carbon (g); α_o = amount of carboxylic acid added to the bottle (g); C_e = concentration of carboxylic acid left in solution at equilibrium (mole/L); α_e = amount of carboxylic acid left in solution at equilibrium in the bottle (g); X = amount of carboxylic acid adsorbed (g); Q_e = adsorption capacity of acids (mg/g).

as shown in Fig. 4. The value of X/m ranges from 0.024 to 0.311 and C_{eq} values from 0.008 to 0.64 as shown in Table 5.

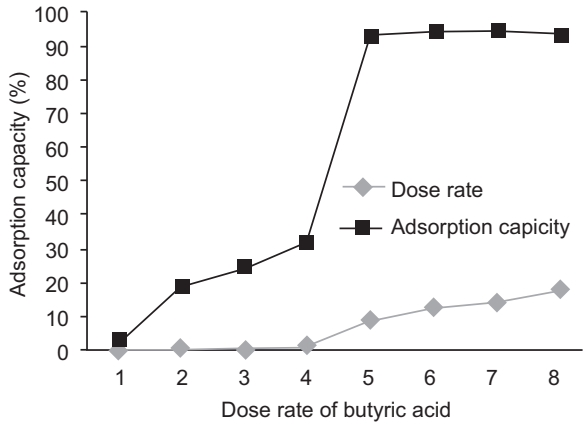

Fig. 4. Effect of dose rate on adsorption capacity of butyric acid.

Conclusion

Percent removal of BA, PA, VA and BUA increases with the increase in adsorbent dose. All acids used in experiments showed better result at acidic pH. Optimum adsorption capacities were found to 91.30%, 65.28%, 41.47% and 93.37% at dosing rate of 2.60 g, 1.47 g, 0.69 g and 8.75 g for BA, PA, VA, BUA, respectively. At different dose rates with same contact time the adsorption capacity increases with an increase of concentration. However, amount adsorbed per amount of adsorbent increases with an increase of dosing rate of each acid.

References

Abe, M., Kawashima, K., Kozawa, K., Sakai, H., Kaneko, K. 2000. Amination of activated carbon and adsorption characteristics of its aminated surface. *Langmuir*, **16:** 5059-5063.

Ania, C.O., Parra, J.B., Pis, J.J. 2002. Influence of oxygen-containing functional groups on active carbon adsorption of selected organic compounds. *Fuel Processing Technology*, **79:** 265-271.

Ayranci, E., Duman, O. 2006. Adsorption of aromatic organic acids onto high area activated carbon cloth in relation to wastewater purification. *Journal of Hazardous Materials*, **136:** 542-552.

Baudu, M., Le Cloirec, P., Martin, G. 1991. Pollutant adsorption onto activated carbon membranes. *Water Science and Technology*, **23:** 1659-1666.

Bertleff, W., Roeper, M., Sava, X. 2005. Carbonylation. In: *Ullmann's Encyclopedia of Industrial Chemistry*, Weinheim: Wiley-VCH, doi:10.1002/14356007.a05_217

Dina, D.J.D., Ntleche, A.R., Ndi, J.N., Ketcha, M.J. 2012. Adsorption of acetic acid onto activated carbon obtained from maize cobs by chemical activation with zinc chloride ($ZnCl_2$). *Research Journal of Chemical Sciences*, **2:** 42-49.

Dong, C., Mei, Y., Chen, L. 2006. Simultaneous determination of sorbic and benzoic acids in food dressing by headspace solid-phase microextraction and gas chromatography. *Journal of Chromatography A*, **1117:** 109-114.

Haghseresht, F., Nouri, S., Lu, G.Q. 2002. Effects of the solute ionization on the adsorption of aromatic compounds from dilute aqueous solutions by activated carbon. *Langmuir*, **18:** 1574-1579.

Kipling, J.I. 1965. *Adsorption from Solutions of Non-Electrolytes*. Academic Press, New York, USA.

Rodriguez-Reinoso, F., Molina-Sabio, M. 1998. Textural and chemical characterization of microporous carbons. *Advances in Colloid and Interface Science*, **77:** 271-294.

Xin, X., Si, W., Yao, Z., Feng, R., Du, B., Yan, L., Wei, Q. 2011. Adsorption of benzoic acid from aqueous solution by three kinds of modified bentonites. *Journal of Colloid and Interface Science*, **359:** 499-504.

Yan, L.G., Wang, J., Yu, H.Q., Wei, Q., Du, B., Shan, X.Q. 2007. Adsorption of benzoic acid by CTAB exchanged montmorillonite. *Applied Clay Science*, **37:** 226-230.

Pak. j. sci. ind. res. Ser. A: phys. sci. 2015 **58** (2) 111-116

Evaluation of Pesticide Residues in Drinking Water in Different Areas of Khyber Pakhtunkhwa, Pakistan

Muhammad Nasimullah Qureshi[a]* and Inayat Ur Rahman[b]

[a]Department of Chemistry, Abdul Wali Khan University, Mardan, Pakistan

[b]Medicinal Botanic Centre, PCSIR Laboratories Complex, Peshawar-25100, Pakistan

(received February 4, 2014; revised April 22, 2014; accepted May 6, 2014)

Abstract. Flood in 2010 severely effected different areas of Khyber Pakhtunkhwa, Sindh, lower Punjab as well as some parts of Balochistan, Pakistan. After the flood, samples of drinking water were collected from the affected areas i.e. Akora Khattak and Buner, Khyber Pakhtunkhwa and pesticides residues were determined quantitatively in these samples employing GC-MS technique. Among the samples collected from Akora Khattak, chlorpyrifos was found in high amounts i.e. 0.040 ppm, in sample no. 6 while methamidophos and methiocarb were found in appreciable quantities i.e. 0.026 ppm and 0.038 ppm, respectively, in sample no. 4. Methamidophos and methiocarb were found in appreciable amounts i.e. 0.039 ppm and 0.034 ppm, respectively, in sample no. 17 among the samples obtained from Buner. Concentrations were found at the level below 0.01 ppm in most of the pesticides under study. From the results it appears that drinking water sources in the area under study have been contaminated with pesticides which is a health hazard and may be a source of various diseases in these areas.

Keywords. flood hit area, drinking water, pesticides, GC-MS technique

Introduction

In Pakistan, in the month of July 2010, water rose up of the level after the heavy monsoon rain fall and came out of brim from the rivers in the form of flood. This flood hit different areas of Pakistan, severely affecting the Khyber Pakhtunkhwa, Sindh, lower Punjab as well as some parts of Baluchistan. About one fifth of Pakistan's total land area was underwater due to the flooding. More than that two thousand people lost their lives and about a million homes perished. As per reports of the United Nations, over 20 million people were suffering and homeless with over 160,000 square kilometers area affected as a result of the floods, exceeding the combined total of the affecters of 2004, due to Indian Ocean Tsunami, the 2005 Kashmir earthquake and the 2010 Haiti earthquake. However, the death toll in each of those three disasters was much higher than the number of people killed so far in these floods (Abid *et al.,* 2010).

Among the provinces of the country, Khyber Pakhtunkhwa was badly damaged, affected primarily the basic necessities of life such as food, shelter and clothing. Unhygienic and contaminated drinking water with pathogenic microorganisms and chemicals like pesticides and herbicides was the most alarming after effects of the flood. The surface water drained the pesticides and herbicides used in agricultural activities into the drinking water resources, making it highly contaminated and harmful for the human consumption.

Use of pesticides to control the insectivorous and herbaceous pests in order to produce good quality and quantity of crops is a fundamental contribution to the Green Revolution. On the other hand some have threatened the long-term survival of major ecosystems by disruption of predator-prey relationships and loss of biodiversity. Pesticides can have significant human health consequences (Hernández *et al.,* 2013; Hayat *et al.,* 2010; Moon *et al.,* 2009) like neurotoxicity (Androutsopoulos *et al.,* 2013; Zaganas *et al.,* 2013; Kanavouras *et al.,* 2011; Bassil *et al.,* 2007; Karalliedde and Senanayake, 1999; Brown *et al.,* 1989) and can produce gastrointestinal, cardiological, dermatological, respiratory, genitor-urinary and musculoskeletal problems (Kesava-chandran *et al.,* 2009; Soomro *et al.,* 2008; Palis *et al.,* 2006; Salameh *et al.,* 2006; Vial *et al.,* 1996; Hueser, 1992). Studies have shown that these chemicals are injurious to immune and endocrine systems (Abhilash and Singh, 2009; Soomro *et al.,* 2008; Luster and Rosenthal, 1993; Chambers, 1992; Arlien-Soberg, 1992).

Contamination of drinking water after flood is a serious environmental issue and a health threat. Flood water can

*Author for correspondence; E-mail: mnasimuq@yahoo.com

be contaminated with a variety of substances including pathogenic microorganisms, automotive fluids, animal wastes, fertilisers, chemicals like pesticides etc. Surface water is drained into the ground water carrying these contaminants. Contamination of drinking water with pesticides cause a number of health problems. Therefore, determination of pesticide residues in drinking water sources is important in order to take appropriate measures for the provision of safe drinking water to public and protection of public health.

Liquid-liquid extraction, which is the most common technique of extracting organic compounds from aqueous phase, is carried out by mixing the aqueous phase with other immiscible organic solvents like ethyl acetate, dichloromethane and hexane. A variety of analytical techniques are used for the analysis of pesticides including chromatographic techniques like GC and HPLC coupled to various detection systems. GC-MS is the method of choice which is a robust and routinely employed for pesticides analyses. This paper presents the results of pesticides residues determination in drinking water samples from different affected areas of Khyber Pakhtunkhwa.

Materials and Methods

Chemicals and reagents. Ethyl acetate (GC grade) and dichloromethane (GC grade) were purchased from Fischer Scientific (Leicestershire, UK). Sodium sulphate anhydrous (analytical grade), potassium dihydrogen phosphate, HCl and sodium chloride (analytical grade) were obtained from Merck (Darmstadt, Germany). GC grade pesticide standards acetamiprid, acetochlor, atrazine, cypermethrin, dichlorvos, difenoconazole, and pyridaben were purchased from AccuStandard New Haven, CT, USA. Aldicarb (99.9%), alpha endosulfan (99.6%), beta-endosulfan (99.9%), chlorpyrifos (99.2%), cyhalothrin (99.7%), fenvalerate (99.8%), methamido-phos (98.4%) and popachlor (99.5%) were procured from Sigma-Aldrich GmbH, Seelze, Germany. Carbofuran (98.5%), dieldrin (98.3%), methiocarb (98.5%), o, p'-DDD (99.6%), o,p'-DDT (99.5%) and p,p'-DDE (98.5%) were obtained from Dr. Ehrenstorfer GmbH Ausburg, Germany. Helium gas (99.9999%) was procured from Pak Gas (United Arab Emirates). Double distilled water was used through out the experimental work.

Preparation of pesticide standard mixture. Stock solutions of the individual pesticides under study were prepared in methanol. From each solution appropriate volume was mixed together in a vial. 2 µL of the standard mixture was injected into the GC column using auto injection system of GC-MS.

Samples collection. Total of 25 samples from drinking water sources (well water) were collected on random basis from Akora Khattak and Buner district in clean and sterilised bottles and numbers were alloted to these samples. Among these: 8 samples were collected from Akora Khattak and 17 samples from Buner. Samples were properly preserved until their use for experimental work. The pesticides selected for the study were those which are most commonly sprayed in these areas as insecticides and herbicides, and are easily available in the form of standards. The data of the most commonly used pesticides in the area has been taken from the Department of Agriculture Training Institute Peshawar, Khyber Pakhtunkhwa. For this study, total of 23 pesticides were selected as shown in Table 1.

Extraction of pesticides and preparation of samples. The procedure adopted was according to the official methods of analysis of AOAC International with some modifications (AOAC, 2002). Water sample (1 L) was adjusted to pH by adding phosphate buffer (pH 7). NaCl (100 g) was dissolved in this solution followed by the addition of 300 mL of ethyl acetate. The mixture was

Table 1. GC-MS data of pesticides standard mixture

Sample no.	Pesticides name	R. Time (min)	Conc. (ppm)	Quantifying ion (base peak) (m/z value)
1	Aldicarb	3.86	38.591	68
2	Methamidophos	4.35	16.657	98
3	Dichlorvos	6.43	18.582	109
4	Carbofuran	7.27	12.680	164
5	Methiocarb	10.02	22.092	168
6	Propachlor	10.69	19.734	120
7	Cyhalothrin	11.76	8.282	198
8	Atrazine	12.24	17.538	200
9	Acetochlor	13.57	17.217	59
10	Chlorpyrifos	14.54	17.066	97
11	α-Endosulfan	16.17	14.907	241
12	p, p'-DDE	16.55	25.480	246
13	Dieldrin	16.69	23.834	79
14	β-Endosulfan	17.30	15.254	195
15	o, p'-DDD	17.36	44.900	235
16	o, p'-DDT	18.06	3.041	235
17	Acetamiprid	18.82	24.242	56
18	Pyridaben	20.92	17.945	147
19	Cypermethrin-1	21.74	46.252	181
20	Fenvalerate-1	22.60	11.544	125
21	Fenvalerate-2	22.85	10.172	125
22	Difenoconazole-1	23.19	10.856	265
23	Difenoconazole-2	23.27	10.622	265

shaken for 1 h at 200 rpm through shaker, then the mixture was poured into separating funnel and the layers were let to separate. The upper organic layer was collected in a round bottom flask, and lower aqueous layer was again treated with 60 mL of ethyl acetate. The mixture was shaken for 15 min. Then the organic layer was separated and mixed with the previously collected layer. Organic layer was dried with sodium sulphate anhydrous. The solution was filtered and evaporated to dry residue through rotary evaporator. The dried residue was reconstituted in 2 µL of dichloromethane. The solution was filtered through 0.45 µmL membrane filter and injected 2 µL into the GC column using auto injection system.

Chromatographic separation of pesticides. A gas chromatograph from Shimadzu hyphenated to a mass spectrometer QP 2010 plus (Tokyo, Japan) equipped with an auto-sampler (AOC-20S) and auto-injector (AOC-20i) was used. Ultra high pure helium was used as carrier gas. All chromatographic separations were performed on a capillary column (DB-5ms; Agilent Technologies, USA) having specifications: length; 30 m, i.d.; 0.25 mm, thickness; 0.250 µm. Other GC-MS conditions were: ion source temperature (EI); 280 °C, interface temperature; 280 °C, solvent cut time; 2 min. 2 µL of samples and standard were injected into the GC column. Injector was operated in a splitless mode. Injection temperature was 250 °C. The column temperature program started at 50 °C for 1 min and ramped to 125 °C at the rate of 25 °C/min. The temperature was further increased to 220 °C at the rate of 10 °C/min and hold for 15 min. Total elution time was 37.5 min. MS was operated in single ion monitoring (SIM) mode. GC-MS solutions software provided by the supplier was used to control the system and to acquire the data. Identification and quantification of the compounds was carried out by comparing the mass spectra obtained with those of external pesticide mixed standard solution. Qualification of the peaks was further authenticated through standard mass spectra from the NIST library (NIST 05).

Results and Discussion

Optimisation of the GC-MS conditions. Multi residues method is essential in the case where nothing is known about the possible contamination. Ideally such method should provide less time consuming, with appropriate base line separation giving quantification of as many pesticides as possible in a single run. The pesticides selected were belonging to different classes of pesticides having different polarity and different thermal properties. For obtaining base line chromatographic separation for such mixture, gradient elution is necessary to obtain precise and accurate quantification at residual level. After optimising the GC conditions using different temperature gradient system, resolution of analytes at the base line was achieved. Column selected was DB-5ms which is mostly used for such analyses. Figure 1 shows the GC chromatogram obtained after analysing the 23 pesticides standards mixture. Detail of the retention times, concentrations and quantifying ion (m/z value) of each pesticide is tabulated in Table 1.

Pesticide residues in drinking water samples. Standard maximum permissible values for pesticide residues in drinking water have been shown in Table 2. Table 3 shows the concentration of pesticides at the level of parts per million (ppm) in the samples collected from Akora Khattak. Aldicarb was detected only in sample AK 1 while in rest it was not detected. Chlorpyrifos was found only in sample no.6 (AK6) while β-endosulfan was detected only in sample no. 3 (AK3). Residues of carbofuran, cyhalothrin, atrazine, acetochlor, α- endosulfan and dieldrin were not detected in

Table 2. Standard maximum permissible values for pesticide residues in drinking water

Sample no.	Pesticide name	Max. permissible limits (ppm)	Reference
1	Aldicarb	0.01	(Hamilton *et al.,* 2003; Jenkins, 1999)
2	Methamidophos	-	(Hamilton *et al.,* 2003)
3	Dichlorvos	0.012	(Moermond *et al.,* 2008)
4	Carbofuran	0.007	(Hamilton *et al.,* 2003)
5	Methiocarb	0.035	(Jenkins, 1999)
6	Propachlor	0.09	(Jenkins, 1999)
7	Cyhalothrin	-	-
8	Atrazine	0.002	(Hamilton *et al.,* 2003)
9	Acetochlor	0.14	((Jenkins, 1999)
10	Chlorpyrifos	-	-
11	α- Endosulfan	0.042	(Jenkins, 1999)
12	p, p'-DDE	0.002	(Hamilton *et al.,* 2003)
13	Dieldrin	0.0002	(Hamilton *et al.,* 2003)
14	β-Endosulfan	0.042	(Jenkins, 1999)
15	o, p'-DDD	0.002	(Hamilton *et al.,* 2003)
16	o, p'-DDT	0.002	(Hamilton *et al.,* 2003)
17	Acetamiprid	-	-
18	Pyridaben	0.0001	(Moermond *et al.,* 2008)
19	Cypermethrin-1	-	-
20	Fenvalerate-1	-	-
21	Fenvalerate-2	-	-
22	Difenoconazole-1	-	-
23	Difenoconazole-2	-	-

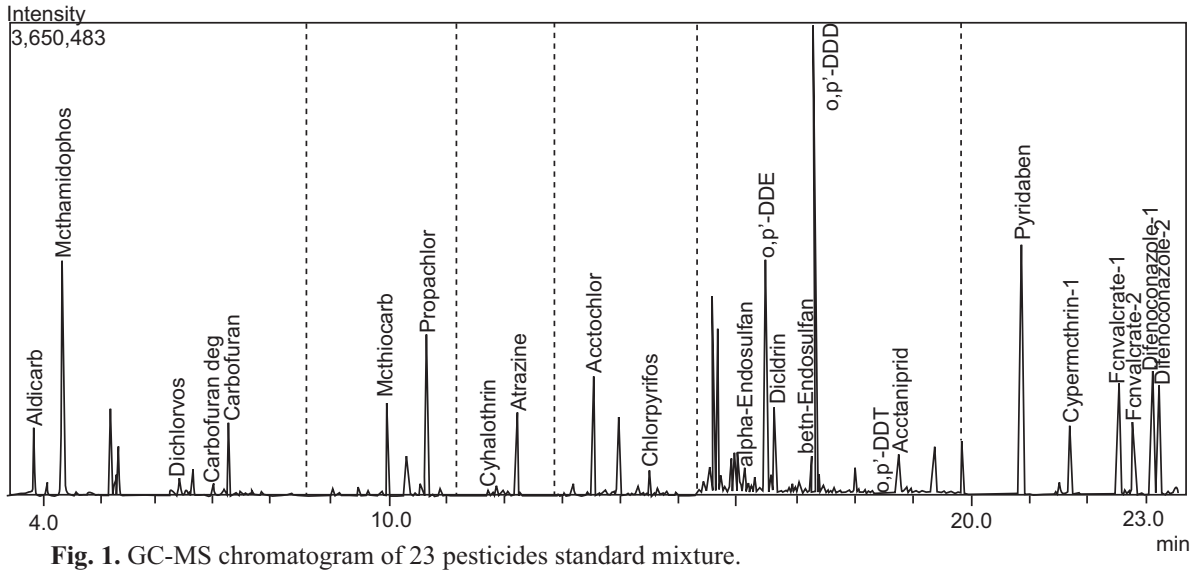

Fig. 1. GC-MS chromatogram of 23 pesticides standard mixture.

Table 3. Quantity (ppm) of pesticides in drinking water samples collected from Akora Khattak (AK) district Nowshera

Sample no.	Pesticide name	AK1	AK2	AK3	AK4	AK5	AK6	AK7	AK8
1	Aldicarb	0.002	ND	ND	ND	ND	ND	ND	ND
2	Methamidophos	0.003	0.006	0.007	0.026	0.010	0.001	ND	0.007
3	Dichlorvos	0.001	0.001	0.003	ND	0.002	ND	0.001	ND
4	Methiocarb	0.011	ND	0.029	0.038	0.012	0.011	ND	0.003
5	Propachlor	ND	<0.001	<0.001	ND	0.001	<0.001	0.001	0.002
6	Chlorpyrifos	ND	ND	ND	ND	ND	0.040	ND	ND
7	p, p'-DDE	<0.001	ND	<0.001	ND	<0.001	ND	0.001	0.005
8	β-Endosulfan	ND	ND	0.001	ND	ND	ND	ND	ND
9	o, p'-DDD	<0.001	<0.001	0.001	<0.001	<0.001	<0.001	0.001	0.003
10	o, p'-DDT	ND	0.001	ND	0.002	0.001	0.001	ND	0.001
11	Acetamiprid	<0.001	ND	0.010	ND	0.002	ND	ND	ND
12	Pyridaben	<0.001	ND	ND	<0.001	<0.001	ND	ND	ND
13	Cypermethrin-1	ND	ND	<0.001	0.001	0.001	ND	ND	ND
14	Fenvalerate-1	ND	ND	<0.001	ND	<0.001	ND	<0.001	0.004
15	Fenvalerate-2	ND	<0.001	0.002	<0.001	0.001	ND	ND	ND
16	Difenoconazole-1	ND	ND	<0.001	<0.001	<0.001	<0.001	<0.001	ND
17	Difenoconazole-2	ND	<0.001	<0.001	ND	ND	ND	ND	ND

Table 4a. Quantity (ppm) of pesticides in drinking water samples collected from district Buner (B)

Sample no.	Pesticide name	B1	B2	B3	B4	B5	B6	B7	B8	B9	B10
2	Methamidophos	0.018	0.011	0.008	0.002	0.001	<0.001	0.002	0.002	0.014	0.001
3	Dichlorvos	ND	<0.001	ND	0.001	ND	ND	<0.001	ND	ND	ND
6	Methiocarb	ND	ND	ND	ND	0.006	ND	ND	ND	ND	0.004
7	Propachlor	0.001	0.001	<0.001	<0.001	ND	<0.001	<0.001	<0.001	<0.001	ND
11	Chlorpyrifos	ND	ND	ND	ND	ND	ND	ND	ND	ND	ND
13	p, p'-DDE	<0.001	0.001	<0.001	<0.001	<0.001	<0.001	<0.001	<0.001	<0.001	ND
16	o, p'-DDD	<0.001	0.001	0.001	0.001	<0.001	0.001	0.001	<0.001	ND	<0.001
17	o, p'-DDT	ND	ND	ND	ND	ND	ND	0.001	ND	ND	ND
18	Acetamiprid	0.001	0.001	<0.001	<0.001	ND	ND	ND	ND	ND	ND
19	Pyridaben	ND	<0.001	<0.001	<0.001	<0.001	ND	<0.001	ND	ND	ND

ND = not detected.

Table 4b. Quantity (ppm) of pesticides in drinking water samples collected from district Buner (B)

Sample no.	Pesticide name	B11	B12	B13	B14	B15	B16	B17
2	Methamidophos	0.002	0.002	<0.001	0.004	0.007	0.002	0.039
3	Dichlorvos	ND	0.001	ND	ND	ND	ND	ND
6	Methiocarb	0.007	0.010	0.001	0.007	0.008	0.012	0.034
7	Propachlor	ND	<0.001	ND	ND	ND	<0.001	ND
11	Chlorpyrifos	0.002	ND	ND	ND	ND	ND	ND
13	p, p'-DDE	<0.001	<0.001	ND	0.001	<0.001	<0.001	0.002
16	o, p'-DDD	<0.001	<0.001	<0.001	0.001	0.001	0.001	0.004
17	o, p'-DDT	ND	ND	ND	<0.001	ND	0.001	ND
18	Acetamiprid	ND	0.001	ND	<0.001	ND	ND	0.009
19	Pyridaben	<0.001	ND	ND	ND	ND	ND	ND

ND = not detected.

any of the water samples collected from Akora Khattak. Chlorpyrifos was found in high amounts i.e. 0.040 ppm, in AK6 while methamidophos and methiocarb were found in appreciable quantities i.e. 0.026 ppm and 0.038 ppm, respectively, in sample no. 4 (AK4). Concentrations of most of the pesticides under study were found at the level below 0.001 ppm. Methiocarb concentration (0.038 ppm) was found beyond the permissible limit (0.035 ppm) in AK4. Amounts of the residues of p, p'-DDE obtained in sample no. 8 (AK8) (0.005 ppm) and of o, p'-DDD in AK8 (0.003) were above the allowed limit (0.002 ppm). Quantified amount o, p'-DDT in AK4 found at the permissible limit (0.002 ppm). Concentrations of rest of the pesticides residues detected were within the range.

Results obtained from the GC-MS analyses of samples collected from Buner are shown in Table 4a and 4b. Aldicarb, carbofuran, cyhalothrin, atrazine, acetochlor, α-endosulfan, dieldrin, β-endosulfan, cypermethrin-1, fenvalerate and difenoconazole were not detected in the water samples collected from Buner. Chlorpyrifos was detected only in sample no. 11 (B11) (0.002 ppm). Methamidophos and methiocarb were found in appreciable amounts i.e. 0.039 ppm and 0.034 ppm, respectively, in sample no. 17 (B17). Rest of the pesticides detected and quantified were below 0.010 ppm. Concentration of methiocarb found (0.034 ppm) is about to the maximum limit (0.035 ppm) while that of p, p'-DDE is at the maximum allowed limit (0.002 ppm) in sample B17 and amount of o, p'-DDD (0.004 ppm) quantified in B17 is beyond the limit (0.002 ppm). Concentrations of rest of the pesticides residues detected in water samples from Buner were within the permissible limits. From the results it appears that drinking waters sources in the area under study have been contaminated with pesticides which is a health hazard and may be a source of various diseases in these areas.

Conclusion

From the data collected in this study, it is evident that the flood water has contaminated the drinking water sources especially in the flood hit areas like Akora Khattak. Therefore, proper measures should be taken to clean the drinking water from such contaminants. It is further suggested that preventive actions should be taken to avoid such occurrence in future leading to health problems.

References

Abhilash, P.C., Singh, N. 2009. Pesticide use and application: an Indian scenario. *Journal of Hazardous Materials,* **165:** 1-12.

Abid, M.H., Qureshi, M.N., Ali, M.J., Ziaurahaman, M. 2010. *A Report on the Bacteriological Investigations of Drinking Water of the Flood 2010 Affected Areas of Khyber Pukhtoonkhwa.* PCSIR Laboratories Complex Peshawar, Pakistan, pp. 1-18.

Androutsopoulos, V.P., Hernandez, A.F., Liesivuori, J., Tsatsakis, A.M. 2013. A mechanistic overview of health associated effects of low levels of organo-chlorine and organophosphorous pesticides. *Toxicology,* **307:** 89-94.

Arlien-Soberg, P. 1992. *Solvent Neurotoxicity*. 373 pp., CRC Press, Boca Raton, FL, USA.

Bassil, K.L., Vakil, C., Sanborn, M., Cole, D.C., Kaur, J.S., Kerr, K.J. 2007. Cancer health effects of pesticides - Systematic review. *Canadian Family Physician,* **53:** 1704-1711.

Brown, S.K., Ames, R.G., Mengle, D.C. 1989. Occupational illness from cholinesterase inhibiting pesticides among agriculture pesticide applicators in California. *Archives of Environmental Health,* **44:** 34-39.

Chambers, H.W. 1992. Organophosphorus compounds: an overview In: *Organophosphates: Chemistry, Fate and Effects,* J.E. Chambers, P.E. Levi (eds.), pp. 3-18, Academic Press, San Diego, CA, USA.

Hamilton, D.J., Ambrus, A., Dieterle, R.M., Felsot, A.S., Harris, C.A., Holland, P.T., Katayama, A., Kurihara, N., Linders, J., Unsworth, J. 2003. Regulatory limits for pesticide residues in water. *Pure and Applied Chemistry,* **75:** 1123-1155.

Hayat, K., Ashfaq, M., Ashfaq, U., Saleem, M.A. 2010. Determination of pesticide residues in blood samples of villagers involved in pesticide application at District Vehari (Punjab), Pakistan. *African Journal of Environmental Science and Technology,* **4:** 666-684.

Hernández, A.F., Parrón, T., Tsatsakis, A.M., Requena, M., Alarcón, R., López-Guarnido, O. 2013. Toxic effects of pesticide mixtures at a molecular level: their relevance to human health. *Toxicology,* **307:** 136-145.

AOAC, 2002. *Official Methods of Analysis of the Association of Official Analytical Chemists.* (AOAC), International, W. Horwitz (ed.), Chapter 10, pp. 97-136, Gaithersburg, Maryland, USA.

Hueser, G. 1992. Diagnostic markers in clinical immunotoxicology and neurotoxicology. *Journal of Occupational Medicine and Toxicology,* **1:** 5-10.

Jenkins, J.J. 1999. *Drinking Water Standards and Guidelines for Pesticides Sampled in Oregon Ground and Surface Water.* pp. 1-8.

Kanavouras, K., Tzatzarakis, M.N., Mastorodemos, V., Plaitakis, A., Tsatsakis, A.M. 2011. A case report of motor neuron disease in a patient showing significant level of DDTs, HCHs and organo-phosphate metabolites in hair as well as levels of hexane and toluene in blood. *Toxicology and Applied Pharmacology,* **256:** 399-404.

Karalliedde, L., Senanayake, N. 1999. Organophosphorus insecticide poisoning. *Journal of the International Federation of Clinical Chemistry,* **11:** 1-9.

Kesavachandran, C.N., Fareed, M., Pathak, M.K., Bihari, V., Mathur, N., Srivastava, A.K. 2009. Adverse health effects of pesticides in agrarian populations of developing countries. *Reviews of Environmental Contamination and Toxicology,* **200:** 33-52.

Luster, M.I., Rosenthal, G.J. 1993. Chemical agents and the immune response. *Environmental Health Perspectives,* **100:** 219-226.

Moermond, C.T.A., Mensink, B.J.W.G., Vos, J.H. 2008. Environmental risk limits for pyridaben. *RIVM Letter Report Number 60176021,* Bilthoven, The Netherlands.

Moon, H.B., Kim, H.S., Choi, M., Yu, J., Cho, H.G. 2009. Human health risk of polychlorinated biphenyls and organochlorine pesticides resulting from seafood consumption in South Korea, 2005–2007. *Food and Chemical Toxicology,* **47:** 1819-1825.

Palis, F.G., Flor, R.J., Warburton, H., Hossain, M. 2006. Our farmers at risk: behaviour and belief system in pesticide safety. *Journal of Public Health,* **28:** 43-48.

Salameh, P.R., Waked, M., Baldi, I., Brochard, P., Saleh, B.A. 2006. Chronic bronchitis and pesticide exposure: a case-control study in Lebanon. *European Journal of Epidemiology,* **21:** 681-688.

Soomro, A.M., Seehar, G.M., Bhanger, M.I., Channa, N.A. 2008. Pesticides in the blood samples of spray-workers at agriculture environment. The toxicological evaluation. *Pakistan Journal of Analytical and Environmental Chemistry,* **9:** 32-37.

Vial, T., Nicolas, B., Descotes, J. 1996. Clinical immunotoxicity of pesticides. *Journal of Toxicology and Environmental Health,* **48:** 215-229.

Zaganas, I., Kapetanaki, S., Mastorodemos, V., Kanavouras, K., Colosio, C., Wilks, M.F., Tsatsakis, A.M. 2013. Linking pesticide exposure and dementia: What is the evidence? *Toxicology,* **307:** 3-11.